SILICIDE FORMATION THROUGH DIFFUSION BARRIERS

by

Maryna Baldé

Dissertation submitted in partial fulfilment of the requirements for the degree of Doctor of Philosophy (Physics)

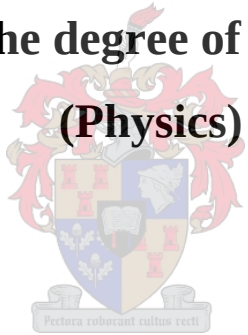

At the

University of Stellenbosch

Promoter: Prof. R. Pretorius

November 2005

DECLARATION

I, the undersigned, hereby declare that the work contained in this dissertation is my own original work and has not in its entirety or in part been submitted at any university for a degree.

Signature: M. Baldé Date:

UITTREKSEL

Die vorming van Ni-, Co- en Fe-silisiedes deur verskillende diffusie sper-tussenlagies is ondersoek. Die diffusie sperlagies onder beskouing was Ta, Ti en Cr. In sommige gevalle is die invloed van die dikte van die sperlagie en van ‘n deklagie ook ondersoek. Die dun-film strukture is voorberei op enkelkristal Si-substrate d.m.v. Elektronbundel Vakuum Deposisie. Die monsters is in vakuum uitgegloei vir tye wat wissel van 10 tot 60 minute by temperature wat wissel van 340 - 800°C en die karakterisering van die monsters is uitgevoer d.m.v. konvensionele RBS, dinamiese RBS, kanaliserings RBS en X-straal diffraksie (XRD).

Die gebruik van a dun (20Å) Ta sperlagie in die Ni-Si sisteem het reaksie verhoed selfs na ‘n uitgloei van 10 min. by 400°C, maar RBS resultate het getoon dat uniforme NiSi skielik gevorm het as eerste fase na ‘n 15 min. uitgloei by 400°C. XRD sowel as dinamiese RBS metings het hierdie abrupte formasie van NiSi in plaas van die normale eerste fase Ni_2Si bevestig. Volgens die Effektiewe Hitte van Formasie (EHF) model toon dit dat die diffusie sperlagie die effektiewe konsentrasie van die Ni-atome verlaag tot ‘n waarde waar die effektiewe hitte van formasie van NiSi meer negatief is as dié van Ni_2Si en sodoende word die eerste fase formasie van NiSi termodinamies bevoordeel. Die dikte uniformiteit van die eerste fase NiSi wat deur die dun Ta sperlaag gevorm het, het verbeter met uitgloei by hoër temperature. ‘n Dikker (100Å) Ta sperlaag het ook Ni diffusie vertraag en nie-uniforme, eerste fase NiSi het eers by 500°C begin vorm. Die uniformiteit van hierde NiSi het ook verbeter met toename in temperatuur, maar die gebruik van die 20Å Ta sperlagie het meer uniforme eerste fase NiSi produseer in die 400 tot 700°C temperatuur gebied. Die gebruik van ‘n dun Cr (30-50Å) sperlagie het ook by 400°C die vorming van hoofsaaklik NiSi opgelewer, maar XRD spektra het Ni_2Si ook aangedui. Die uniformiteit van NiSi het verbeter by hoër temparatuur uitgloeiings. Soortgelyke resultate is verkry van monsters met ‘n dikker (100Å) Cr sperlaag by laer temperature, d.w.s die vorming van NiSi as eerste fase by 400°C, maar die eerste fase NiSi wat by 500 tot 700°C gevorm het, was nie-uniform. In die geval van Ti-sperlagies was die dikker (100Å) Ti minder effektief as die dunner Ti sperlagies vir die verkryging van uniforme eerste fase NiSi in die 500 tot 700°C temperatuur gebied. Die gebruik van ‘n dun (30-50Å) Ti sperlagie het ‘n mengsel van Ni_2Si en NiSi as eerste reaksie gevorm by 400°C, maar ‘n 10 min. uitgloei by 500°C het uniforme NiSi gevorm, soos bevestig is deur RBS en XRD metings. Die uniformiteit van die NiSi het verbeter met toename in uitgloei-temperatuur tot by 700°C. In die geval van die dikker Ti sperlagie het geen reaksie by 400°C plaasgevind nie en nie-uniforme eerste fase NiSi het by 500°C gevorm. Al drie dun sperlagies het $NiSi_2$ gevorm by temperature van 750°C en hoër, maar die dun Ti sperlaag het die mees uniforme di-silisied gevorm. Die $NiSi_2$ wat deur al drie die dikker sperlae by 800°C gevorm het, was nie-uniform.

Die gebruik van ‘n dun (10-30Å) Ta diffusie sperlagie het Co-silisied formasie voorkom tot by 560°C. Die effektiewe Co-konsentrasie by die groei-intervlak is verlaag, derhalwe word die gewone eerste fase formasie van Co_2Si by 450°C oorgeslaan. By 560°C het ‘n mengsel van CoSi en $CoSi_2$ gevorm, soos bevestig deur XRD. Die $CoSi_2$ wat by 640°C gevorm het (‘n hoër formasie temperatuur as sonder ‘n sperlagie) se dikte was redelik uniform, maar XRD metings het getoon dat daar ook CoSi teenwoordig was. Die gebruik van dikker (100Å) Ta sperlae het die diffusie van Co-atome vertraag tot by temperature so hoog as 600°C. Uitgloei by 700°C het $CoSi_2$ sowel as CoSi gevorm en by 800°C het nie-uniforme $CoSi_2$ gevorm. Die toevoeging van ‘n Ta deklagie (van verskillende diktes) in samehang met ‘n 30Å Ta diffusie sperlagie het nie Co-silisied formasie wesentlik beïnvloed nie. Die gebruik van dun (10-30Å) Ti sperlagies het gelei tot die oorslaan van die Co_2Si voorloper fase en die vorming van redelik uniforme eerste fase CoSi by 520°C. Uniforme $CoSi_2$ het by 560°C begin vorm en by hoër temperature was die $CoSi_2$ steeds uniform. Die teenwoordigheid van ‘n dikker (100Å) Ti sperlagie het die effektiewe konsentrasie van Co by die groei-intervlak so verlaag dat $CoSi_2$ as eerste fase begin vorm het na ‘n 30 min. uitgloei by 600°C. By 700 en 800°C het nie-uniforme $CoSi_2$ gevorm.

Vir Fe-silisied formasie het die gebruik van 50Å en 100Å Cr sperlae, sowel as $CrSi_2$ sperlae, soortgelyke resultate opgelewer. Daar was geen verandering in die gewone Fe-silisied fase formasie volgorde nie, want nie-uniforme FeSi was die eerste fase wat by 500°C gevorm het en daarna het $FeSi_2$ begin vorm by 600°C. Uitgloei by 700°C deur Cr sperlagies het gelei tot die volledige formasie van $FeSi_2$ wat meer uniform was as dié wat in die Fe-Si binêre sisteem gevorm het sonder ‘n diffusie sperlagie.

In hierdie studie is dinamiese intydse RBS vir die eerste keer gebruik om bo enige twyfel te bewys dat diffusie sperlae gebruik kan word om die “oorslaan” van fases te bewerkstellig. Hierdie resultate is interpreteer in terme van die Effektiewe Hitte van Formasie (EHF) model en is goeie voorbeelde van konsentrasie-gekontroleerde fase seleksie. In die algemeen is bevind dat hoe dikker die diffusie sperlagie, hoe hoër die temperatuur van silisied-formasie. Bowendien was silisied-formasie oor die algemeen meer uniform by hoër uitgloei-temperature en met die gebruik van dunner diffusie sperlagies.

ABSTRACT

The formation of Ni-, Co- and Fe-silicides through different diffusion barrier interlayers was investigated. The diffusion barrier layers examined were Ta, Ti and Cr. In some cases the thickness of the barrier layer and the influence of a capping layer was also investigated. The thin-film structures were prepared on single crystal Si-substrates by Electron Beam Vacuum Deposition. The samples were vacuum annealed for times ranging from 10 to 60 min at temperatures ranging from 340 - 800°C and sample characterization was carried out by conventional RBS, dynamic RBS, channeling RBS and X-ray diffraction (XRD).

The use of a thin (20Å) Ta diffusion barrier in the Ni-Si system allowed no reaction even after annealing for 10 min at 400°C, but RBS measurements showed that after annealing for 15 min at 400°C uniform NiSi formed suddenly as first phase. XRD as well as dynamic RBS measurements confirmed this abrupt formation of NiSi instead of the normal first phase Ni_2Si. According to the Effective Heat of Formation (EHF) model this shows that the diffusion barrier reduces the effective concentration of the Ni atoms to a value where the effective heat of formation of NiSi is more negative than that of Ni_2Si and first phase formation of NiSi is thus thermodynamically favoured. The thickness uniformity of the first phase NiSi that formed through the thin Ta barrier improved at higher annealing temperatures. A thicker (100Å) Ta barrier also retarded the Ni diffusion and first phase, non-uniform NiSi only started to form at 500°C. The uniformity of this NiSi also improved with increased temperature but the use of the 20Å Ta barrier produced more uniform first phase NiSi in the 400 to 700°C temperature range. The use of a thin (30-50Å) Cr barrier also allowed the formation of mainly NiSi at 400°C, although XRD spectra indicated the presence of some Ni_2Si. The uniformity of NiSi improved at higher temperature anneals. Similar results were obtained from samples with a thicker (100Å) Cr barrier layer at lower temperatures, i.e. the formation of NiSi as first phase at 400°C, but the first phase NiSi that formed at 500 to 700°C was non-uniform. In the case of Ti-barriers, the thicker (100Å) Ti barrier seems less effective than the thinner Ti barriers in delivering uniform first phase NiSi in the 500 to 700°C temperature range. The use of a thin (30-50Å) Ti barrier produced a mixture of Ni_2Si and NiSi as first reaction at 400°C, but a 10 min anneal at 500°C formed uniform NiSi as confirmed by RBS and XRD measurements. The uniformity of the NiSi improved with an increase in annealing temperature up to 700°C. In the case of the thicker Ti interlayer no reaction occured at 400°C and non-uniform first phase NiSi formed at 500°C. All three thin barriers formed $NiSi_2$ at temperatures of 750°C and above, but the thin Ti barrier formed the most uniform di-silicide. The $NiSi_2$ that formed at 800°C through all three of the thicker barriers was non-uniform.

The use of a thin (10-30Å) Ta diffusion barrier prevented Co-silicide formation up to 560°C. The effective Co concentration at the growth interface is lowered, thus skipping the usual first phase formation of Co_2Si at 450°C. At 560°C a mixture of CoSi and $CoSi_2$ formed, as was confirmed by XRD. The $CoSi_2$ that formed at 640°C (a higher formation temperature than without barrier) was of quite uniform thickness, but XRD measurements indicated that some CoSi was present as well. The use of thicker (100Å) Ta barrier layers retarded the diffusion of Co atoms for temperatures of up to 600°C. Annealing at 700°C formed $CoSi_2$ and some CoSi and at 800°C non-uniform $CoSi_2$ formed. The addition of a Ta capping layer (of different thicknesses) in conjunction with a 30Å Ta diffusion barrier layer did not significantly improve Co-silicide formation. The use of thin (10-30Å) Ti barrier layers resulted in the skipping of the Co_2Si precursor phase and the formation of quite uniform first phase CoSi at 520°C. Uniform $CoSi_2$ started forming at 560°C and the $CoSi_2$ remained uniform at higher temperatures. The presence of a thicker (100Å) Ti barrier lowered the effective concentration of Co at the growth interface to such an extent that $CoSi_2$ started to form as first phase after annealing for 30 min at 600°C. At 700 and 800°C non-uniform $CoSi_2$ formed.

For Fe-silicide formation the use of 50Å and 100Å Cr barriers, as well as $CrSi_2$ barriers, delivered very similar results. There was no change in the normal Fe-silicide phase formation sequence, as non-uniform FeSi was the first phase to form at 500°C and thereafter $FeSi_2$ started to form at 600°C. At 700°C the use of Cr barriers resulted in the complete formation of $FeSi_2$ of greater uniformity than was formed in the Si-Fe binary system without the presence of a diffusion barrier.

In this study dynamic real-time RBS has been used for the first time to prove without any doubt that diffusion barrier layers can be used to bring about “phase skipping”. These results have been interpreted in terms of the Effective Heat of Formation (EHF) model and are good examples of concentration controlled phase selection (CCPS). In general it was found that the thicker the diffusion barrier layer, the higher the temperature of silicide formation. Furthermore, silicide formation was generally found to be more uniform at higher annealing temperatures and when thinner diffusion barrier layers were used.

ACKNOWLEDGEMENTS

I would like to thank the following people and organisations without whose support and assistance this investigation would not have been possible.

- **Prof. R. Pretorius**, University of Stellenbosch, for the very knowledgeable supervision and guidance of the study.
- **Dr C. C. Theron**, iThemba Labs, for guidance, help and advice during the execution of the study, as well as the use of his dynamic RBS system.
- **Messrs. K. Springhorn, L. Ashworth** and **C. Doyle**, iThemba Labs, for humour, patience and assistance with the practical side of things!
- **Mr T. Ntsoane**, XRD facility iThemba Labs, for help in doing and analyzing the X-ray diffraction measurements.
- All the staff at iThemba Labs for help, acceptance and good times.
- The **National Research Foundation** for the generous financial support during the first three years of the study.
- My **Father** for the dream.
- My **Mother** for practical and mental support.
- My children, **Jean** and **Martinique** for their help in running the household and buying groceries!
- My husband **Erwin** for moral and financial support, as well as for continuing to believe in me.
- The **Creator** for health, talents and opportunities.

TABLE OF CONTENTS

LIST OF TABLES

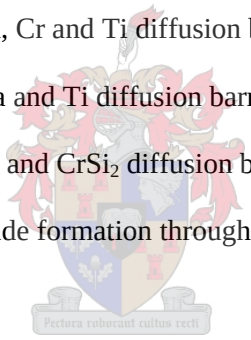

Chapter 1

INTRODUCTION AND SCOPE

1.1 Introduction

Layered thin film structures are used as primary components in technologies such as integrated circuits, solid state lasers and opto-electronic devices and this underlines the importance of the study of thin film solid state interaction and phase formation. This thesis is concerned with the effects of different metallic diffusion barrier interlayers on first phase formation and phase formation sequence in binary thin film systems. Knowing beforehand which phase can be expected to form first, at what temperature the reaction would occur, as well as being able to predict the reaction sequence obviously holds great advantages for the device technologist.

The Effective Heat of Formation Model (EHF model) **[1,2]** showed for the first time that thermodynamic data can be used to explain and predict phase formation in the solid state. This model defines an effective heat of formation that depends upon the concentrations of the reacting species at the interface between two materials in contact. It also illustrates how new phases can be formed by controlling the effective concentration at the growth interface. This approach to the formation of materials is known as Concentration Controlled Phase Selection (CCPS) **[3].**

In this study of thin film metal-silicon binary systems different metallic diffusion barriers are used to control the silicide phase that forms by controlling the effective concentration at the growth interface. This approach is very important as it enables the device technologist to select the desired device characteristics, like low resistivity, uniformity and good thermal stability. For example, the different phases of nickel silicide have different resistivities: $NiSi_2$ has a relatively high resistivity of ~ 34 μΩ.cm, compared to NiSi with a resistivity of only ~ 10 μΩ.cm. This low resistivity of NiSi makes it a desirable silicide phase for use in certain applications and thus also a desirable phase to attempt forming by using concentration controlled phase selection.

1.2 Metal silicide formation

The heating or annealing of a thin metal film in contact with a silicon substrate usually leads to the formation of a metal silicide. The phase of the metallic silicide depends on the temperature of formation which in turn is determined by the reaction between the two different solid phases in direct contact at the growth interface. These two phases are the Si substrate, which is covalently bonded single crystal, and the thin metal film which is usually poly-crystalline.

The metallic silicides can roughly be grouped in three main classes, i.e. metal-rich silicides, monosilicides and disilicides, which typically start to form around 200, 400 and 600 °C respectively **[4].** In the normal formation sequence for nickel silicides, for example, the metal-rich Ni_2Si phase forms as first phase at temperatures above 200°C, the monosilicide NiSi forms at 350 °C and the disilicide $NiSi_2$ at about 750 °C. This last phase is called the "end phase" as no phase changes occur at higher temperatures.

In phase diagrams of metal-silicon systems there are generally more than three silicide phases present, as will be seen in later chapters, but it has been established experimentally **[4,5,6]** that not all the equilibrium phases of the bulk case are present as dominant growth phases during silicide formation in thin film systems. These other phases may nucleate but do not grow to detectable macroscopic dimensions.

1.3 Epitaxial metal silicides

Epitaxial growth of metallic silicide occurs when the atoms in the silicide are aligned with the atoms in the underlying single crystal Si substrate. The formation of epitaxial silicide films is important, as these films are usually more uniform and stable and have improved electrical characteristics.

In determining if a silicide will grow epitaxially or not, the lattice match η is a very important parameter and can be defined as:

$$\eta = (a_{silicide} - a_{Si}) / a_{Si}$$

where $a_{silicide}$ is the lattice parameter of the crystalline plane of the silicide that is being matched to the silicon substrate and a_{Si} is the lattice parameter of the Si substrate **[4].** For good epitaxial growth the lattice mismatch should not be more than a few percent. The silicides with small unit cell areas and small lattice mismatches like $NiSi_2$ and $CoSi_2$ are easiest to grow epitaxially and form high quality silicides.

In this investigation the quest has been to use metallic diffusion barrier interlayers to enable possible epitaxial growth of certain desirable metal silicide phases at lower formation temperatures, and with the possible exclusion of other, less desirable, phases. The desirability of a particular silicide phase is largely determined by its importance and applications in the thin film industry.

1.4 Kinetics of phase formation

A typical example of a thin film reaction couple is shown in **Fig. 1.1**. The thickness of the two thin films ranges from several hundred to several thousand angstroms. When the system is heated the materials in the two films (A and B) mix to form a chemical compound phase of a different composition ($A_\alpha B$). This could be an equilibrium compound phase, an amorphous phase or a metastable phase. In thin film systems only one phase usually grows at any one time and this phase will continue to grow until one of the components has been consumed. During phase formation there are three important processes taking place, namely nucleation, reaction and diffusion. In a given system, the kinetics of the phase formation is characterized by the slowest of these three processes.

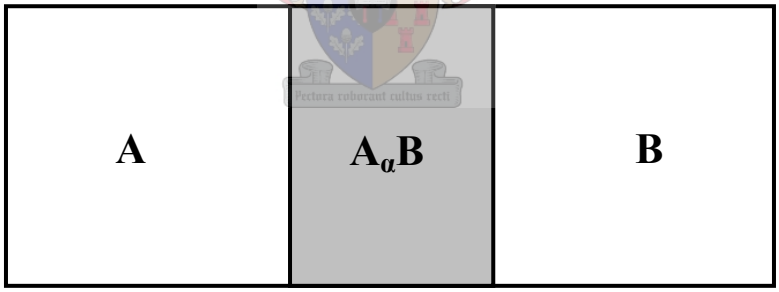

Figure 1. 1. Schematic representation of a thin film binary reaction couple. The two thin films composed of A and B respectively react to form a thin film of the $A_\alpha B$ phase.

Nucleation is the process whereby $A_\alpha B$ first forms at the A-B interface. At this point neither A nor B has to move in order to take part in the reaction. The phase will only nucleate if its formation causes a drop in free energy that is larger than the increase in surface energy which results from the extra interface which is formed.

In some systems there is a nucleation barrier which must first be overcome. The energy needed to overcome this barrier is the activation energy of nucleation and such systems are governed by so called nucleation-limited kinetics. Due to the high

temperatures needed to overcome the nucleation barrier and initiate reaction in these systems, subsequent phase growth is usually very fast.

The actual chemical reaction in which the new phase is formed occurs at one of the interfaces, A/$A_\alpha B$ or $A_\alpha B$/B. The determination of the actual reaction interface depends upon whether A or B is the dominant diffusing species through the $A_\alpha B$ phase. For instance, if A is the dominant diffusing species there will be a movement of A atoms through the already formed $A_\alpha B$ film to the $A_\alpha B$/B interface where the reaction between A and B atoms will occur.

The relationship between the rate at which the $A_\alpha B$ phase increases in thickness and the time depends upon whether the diffusion or the reaction is the slowest part of the phase formation process. The slower of the two processes will dominate the reaction kinetics. Nucleation limited formation depends linearly on time t, while diffusion limited growth kinetics has a $t^{1/2}$ dependence.

1.5 Thermodynamics of phase formation

1.5.1 Sequence of phase formation

Binary equilibrium phase diagrams usually show several chemically stable equilibrium compound phases. In a bulk system any of these equilibrium phases could be produced given the correct composition, pressure and temperature. If bulk pieces of two materials A and B were joined to form a bulk diffusion couple several, and in some cases all of the compound phases on the phase diagram would be present if the two materials were allowed to react with each other. A striking feature of phase formation in thin film diffusion couples (several hundred nanometers of material) is that usually only one compound phase grows at a time (say $A_\alpha B$). This phase then grows until one of the materials has been consumed (e.g. A). If there is still B left then this will react with the phase $A_\alpha B$ to form a new more B-rich phase $A_\beta B$. This will continue until either B or $A_\alpha B$ has been consumed.

It is necessary to try and understand the actual mechanisms of interaction in these thin film systems in order to be able to forecast which phases will form first and also what the subsequent phase formation sequence will be. In the thin film industry it is often desirable to form a second or third phase directly as a first phase. In order to manipulate phase formation the driving forces and influencing factors should be

understood. The following thermodynamic models attempt to give the necessary tools to do this.

1.5.2 Walser-Bené model

Walser and Bené **[7]** stated one of the first rules for predicting phase formation: **The first compound phase nucleated in planar binary reaction couples is the most stable congruently melting compound adjacent to the lowest temperature eutectic on the bulk equilibrium phase diagram.**

This rule was relatively successful in predicting first phase formation in metal-silicon systems and was later extended by Tsaur *et al*. **[8]** to subsequent phase formation sequence in metal-silicon systems as follows: **The second phase formed is the compound with the smallest ΔT that exists in the phase diagram between the composition of the first phase and the un-reacted element.**

Here ΔT is defined as the temperature difference between the liquidus curve and the peritectic point (point where a solid breaks up into a liquid and a solid, both with new composition) of the phase. ΔT is zero for so called congruently melting compounds. Bené subsequently extended the Walser-Bené rule to metal-metal reactions **[9]** by relaxing the requirement that the first phase should be a congruently melting phase.

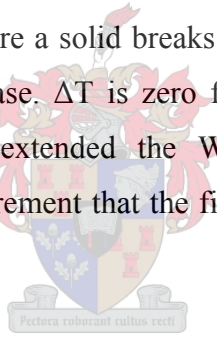

1.5.3 Effective Heat of Formation model

Pretorius **[1,2,3]** used a much more fundamental approach in predicting first phase formation by postulating the Effective Heat of Formation (EHF) model. The model shows how heats of formation, when expressed as effective heats of formation, ΔH', can be used in conjunction with the composition of the lowest eutectic (or liquidus minimum) of the binary system, to predict both the first phase and subsequent phases which form. This model combines thermodynamics with the availability or effective concentration of the elements at the interface.

The driving force for a process like phase formation is given by the change in the Gibbs free energy, $\Delta G^\circ = \Delta H^\circ - T\Delta S^\circ$ where ΔH° is the change in enthalpy during the reaction at a temperature T and ΔS is the change in entropy. Since thin film reactions occur in the solid state, the Gibbs free energy can be approximated by the standard enthalpy of reaction alone, as the change in entropy may be considered to be

close to zero for most systems. Thus $\Delta G^\circ_T \approx \Delta H^\circ_{298}$. According to the Neumann-Kopp rule **[10]** the standard values (T = 298K) of enthalpy and entropy in solids can be used for thermodynamic calculations at any temperature. An effective heat of formation **[3]** is defined as:

$$\Delta H' = \Delta H^\circ \left(\frac{\text{effective concentration of limiting element}}{\text{compound concentration of limiting element}} \right) \qquad \textbf{1. 1}$$

where $\Delta H'$ and ΔH° are expressed in kJ $(\text{mol.at})^{-1}$. According to the EHF model, solid-state phase formation is controlled by the effective concentrations of the reacting species at the growth interface.

For example consider a silicon-cobalt growth interface and the prospective formation of CoSi. If the effective concentration at the interface was 20 at.% Si, then Si would be the limiting species. Obviously the compound concentration of Si in CoSi is 50 at.% and the standard enthalpy value $\Delta H^\circ = -50.0$ kJ $(\text{mol.at})^{-1}$ for the formation of CoSi. This gives an effective heat of formation value of:

$$\Delta H' = -50.0 \left(\frac{0.2}{0.5} \right) = -20.0 \text{ kJ } (\text{mol.at})^{-1}$$

Eq. 1.1 shows that there is a linear relationship between the effective heat of formation (or heat released) and the concentration of the limiting element.

Using this linear relationship an effective heat of formation diagram can be drawn for any binary system (see **Fig. 1.2)**. The EHF model states the following rule to predict first phase formation: **The first compound phase to form during metal-silicon interaction is the congruently melting phase with the most negative effective heat of formation (ΔH′) at the concentration of the lowest eutectic temperature (or liquidus minimum) of the binary system [3,5].**

Subsequent phase formation can also be predicted as follows: **After first silicide formation, the next phase formed at the interface between the compound and the remaining element is the next congruent phase richer in the unreacted element, which has the most negative effective heat of formation. If the compounds between a formed phase and the remaining element are all non-congruent, the next phase that will form is the non-congruent phase with the most negative effective heat of formation [3,5].**

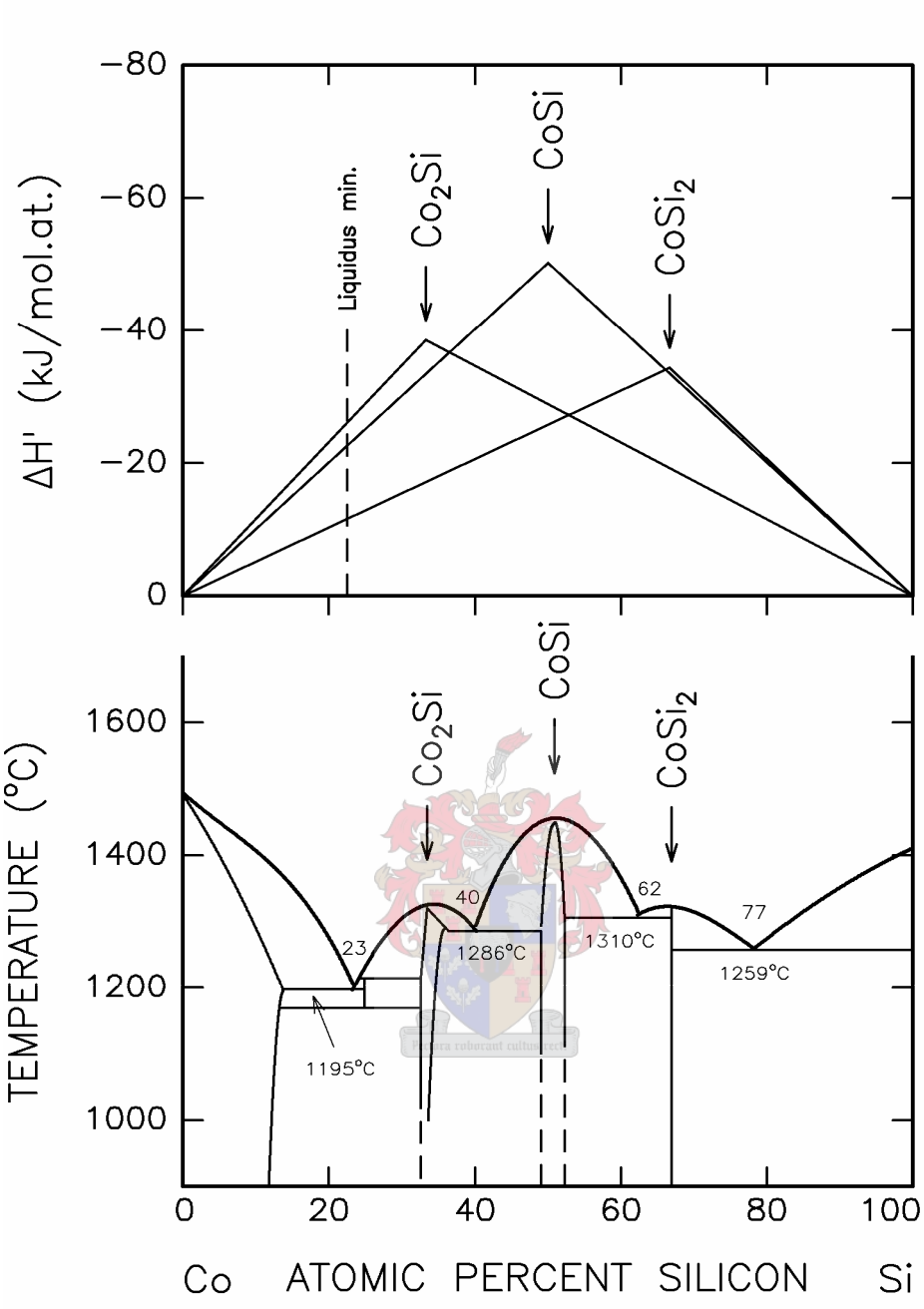

Figure 1.2. Phase diagram **[10]** and EHF diagram for the Co-Si binary system, showing the linear relationship between effective heat of formation (or heat released) and the concentration of the limiting element. Note that at the concentration of the liquidus minimum the phase Co_2Si has the most negative effective heat of formation and would thus be the first phase to form.

The EHF model has been successfully used in metal-metal, metal-silicon and metal-germanium systems to predict first phase formation as well as phase formation sequence.

1.6 Diffusion barrier interlayers

A diffusion barrier interlayer is used in a binary system, for example a silicon-metal binary system, to control the effective concentration at the growth interface. It consists of a thin layer of a third material deposited between the silicon substrate and the metal and this material should be unreactive with the metal. A diffusion barrier is sometimes also referred to as a marker, as it marks or indicates the direction of motion of the diffusion species by moving in the opposite direction. The thickness of a diffusion barrier can be anything from a few Å to a few hundred Å. In general a diffusion barrier can influence the following factors: the diffusion of a particular species and thus the effective concentration of that species at the growth interface, the phase formation sequence by the skipping of certain precursor phases, the formation temperature of a particular phase, and also the uniformity and epitaxiality of phases.

In accordance with the effective heat of formation model the "*efficiency*" of a diffusion barrier for a metal-silicide system can be expressed in terms of the *ability* of the barrier to:

- prevent or inhibit the normal diffusion of the diffusing species at the growth interface, and / or
- lower the effective concentration of the diffusing species at the growth interface
- enable the skipping of initial phases in the normal phase sequence by lowering the effective concentration at the growth interface, and / or
- lower the formation temperature of a particular desired silicide phase, and /or
- improve the uniformity of a desired formed silicide phase by the skipping of initial phases in the normal phase sequence, and / or
- improve the epitaxiality of a desired formed silicide phase.

1.7 Scope of the investigation

In this study the application of concentration controlled phase formation in different metal-silicon binary systems was investigated. Different diffusion barriers were used as a means of trying to control the concentration of a species at the reaction interface. The results are discussed in terms of the effective heat of formation model, which describes phase formation in terms of thermodynamics and the effective concentrations at the growth interface.

The samples consisted of a variety of metallic thin film structures with different diffusion barriers deposited onto silicon substrates and the depositions were done using vacuum electron beam evaporation. Reaction was usually induced in the samples by annealing in a vacuum furnace at pressures below 2×10^{-7} Torr. This was done to limit oxidation or other forms of contamination.

Rutherford Backscattering Spectrometry (RBS) with 2 MeV alpha particles was used to determine the composition of the samples. RBS was also done in channeling mode to study the possible epitaxial quality of the silicide films. Dynamic RBS (in-situ, real time RBS) was used to confirm the precise phase formation sequence i.e. which phase formed as first phase, the abruptness of the phase change and the temperature of formation of each phase. X-ray diffraction (XRD) was used to try and identify the various silicide phases.

Chapter 2 attempts to give an overview on all research done during the past decade or so on the formation of metal silicides through diffusion barrier interlayers. The metal-silicides that have been most researched in this regard are the silicides of cobalt, nickel, titanium and iron and a short discussion of this research is given. The sample preparation techniques as well as the methods of characterization of samples are discussed in **Chapter 3.**

The formation of Ni-silicides through different diffusion barriers is discussed in **Chapter 4**. The study of Ni-silicide formation is important because of the suitability of nickel silicides, particularly NiSi with its very low resistivity, for applications in the ULSI technology. NiSi is of special interest because it is possible to grow uniform NiSi layers with good thermal stability and very low resistivity **[11]**. It is known that, in the Ni-Si binary system, Ni is the diffusing species. When a thin metallic interlayer is placed between the silicon substrate and the nickel layer, this interlayer acts as a diffusion barrier through which the nickel has to diffuse before it reacts with the silicon. The presence of the barrier layer influences the nickel silicide phase formation sequence and might possibly favour the formation of NiSi as first phase (instead of the usual Ni_2Si), or lower the formation temperature of NiSi, with obvious benefits to the industry. The interlayers investigated were Ta, Cr and Ti.

Chapter 5 describes the formation of Co-silicides, in particular $CoSi_2$, through Ti or Ta diffusion barriers. In recent years $CoSi_2$ has become one of the most researched silicides (see **Table 2.6** in **Chapter 2**). This can be ascribed to the fact

that, like NiSi, $CoSi_2$ has a low resistivity **[11]**, it also has excellent uniformity and high thermal stability **[12,13],** all properties that are of great interest in the ULSI industry. A Ti diffusion barrier has been successfully used to influence the diffusion of Co atoms in the presence of different ambient atmospheres and/or different capping layers to form epitaxial $CoSi_2$ directly as first phase **[11,12]** instead of Co_2Si which is usually found as first phase. In this investigation however, no ambient atmospheres were used as all depositions and annealing were done in vacuum. A comparative study was done using a 30 Å Ta diffusion barrier together with Ta capping layers of differing thickness.

Chapter 6 reports on Fe-silicide formation by controlling the diffusion of Fe atoms through Cr and $CrSi_2$ diffusion barrier interlayers. Fe-silicide formation is interesting due to the fact that β-$FeSi_2$ is a semi-conductor that has a small band gap and can be used for infrared sensors.

Finally, the experimental results and outcomes obtained in this investigation are summarized and final conclusions are drawn in **Chapter 7.**

Chapter 2

REVIEW OF SILICIDE FORMATION THROUGH BARRIER LAYERS

2.1 Introduction

The formation and characterization of thin epitaxial metallic silicide layers on Si substrates has been the subject of a vast number of fundamental studies as metal silicides are widely used as gates, contacts and interconnects in silicon based micro-electronic devices. The studies of the formation of the silicides of cobalt, nickel and titanium have been most prolific due to the suitability of some of their silicides for applications in ULSI technology. For ULSI devices, in particular, it is crucial that these silicide layers not only have low resistivity but are very uniform and have good thermal stability. The silicides which have the lowest resistivity (between 10 and 15 μΩ-cm) are $CoSi_2$, $TiSi_2$ (C54 phase) and NiSi **[11].** The formation of epitaxial silicides has also received a lot of interest as these usually have excellent uniformity and high thermal stability **[12,13].** The silicides that produce high quality epitaxial films and are the easiest to grow, are the ones which have the smallest lattice mismatch to single crystal silicon and the smallest unit cell areas. The lattice mismatch of $TiSi_2$ with silicon is large and epitaxy is therefore difficult to achieve. However, the epitaxial formation of $CoSi_2$ or NiSi is possible as they have lattice mismatches of only 1.2 % and 0.4 % and unit cell areas of 18 $Å^2$ and 51 $Å^2$ respectively **[11].**

Epitaxial $CoSi_2$ has been grown on Si(111) using methods such as solid-phase epitaxy, molecular-beam epitaxy and ion-beam synthesis **[14].** The formation of good quality epitaxial $CoSi_2$ on Si(100) without an interlayer as barrier is normally very difficult, requiring UHV conditions and utilisation of a template method **[12,15-17].**

In this chapter it will be attempted to give a short review of most of the research that has been done on metal silicide formation through diffusion barrier interlayers, with special attention given to the formation of the silicides of cobalt, nickel, titanium and iron.

2.2 Cobalt Silicides

Normally when a thin cobalt film is deposited on silicon the phase formation sequence is Co_2Si as first phase, then CoSi and finally $CoSi_2$. However, by placing a thin Ti interlayer (~ 50 Å) between the cobalt and silicon, the first and second phases are skipped and this leads to the direct formation of excellent epitaxial quality $CoSi_2$ on Si(100) and Si(111) substrates **[18,19].** This is because no bond breaking of any precursor phase is required and random nucleation is prevented, thereby ensuring good epitaxy. This approach is usually referred to as titanium interlayer mediated epitaxy – TIME **[19,20]**.

Table 2.1 lists all the different barrier layers that have been used to research the possibility of enhanced formation of cobalt silicides. In all the tables given in this chapter the systems are listed in alphabetical order according to the barrier layer. The discussion of a particular metal-silicide system usually starts with the diffusion barrier layer that has been most researched and ends with the least researched barrier. In cases where the type of Si substrate is not indicated in the abstract, it is generally thought to be Si(100).

2.2.1 Ti barrier layers

It is clear from **Table 2.1** that, for the formation of Co-silicides, most of the research **[14,21-50]** has been done on the Si(100)/Ti/Co system in non-reactive ambient atmosphere (vacuum) and most results confirm the formation of a stable, epitaxial layer of $CoSi_2$ on the Si substrate with a Ti layer on top – the so-called "reversal" of the deposited layers. This reversal occurs because the Co diffuses through the barrier to react with the Si substrate. In this instance it has been shown **[28-31]** that this barrier is actually a ternary Co-Ti-Si compound. Titanium interlayers have proven to be the best epitaxy promoters for the formation of $CoSi_2$ and increasing the Ti thickness seems to improve its efficiency **[33-36].**

It is commonly believed that the Ti interlayer serves as an oxygen scavenger as well as a diffusion barrier limiting the Co-Si interaction up to 500°C. This allows one (Co_2Si) or both (Co_2Si and CoSi) precursor phases in the ordinary Co-Si reaction sequence to be skipped **[12,19,26,51].**

Table 2.1. Review of Co-silicide formation through diffusion barrier layers.

COBALT SILICIDES				
SYSTEM	**AMBIENT**	**TYPE Si**	**REFERENCES**	**RESULTS**
Si/C/Co	vacuum		102	Thick C – epitaxial $CoSi_2$; thin C – epitaxial $CoSi_2$ nucleate higher temp
Si/CoC/Co	vacuum	(100)	103	Epitaxial $CoSi_2$
Si/Cr/Co	vacuum		91,92	Partial layer reversal, 3 regimes depend on thickness interlayer
Si/Fe/Co	vacuum	(100)	93	Epitaxial $CoSi_2$ nucleate higher temp
Si/Ge/Co	vacuum	(100)	93,94	Epitaxial $CoSi_2$ nucleate higher temp
	vacuum	(111)	95	Buried B-type epitaxial $CoSi_2$
Si/Hf/Co	vacuum	(100)	25,33,34,35, 36,88	Complex phase sequence leads to epitaxial $CoSi_2$; Hf forms stable reaction barriers
	N_2		53	TEM shows intermediate CoSi phase raises nucleation temp
	vacuum	(100), poly	34,89	Epitaxial $CoSi_2$; the CoSi-$CoSi_2$ phase transition temp lower on poly-Si than on Si(100)
Si/Mo/Co	vacuum		91	3 regimes depend thickness interlayer
Si/Nb/Co	vacuum	(100)	33,35,36	Only non-epitaxial $CoSi_2$, no stable barriers form
Si/Ni/Co	vacuum	(100)	93	Lowers nucleation temp
Si/SiO_x/Co	vacuum	(100)	15,16,17,20, 44,64,65,66, 67,68,69,70, 71	Epitaxial $CoSi_2$; epitaxial $CoSi_2$ first phase, suppression of intermediate phases
	vacuum	(111), (110), (211), (511)	17,20,70	Thicker excellent quality epitaxial single crystal $CoSi_2$ films at elevated temps ; epitaxial $CoSi_2$ at 500-700°C
Si/SiO_x/Co/Cr_{cap}	vacuum		13	Amorph mixing layer at 450 °C controls diffusion - epitaxial $CoSi_2$
Si/SiO_x/Co/Mo_{cap}	vacuum		13	Amorph mixing layer at 450 °C controls diffusion - epitaxial $CoSi_2$
Si/SiO_x/Co/Ti_{cap}	vacuum	(100)	13,40,65,72, 73,74,75,76	Epitaxial quality depends upon temp, Ti and Co thickness; Ti cap eliminates sensitivity of $CoSi_2$ formation to O_2 contamination
	gas	(100)	77	Epitaxial $CoSi_2$ with capping layer on top
Si/SiO_x/Co/Zr_{cap}	vacuum		13	Amorph mixing layer at 450°C controls diffusion - epitaxial $CoSi_2$
Si/SiO_x/Ti/Co	vacuum	(100)	40,78,79	Self-aligned formation of uniform epitaxial $CoSi_2$
Si/Ta/Co	vacuum	(100)	80,81	Co_2Ta appeared first, CoSi at 700°C, end $CoSi_2$ with $TaSi_2$ on top
	vacuum	(111)	80,81	CoSi at 700°C, then $CoSi_2$ and then $TaSi_2$, reaction on (111) at faster rate
	NH_3	(100)	82,83	Ta layer reduces native oxide, limits flow of Co atoms- epitaxial $CoSi_2$ at early stage of annealing
	N_2	(100)	84	600°C epitaxial $CoSi_2$, epitaxiality improves at higher temps
	N_2	(100), Poly	85,86	Deposited as Co-Ta alloy
Si/Co/Ta/Co_{cap}	vacuum	(100)	87	After 30 min at 650°C nearly all the Co above and below the 30 Å Ta converts to $CoSi_2$.

Si/Ti/Co	vacuum	(100)	14,21,22,23, 24,25,26,27, 28,29,30,31, 32,33,34,35, 36,37,38,39, 40,41,42,43, 44,45,46,47, 48,49,50	Growth of inhomogeneous $CoSi_2$ layer with Ti-rich surface layer ; Ti increases $CoSi_2$ nucleation temp ; stable epitaxial $CoSi_2$, ternary Co-Ti-Si compound as diffusion barrier ; Ti thickness determines cap formed and epitaxial quality
	N_2	(100), (111)	18,53,54,55, 56	TEM shows intermediate CoSi phase ; raises nucleation temp, Ti better than Hf ; thin TiN cap forms
	N_2 +O_2	(100)	58	Oxygen needed in N_2 to form stable Co-Ti-O (spinel) barrier ; single crystal epitaxial $CoSi_2$; anneal in vacuum leads to polycrystalline $CoSi_2$
	N_2, N_2+H_2, He+H_2	(100), (111)	14,45,46	Reactive ambient Ti bound near surface as oxide or nitride on top epitaxial $CoSi_2$ layer
	vacuum	Poly	19,34,59,60	$CoSi_2$ in single step, thermally unstable; Si-pile-up at poly-Si surface, unlike Hf
	NH_3	(100)	18,19,57	Layer reversal to form epitaxial $CoSi_2$ with TiN on top
Si/Ti/Co/Ti_{cap}	vacuum	(100)	19,24,49,60, 61,62,63	Improved stability and uniformity of $CoSi_2$ due to reduced surface and interface diffusion during anneal
Si/Ti/Co/TiN_{cap}	N_2		19,49,60	TiN cap increases uniformity and stability due to reduced surface and interface diffusion during anneal
Si/$TiSi_x$/Co	vacuum	(100)	99	Epitaxial $CoSi_2$
Si/Ti/a-Si/Co	vacuum	(100)	100,101	Epitaxy improved by adding a-Si, because form multi-element barrier
Si/V/Co	vacuum		92	Complete layer reversal
Si/W/Co	vacuum		90	Form CoSi at 450°C ; 2nd anneal at 750°C forms $CoSi_2$
Si/Zr/Co	vacuum	(100), (111), a-Si	96,97,98	Formation temp on a-Si lower; interface more uniform ; $CoSi_2$ forms on Si and a-Si above 600°C
Si/ZrN/Co	NH_3	(100)	96	Deposited as Co-Zr alloy. Below 600°C oxide layer retards formation of $CoSi_2$; above 600°C two reactions (i) $CoSi_2$ forms at substrate interface and (ii) ZrN diffusion barrier

It is also a well known fact **[2,48]** that temperature hardly has any effect on the thermodynamics of solid state interaction. Forcing interaction at a higher temperature by using a barrier interlayer therefore does not give a thermodynamic reason why the Co_2Si and CoSi phases are skipped.

It has been proposed that the Co flux is controlled by the barrier layer, thereby leading to direct $CoSi_2$ formation. It was, however, only after formulation of the effective heat of formation model **[1-3,51]** that a thermodynamic explanation could be given. Pretorius and Mayer **[2]** used this model to define the concept of concentration controlled phase selection – CCPS. The CCPS approach is not only applicable to silicide formation, but should in general enable materials scientists to form phases with

desirable properties by controlling the concentrations of the reactants at the growth interface **[2,48,52].** Deposition rate and substrate temperature seems to be crucial in determining epitaxy, which seems to be better with low deposition rates (~ 0.1Å /s) and high substrate temperatures (600°C) **[48].** However, the growth of inhomogeneous $CoSi_2$ through a Ti barrier has also been reported **[21-23],** and in non-reactive ambient at high temperature the formed $CoSi_2$ and the Ti has been found to react further to form $Co_{0.25}Ti_{0.75}Si_2$ and $CoSi_2$ **[50].**

Epitaxial single crystal $CoSi_2$ with a thin TiN layer on top has been formed for both Si(100) and Si(111) substrates using a Ti interlayer in a nitrogen ambient **[18,53-56]** or on Si(100) in a NH_3 ambient **[19,57].** The addition of oxygen to the N_2 ambient **[58]** showed the formation of a stable Co-Ti-O (spinel) membrane acting as diffusion barrier. Other reactive ambients (N_2, N_2+H_2 or He+H_2) also bound the Ti near the surface in an oxide or nitride layer **[14,45,46]** on top of an epitaxial $CoSi_2$ layer. Research done on poly-crystalline Si substrates using a Ti barrier layer reported that thermally unstable $CoSi_2$ has been formed in a single step **[19,34,59,60].** The use of a Ti capping layer in vacuum **[19,24,49,60-63];** the use of Ti/Co multilayers **[61,62]**; as well as the use of a TiN cap in an N_2 ambient **[19,49,60]**, was found to increase the uniformity and stability of $CoSi_2$ on crystalline Si substrates.

2.2.2 Oxide barrier layers

It has been shown **[13,15-17,20,44,64-71]** that a SiO_x (Shiraki oxide) interlayer can also be used successfully on Si(100) as a diffusion barrier for $CoSi_2$ epitaxy instead of titanium. This approach is usually referred to as oxide mediated epitaxy (OME) and has also been used on Si (111), (110), (211) and (511) surfaces **[17,20,70]** to form thicker, excellent quality, epitaxial, single crystal $CoSi_2$ films at elevated temperatures.

The $Si/SiO_x/Co$ system has also been used with different metallic capping layers i.e. Cr, Mo, Zr **[13],** as well as Ti **[13,40,65,72-76]** and it was found that the cap eliminates the sensitivity of $CoSi_2$ formation to O_2 contamination. An amorphous TiCo layer that controls diffusion **[13]** was reported to form at 450°C leading to the formation of uniform epitaxial $CoSi_2$. When an ambient forming gas **[77]** was used with the capped OME system it resulted in the formation of epitaxial $CoSi_2$ with a capping layer on top, which could easily be removed by wet chemicals.

As both Ti and SiO_x interlayers delivered such excellent results as diffusion barriers for the Si/Co system, a combination of the two has also been researched **[40,78,79]** yielding the self-aligned formation of uniform epitaxial $CoSi_2$.

The process of using different interposed layers [mostly metallic] as diffusion barriers in order to expedite the formation of epitaxial silicides is in general referred to as interlayer mediated epitaxy – IME. Except for Ti (used in TIME), the other metals most researched as barriers to promote uniform $CoSi_2$ formation have been Ta, Hf, Nb, W, Cr, Mo, Ge, Ni and Zr (see **Table 2.1**).

2.2.3 Ta barrier layers

Tantalum has been used as a barrier on both Si(100) and Si(111) substrates and annealing in vacuum **[80,81]** initially forms Co_2Ta, which is then followed by CoSi forming at 700°C, and finally $CoSi_2$ forms with $TaSi_2$ on top. All phase formations occur at higher temperatures on Si(111) than on Si(100) and at higher temperatures than for the binary Si/Co system.

Annealing the Si(100)/Ta/Co system in NH_3 **[82,83]** showed the formation of an intermediate Ta layer having 2 functions, i.e. to reduce native oxide and also to limit the flow of Co atoms to the Si surface and this made it possible to form epitaxial $CoSi_2$ even at the early stage of annealing. When N_2 was used as ambient **[84]** for the same system, epitaxial $CoSi_2$ grains started forming at 600°C and $CoSi_2$ epitaxiality improved at higher temperatures, but at 900°C Ta lost its barrier function, due to $TaSi_2$ formation.

Similar results were obtained by using Co-Ta alloys on Si(100) and poly-Si substrates in N_2 ambient **[85,86],** except that CoSi formed first. The $CoSi_2$ that formed on poly-Si from the deposition of a Co-Ta alloy was found to maintain low sheet resistance up to 950°C. It seems as if the mere presence of Ta, whether deposited as an interlayer or an alloy, has a beneficial effect on the formation of cobalt silicides.

A slightly different study on the effect of the presence of Ta on cobalt diffusion mechanisms was done using the $Si/Co/Ta/Co_{cap}$ system **[87]** and it was found that the formation temperature for $CoSi_2$ depends upon the thickness of the Ta layer. After only 30 min at 650°C nearly all the Co above and below a 30 Å Ta barrier had converted to $CoSi_2$.

2.2.4 Hf barrier layers

It has been reported that Hf forms a stable reaction barrier for Co diffusion on Si(100) and a complex phase sequence leads to the formation of both epitaxial and non-epitaxial $CoSi_2$ **[25,33-36,88].** This result differs from the use of a Ti barrier, in which case only epitaxial $CoSi_2$ formed. TEM studies using an Hf interlayer in a N_2 ambient **[53]** show the presence of an intermediate CoSi phase that raises the $CoSi_2$ nucleation temperature, but not as much as a Ti barrier would.

Studies were done to compare the use of a Hf interlayer on Si(100) and poly-Si **[34,89]** and it was found that the CoSi - $CoSi_2$ phase transition temperature was lower on poly-Si than on Si(100) and there was no Si pile-up at the poly-Si surface, as had been found in the case of a Ti barrier.

2.2.5 Other barrier layers

The use of a Nb interlayer **[33,35,36]** has not proven very useful for promoting epitaxiality, as only non-epitaxial $CoSi_2$ formed. A W barrier **[90]** reportedly forms CoSi at 450°C but $CoSi_2$ only forms after a second anneal at 750°C. Using either Mo **[91]** or Cr **[91,92]** interlayers three different regimes were reported, depending upon the thickness of the interlayer – for thin layers CoSi formed first, for thicker layers $CoSi_2$ formed first and for thick layers, $MoSi_2$ (or $CrSi_2$) formed first and then only did $CoSi_2$ form. Epitaxial $CoSi_2$ nucleates at higher temperatures with the use of Fe **[93]** or Ge **[93,94]** barriers, while Ni **[93]** lowers the nucleation temperature. When Ge is used as a barrier on Si(111), buried B-type epitaxial $CoSi_2$ forms at 460°C **[95]** and the use of a V/Co bilayer **[92]** leads to complete layer reversal.

Comparative studies using Zr as an interlayer **[96-98]** on Si(100), Si(111) and amorphous Si substrates, showed that the formation temperature of crystalline $CoSi_2$ was lower and the interface was more uniform on a-Si, but the sheet resistance was lower on crystalline Si at high temperatures. When this Si(100)/Zr/Co system was annealed in NH_3 ambient atmosphere at temperatures above 600°C, two reactions occurred simultaneously: (i) $CoSi_2$ formation at the substrate interface and (ii) the formation of ZrN **[96]** which stops diffusion of Si to the surface.

A $TiSi_x$ interlayer **[99]**; a Ti/a-Si double interlayer **[100,101]**; a C interlayer **[102] ,** as well as a CoC interlayer **[103]** have also been used to try and enhance $CoSi_2$ formation and these met with varying degrees of success.

2.3 Nickel Silicides

Although less researched than cobalt-silicide formation, the formation of nickel silicides through diffusion barriers has received a lot of research attention.

NiSi has, due to its very low resistivity, become a promising candidate as contact material in ultra large scale integrated circuits **[104-106].** Unlike $TiSi_2$ (C54), currently the most widely used contact material, the sheet resistance of NiSi remains unchanged even for line widths down to 0.1μm **[41,107].** An added advantage of NiSi when compared to $TiSi_2$ and $CoSi_2$, is the relatively low consumption of silicon, making it very suitable for shallow junction applications.

However, the phase transition from NiSi to high resistivity $NiSi_2$ at temperatures greater than 750°C poses a serious problem. Fortunately the thermal stability of NiSi has recently been significantly improved by the addition of platinum barrier interlayers.

2.3.1 Pt barrier layers

Pt diffusion barrier layers was introduced either as a $Ni_{0.95}Pt_{0.05}$ alloy **[108],** or by using Ni/Pt bi-layers on Si(100) substrates **[109-111]** and from **Table 2.2** it is clear that most research done on Ni-silicide formation has, in fact, utilized Pt interlayers. The enhanced thermal stability of NiSi up to temperatures of nearly 900°C is ascribed **[108-111]** to formation of highly textured Ni(Pt)Si films significantly lowering the interfacial energy and therefore also lowering the free energy change, ΔG, for the reaction $NiSi + Si \rightarrow NiSi_2$. When the Ni-Pt alloy was used on Si(111) substrates, Ni_2Si formed first and then NiSi only formed when all the Ni had reacted, indicating that the Pt never reached high enough concentration to inhibit Ni_2Si growth **[108-110, 112-114].** The thermal stability of the NiSi was found to be greater on Si(111) than on Si(100) **[110].**

2.3.2 Pd barrier layers

Palladium interlayers **[114,115]** have been used to retard the formation of Ni_2Si and subsequently delay the formation of NiSi. In this case it was found that a thin Pd_2Si layer, formed at low temperatures, acted as the diffusion barrier. The thermal stability of NiSi can also be improved by using Pd interlayers, but Pt has a greater effect **[114].**

Table 2. 2. Review of Ni-silicide formation through diffusion barrier layers.

NICKEL SILICIDES				
SYSTEM	**AMBIENT**	**TYPE Si**	**REFERENCES**	**RESULTS**
Si/Co/Ni	vacuum	(100)	121,122,123	Co-Ni co-deposited Ni_2Si, $NiSi_2$ and $CoSi_2$ formed ; NiSi films with low sheet resistance and significantly improved thermal stability; in thin bilayer $CoSi_2$ and $NiSi_2$ form, but in thick NiSi forms as well
Si/Ir/Ni	vacuum		121	Improved thermal stability of $NiSi_2$
Si/Mo/Ni	vacuum		124	NiSi lower sheet resistance, at 700°C NiSi transformed into $NiSi_2$ and $MoSi_2$ forms
Si/NiZr/Ni	vacuum		116	Diffusion of Ni at 350°C through NiZr leads to formation of epitaxial $NiSi_2$
	O_2		116	Forms $NiSi_2$ /ZrO_2 on Si substrate
Si/Pd/Ni	vacuum		114,115	Thicker Pd layers increased temp of complete formation of NiSi and Ni_2Si Enhanced thermal stability for NiSi films
Si/Pt/Ni	vacuum	(100)	108,109,110, 111	Improved thermal stability ; Pt increases $NiSi_2$ nucleation temp to 900°C – more stable NiSi at higher temps
	vacuum	(111)	108,109,110, 112,113,114	Ni-Pt alloy-first form Ni_2Si-then NiSi - this Pt not barrier ; NiSi at 640°C ; thermal stab of NiSi on (111) greater than on (100) ; increased activation energy for $NiSi_2$
Si/SiO_x/Ni	vacuum		125	SIMOX- separation-by-implantation-of-oxygen – leads to uniform $NiSi_2$ on SiO_2/Si (no layer reversal)
SI/Ti/Ni	vacuum	(111)	117	Preferential growth of epitaxial $NiSi_2$ at 475°C and at 500°C orthorhombic NiSi ; TEM shows amorphous interlayer
	N_2(10%H_2)	(100)	118	Growth of Ni_2Si at 400°C and NiSi at 500°C depends on barrier formed during annealing
Si/Ti/Ni/Ag_{cap}	Forming gas	(111)	119	Preferential growth of epitaxial $NiSi_2$ at 450°C – at 500°C orthorhombic NiSi ; TEM shows amorphous interlayer

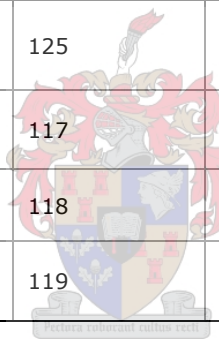

2.3.3 Zr barrier layers

Zirconium was one of the first metals used successfully as a diffusion barrier for the Ni-Si system in the form of an amorphous NiZr interlayer. High resistivity epitaxial $NiSi_2$ was found to form first **[116]** at 350°C and in an O_2 ambient a ZrO_2 layer formed on top of the $NiSi_2$, indicating complete layer reversal.

2.3.4 Ti barrier layers

As Ti barriers had been used with such success to enhance Co-silicide formation, Ti has also been researched **[117,118]** as a diffusion barrier for nickel silicide formation. On Si(111) the use of a Ti barrier under vacuum conditions resulted in the formation of $NiSi_2$ as first phase **[117]** at 450°C. TEM studies showed that in this instance an amorphous interlayer was acting as diffusion barrier. On Si(100) substrates in a N_2(10%H_2) ambient **[118],** the Ti barrier resulted in the growth of

Ni_2Si at 400°C and NiSi at 500°C. It seems that the diffusion barrier that forms during annealing determines the specific silicide that results. This diffusion barrier, in turn, depends upon **[118]** the interlayer, type of Si substrate, temperature and specific annealing conditions, like ambient atmosphere. The same group found that the Si(111)/Ti/Ni/Ag_{cap} system under forming gas atmosphere **[119]** forms epitaxial $NiSi_2$ at 450°C and orthorhombic NiSi at 500°C.

2.3.5 Other metallic barrier layers

The metals Cr, Co, Ir, and Mo have also been used in IME for the Si/Ni system (see **Table 2.2**). Nickel-monosilicide formed as first phase **[120]** by utilizing the presence of a segregated Cr-rich amorphous interlayer after thermal processing of samples formed by sputter-deposited Ni80Cr20 alloy films on Si substrates. The use of Co or Ir barrier-layers on Si(100) substrates **[121]** has lead to the formation of NiSi films with low sheet resistance and significantly improved thermal stability. Ultra-thin Co/Ni bilayers on Si(100) formed $CoSi_2$ and $NiSi_2$ **[122],** but thicker layers formed NiSi as well. In another study $CoSi_2$, Ni_2Si, and $NiSi_2$ nano-crystalline regions **[123]** were identified by HRTEM in Co/Ni films co-deposited on Si(100) by Pulsed Laser Deposition. NiSi with lowered sheet resistance has also been formed by using a Mo interlayer **[124].**

2.3.6 Oxide barrier layers

Crystalline $NiSi_2$ thin films have been formed on SIMOX (separation by implantation of oxygen) Si-on-oxide substrates **[125]** in which case the oxide layer acted as diffusion barrier.

2.4 Titanium Silicides

As mentioned earlier, the studies of the formation of the silicides of cobalt, nickel and titanium are important because of their low resistivity, uniformity and good thermal stability. The silicide of Ti which usually forms first in the binary Si/Ti system is C49 $TiSi_2$. The C54 $TiSi_2$ phase, which has the lowest resistivity, only forms at about 750°C. Furthermore, as the relatively large lattice mismatch of $TiSi_2$ with silicon makes epitaxy difficult to achieve, quite a lot of research has been done trying to find metallic barrier interlayers that would either cause the C54 phase to form as first phase,

lower the C49 - C54 phase transition temperature significantly, improve the thermal stability and/or lower the sheet resistance of the disilicide. The metals which have been most researched as diffusion barrier interlayers for Ti-silicide formation are Mo, Ta and Ti and of these, Mo has received most attention as can be seen in **Table 2.3.**

2.4.1 Mo barrier layers

Mo interlayers have proven useful in lowering the formation temperature of the C54 $TiSi_2$ phase on Si(100) substrates by 100°C **[126-129].** The pathway for the formation of the C54 $TiSi_2$ phase is altered from the usual C49 – C54 phase transformation to the direct epitaxial growth of the C54 $TiSi_2$ phase at 450°C by the use of a thicker Mo (180 Å) interlayer that forms a C40 $(Ti,Mo)Si_2$ barrier **[130-136].** This direct formation yields a lowered sheet resistance for the C54 $TiSi_2$ and this makes the use of Mo very promising for sub-micron applications. The thermal stability and morphology of $TiSi_2$ is improved by using Mo interlayers and the effects of Mo is the same whether the Mo is deposited or implanted **[134-136].** When the Si/Mo/Ti system is annealed in nitrogen **[135]** instead of He, the formation of a surface layer of TiN competes with the formation of silicides. On poly-Si the use of a Mo interlayer leads to the complete prevention of C49 formation **[137]** and the lowering of the formation temperature of C54 by 75°C **[132].** The impact of Mo on the thermal stability of $TiSi_2$ seems to be complex and depends upon the type of Si substrate used.

2.4.2 Ta barrier layers

The Si(100)/Ta/Ti system has also received a lot of attention. The use of Ta barriers was reported to lower the C49-C54 transition temperature from 830 to 630°C **[138-140],** to retard the agglomeration of $TiSi_2$ and to slightly improve the thermal stability of $TiSi_2$ **[132].** Depending upon the concentration of Ta present, direct formation of C54 has also been reported through the formation of an intermediate template C40 $TaSi_2$ phase **[140,141].** Based on crystallographic considerations, the in-plane lattice mismatch between the basal planes of the hexagonal $TaSi_2$ phase and the (010) planes of the C54 phase is within 0.3% **[142],** a factor of 10 times better than between the basal planes of the hexagonal $(Mo,Ti)Si_2$ phase and the (010) planes of the C54 phase. This offers some explanation for the fact that Ta is even more effective than Mo as a diffusion barrier for the enhanced formation of Ti-silicide. Recently it has

been shown that the formation temperature of C54 $TiSi_2$ has been lowered by 100°C with a Ta interlayer **[143]** due to the formation of a pure C40 $TiSi_2$ precursor phase.

Table 2.3. Review of Ti-silicide formation through diffusion barrier layers.

TITANIUM SILICIDES				
SYSTEM	**AMBIENT**	**TYPE Si**	**REFERENCES**	**RESULTS**
Si/Al/Ti	vacuum		148	Enhances formation of C49 $TiSi_2$ and retards transition from C49 to C54 (formation temp 767°C increases to 853°C)
Si/Mo/Ti	vacuum	(100)	126,127,128, 129,130,131, 132,133,134, 135,136	Enhanced form of C54 due to increased density of nucleation sites ; Temp range for stable C49 is decreased by 80 deg Formation of C54 at 600°C instead of 700°C Effects of Mo same for deposited or implanted into Si
	He,N_2		135	For thick Mo layer C40 (Ti,Mo)Si_2 forms, and this leads to direct forms of C54. Thin Mo no C40 ; anneals in N_2 suppress formation of C54, due to surface TiN
	vacuum	poly	132,137	Complete prevention of C49 formation to form epitaxial C54 $TiSi_2$; impact of Mo on thermal stability of $TiSi_2$ complex and depends upon **type** of Si . Temp for $TiSi_2$ formation is decreased by 75 deg on poly Si
Si/Nb/Ti	vacuum		149	Formation of C40(Nb,Ti)Si_2 on substrate; Phase depends on amount Nb and type of substrate
Si/Ta/Ti	vacuum	(100)	132,138,139, 140,141,142, 143	Change in temp of phase (C49-C54) transition from 830°C to 630°C , Ta retards agglomeration of $TiSi_2$. Using Ta instead of Mo leads to direct formation of C54, without forming C49 first
	vacuum	(111)	144,145,146	Ta remains at interface, the C49-C54 phase transition lowered by 200 deg using 5 Å Ta (550°C instead of 750°C), less surface agglomeration of C54 $TiSi_2$ film
	vacuum	poly	147	Temp for $TiSi_2$ formation is decreased by 75 deg on poly Si by use of Ta barrier
Si/TiW/Ti	vacuum		150	TiW barrier is effective to Si and O_2 out-diffusion as well as the incorporation of ambient gasses
Si/W/Ti	vacuum		126	Formation temp of C54 lowered by 100°C, enhanced formation of C54 due to increased nucleation sites for C49-C54 phase transformation
Si/Zr/Ti	vacuum	(100), amorph	151	Phase transition temp increased with amount of Zr, depending also on type Si substrate

On Si(111) substrates the C49-C54 phase transition temperature is lowered by 200°C **[144-146]** through the use of a 5 Å Ta interlayer. The sheet resistance is also lowered, the C54 phase displays different crystal orientation and there is less surface agglomeration of the C54 $TiSi_2$ film. It is interesting that AES analysis **[145]** indicated that the Ta layer remained at the interface between the formed $TiSi_2$ and the Si(111)

substrate. The temperature for $TiSi_2$ formation on poly-Si is decreased by 75°C by utilizing a Ta interlayer **[147].**

2.4.3 Other barrier layers

Other metals that have been researched as diffusion barriers for Ti-silicide formation are Al, Nb, W and Zr. Aluminium as barrier **[148]** enhances the formation of C49 $TiSi_2$ and retards the transformation of C49 to C54. The use of a Nb interposed layer leads to the formation of C40 $(Nb,Ti)Si_2$ and the silicide phase that forms depends upon the amount of Nb present as well as the type of Si substrate **[149].** The formation temperature of C54 is lowered by 100°C by a W interlayer **[126]** and the formation of C54 $TiSi_2$ is also enhanced by the presence of W due to increased nucleation sites for the C49-C54 phase transformation, whereas a TiW barrier **[150]** is effective to Si and O_2 out-diffusion as well as the incorporation of ambient gases. For the Si/Zr/Ti system the phase transition temperature increases as the amount of Zr increases **[151],** depending on the type of Si substrate used.

2.5 Iron Silicides

The formation of the silicides of iron through diffusion barrier layers has also been researched (see **Table 2.4)**. By analogy to reactive deposition epitaxy and TIME experiments, an attempt was made to restrain the supply of reactants to the reaction interface in the solid phase reaction between Si and Fe. The goal being to change the normal phase formation sequence by using a suitable diffusion barrier, so that the β-$FeSi_2$ phase forms directly.

Table 2.4. Review of Fe-silicide formation through diffusion barrier layers.

IRON SILICIDES				
SYSTEM	**AMBIENT**	**TYPE Si**	**REFERENCES**	**RESULTS**
Si/Fe-Cr/Fe	vacuum	(100)	52	β-$FeSi_2$ forms at 800°C
Si/FeV/Fe	vacuum		152	First phase formation of ε-FeSi, no direct formation of β-$FeSi_2$, layers more smooth
Si/FeZr/Fe	vacuum		152	First phase formation of ε-FeSi, no direct formation of β-$FeSi_2$, Zr barrier fails structurally at high temps
Si/Fe-Ni/Fe	vacuum	(100)	52	β-$FeSi_2$ forms at 800°C
Si/SiO_x/Fe	O_2	(100)	154	With O_2 present Fe main diffusing species (not Si), more O_2 than 2 at% formed FeO and no silicide
Si/Ti/Fe	vacuum	(100)	153	Semi-conducting β-$FeSi_2$ films formed

In a study making use of CCPS **[52],** samples with an evaporated layer of $Fe_{30}M_{70}$ (M = Cr, Ni) were used. For both Cr and Ni it was found that β-$FeSi_2$ forms after annealing for 10 minutes at 800°C. A further 3 hr anneal and a 60 mJ excimer laser anneal forms α-$FeSi_2$, and then after a final 3 hr anneal at 800°C complete reversal to the desired semiconducting β-$FeSi_2$ phase occurs.

Both Fe-V and Fe-Zr barriers **[152]** showed first phase formation of ε-FeSi, but first phase formation of the β-$FeSi_2$ phase was not observed. The Fe-V interlayer did, however, result in smoother layers of β-$FeSi_2$.

Semi-conducting β-$FeSi_2$ films have been formed by using Ti interlayers **[153]** and in an O_2 ambient **[154]** Fe was found to be the main diffusing species during silicide formation and the diffusion barrier in this case was SiO_x , where $1 \leq x \leq 2$.

2.6 Other Metal Silicides

Table 2.5 shows the research done on the formation of the silicides of molybdenum, chromium and tantalum through diffusion barrier interlayers. The formation temperature of $MoSi_2$ was lowered, the rate of Si diffusion enhanced and the hindrance of the natural oxide layer avoided by using Co or Ni interlayers **[155].**

Table 2.5. Review of other metal-silicide formation through diffusion barrier layers.

OTHER METAL SILICIDES				
SYSTEM	**AMBIENT**	**TYPE Si**	**REFERENCES**	**RESULTS**
Si/Co/Mo	vacuum	(100)	155	Formation temp $MoSi_2$ lowered to 500-550°C, rate of Si diffusion enhanced
Si/Ni/Mo	vacuum	(100)	155	Formation temp $MoSi_2$ lowered to 500-550°C, rate of Si diffusion enhanced
Si/Pd_2Si/Cr	vacuum	(100), (111)	156	$CrSi_2$ form by diffusion of Si through barrier
Si/Ti/Ta	vacuum	poly	157, 158	Below 1000 °C 2 phases -$TiSi_2$/$TaSi_2$, above 1000 °C ternary phase (TiTa)Si_2

It has been shown that $CrSi_2$ can be formed on Si(100) and Si(111) substrates by diffusion of Si through a Pd_2Si barrier **[156].** Formation kinetics of $CrSi_2$ on top of the underlying Pd_2Si was found to be much faster for Si(100) substrates as compared to Si(111). This is ascribed to the fact that Pd_2Si forms epitaxially on Si(111).

A $TiSi_2$/$TaSi_2$ bilayer formed when Ti/Ta bilayers were used on poly-Si **[157]**, silicidation of the Si/Ti/Ta system proceeded sequentially, as first Ti and then Ta **[158]** converted to their respective silicides. During the growth of the $TiSi_2$, adsorbed oxygen moved to the Ti/Ta interface and formed SiO_2 which acted as a barrier to Si diffusion.

2.7 Summary

A summary of silicide formation through barrier layers is given in **Table 2.6**.

Table 2. 6. Summarized review of silicide formation through diffusion barrier layers.

SYSTEM	REFERENCES	SYSTEM	REFERENCES
COBALT SILICIDES		**NICKEL SILICIDES**	
Si/C/Co	102	Si/Co/Ni	121,122,123
Si/CoC/Co	103	Si/Ir/Ni	121
Si/Cr/Co	91,92	Si/Mo/Ni	124
Si/Fe/Co	93	Si/NiZr/Ni	116
Si/Ge/Co	93,94,95	Si/Pd/Ni	114,115
Si/Hf/Co	25,33,34,35,36,53,88,89	Si/Pt/Ni	108,109,110,111,112,113,114
Si/Mo/Co	91	Si/SiO_x/Ni	125
Si/Nb/Co	33,35,36	Si/Ti/Ni	117,118
Si/Ni/Co	93	Si/Ti/Ni/Ag_{cap}	119
Si/SiO_x/Co	15,16,17,20,44,64,65,66,67, 68,69,70,71	**TITANIUM SILICIDES**	
Si/SiO_x/Co/Cr_{cap}	13	Si/Al/Ti	148
Si/SiO_x/Co/Mo_{cap}	13	Si/Mo/Ti	126,127,128,129,130,131,132, 133,134,135,136,137
Si/SiO_x/Co/Ti_{cap}	13,40,65,72,73,74,75,76,77	Si/Nb/Ti	149
Si/SiO_x/Co/Zr_{cap}	13	Si/Ta/Ti	132,138,139,140,141,142,143, 144,145,146,147
Si/SiO_x/Ti/Co	40,78,79	Si/TiW/Ti	150
Si/Ta/Co	80,81,82,83,84,85,86	Si/W/Ti	126
Si/Co/Ta/Co_{cap}	87	Si/Zr/Ti	151
Si/Ti/Co	14,18,19,21,22,23,24,25,26, 27,28,29,30,31,32,33,34,35, 36,37,38,39,40,41,42,43,44, 45,46,47,48,49,50,53,54,55, 56,57,58,59,60	**IRON SILICIDES**	
		Si/Fe-Cr/Fe	52
		Si/FeV/Fe	152
Si/Ti/Co/Ti_{cap}	19,24,49,60,61,62,63	Si/FeZr/Fe	152
Si/Ti/Co/TiN_{cap}	19,49,60	Si/Fe-Ni/Fe	52
Si/$TiSi_x$/Co	99	Si/SiO_x/Fe	154
Si/Ti/a-Si/Co	100,101	Si/Ti/Fe	153
Si/V/Co	92	**OTHER SILICIDES**	
Si/W/Co	90	Si/Co/Mo	155
Si/Zr/Co	96,97,98	Si/Ni/Mo	155
Si/ZrN/Co	96	Si/Pd_2Si/Cr	156
		Si/Ti/Ta	157, 158

Pectora roborant cultus recti

Chapter 3

EXPERIMENTAL TECHNIQUES

3.1 Preparation of samples

In this investigation the substrates used were mainly commercial wafers of single crystal Si<100> and in some instances single crystal Si<111> were used. Si wafers offer a firm, clean substrate with a relatively low mass making it favorable for Rutherford Backscattering Spectrometry (RBS) analysis as the deposited metals are all heavier than Si and can therefore be resolved easily.

3.1.1 Silicon substrate preparation

The silicon substrate wafers were cut into 9 mm square samples and the samples were de-greased in an ultrasonic bath with organic solvents using the following sequence during the wash procedure:

- methanol
- acetone
- trichloroethylene
- acetone
- methanol
- nanopure water
- 20 % hydrofluoric acid (HF) solution.

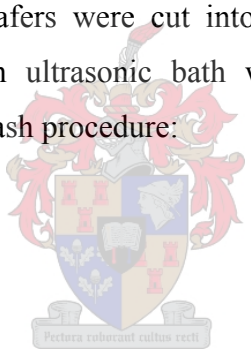

Care was taken to avoid contamination between solvents by including an additional rinse between each pair of solvents. After the washing procedure, the samples were immediately loaded into the ultra high vacuum (UHV) evaporation system to decrease the risk of contamination.

3.1.2 Electron Beam Vacuum Deposition

The different metal layers were then deposited sequentially on the Si-substrate samples by making use of electron beam vacuum deposition. The system was fitted with a rotary roughing pump and a turbo molecular pump that could pump the deposition chamber down to 10^{-5} Torr. A set of six ionization pumps and a liquid nitrogen cold trap were used to take the pressure down to below 10^{-7} Torr. The pressure was kept in the low 10^{-7} range for the duration of the depositions.

Evaporation was accomplished by electron beam melting of the materials in water-cooled copper crucibles. A substrate heater was used for the deposition of $CrSi_2$.

3.1.3 Vacuum annealing

The samples were subsequently annealed in a quartz tube vacuum furnace fitted with a mechanical fore pump, a turbo molecular pump and a liquid nitrogen cold trap. A pressure of 10^{-7} Torr was maintained during annealing. The temperature was controlled by a Eurotherm microprocessor which was part of a feedback system between a thermocouple mounted in the furnace and the furnace power supply. After annealing the samples were left in the vacuum chamber for at least an hour to cool down and vacuum was broken by means of high purity nitrogen to further reduce the possibility of oxidation.

3.2 Characterization of Samples

3.2.1 X-ray Diffraction (XRD)

X-ray diffraction (XRD) is a useful and efficient characterization technique for identifying different compound phases depending on their crystal structure. The incident X-rays are reflected from the different planes in the crystal (see **Fig. 3.1**) and therefore X-rays arriving at the same point from different planes have traveled different distances and this causes a phase shift and a resulting interference **[159].** Constructive interference occurs when the difference in distance traveled is equal to a multiple of a wavelength and is given by the well known Bragg equation:

$$2d\sin\theta = n\lambda \qquad \textbf{3. 1}$$

where d is the interplanar spacing, n the order of the reflection, λ the wavelength and θ the incident angle of the radiation. From this equation constructive interference will occur at a scattering angle of θ for a given interplanar distance and X-ray energy. By varying the incident angle θ and recording the positions of constructive interference it is possible to measure the d-spacing of the crystal planes. A plot of X-ray counts versus θ gives a series of peaks and the position of each peak defines the spacing between a set of planes. The intensity of the peak is determined by the interference of the X-rays reflecting off the other sets of planes in the crystal. A discussion of the identification of silicides by X-ray diffraction is given in **Appendix A**.

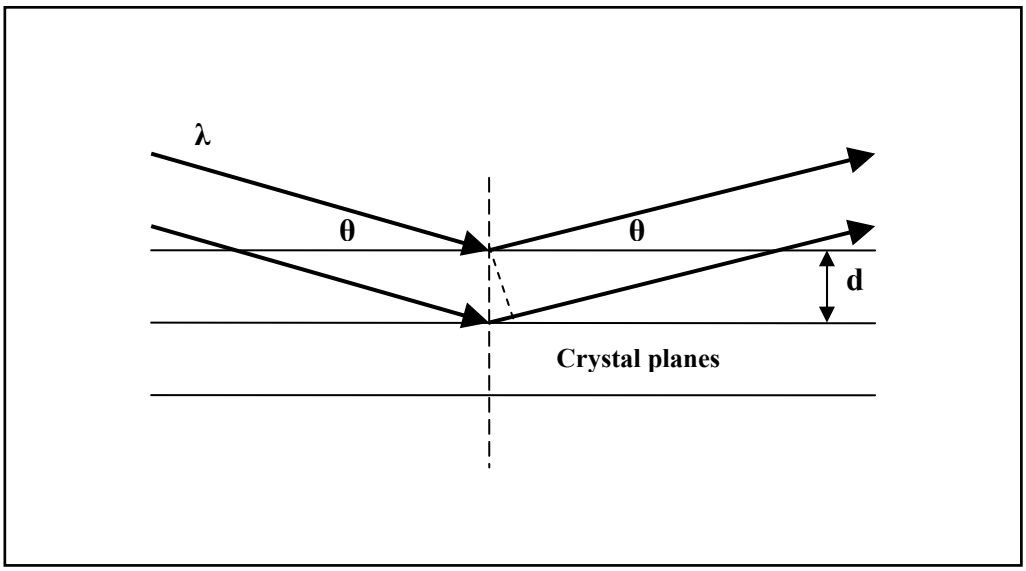

Figure 3. 1. Line diagram of X-rays reflected off crystal planes. Interference between the reflected rays gives rise to the well known Bragg equation. By varying the angle θ and using constructive interference the d -spacing of the crystal planes can be measured.

In this investigation the XRD spectra were obtained by using standard θ-2θ geometry. The sample was rotated horizontally while both the detector and the X-ray tube moved symmetrically through an angle θ. The X-ray yield was plotted as a function of 2θ. The powder diffraction data used for phase identification was from the Internatonal Centre for Diffraction Data (ICDD) CD released in 1998.

3.2.2 Rutherford Backscattering Spectrometry (RBS)

Rutherford Backscattering Spectrometry (RBS) is a very simple, fast and efficient way of characterizing thin films. To obtain an RBS spectrum, the sample is subjected to a beam of mono-energetic charged particles **[160].** In this investigation a 2 MeV He^+ beam (alpha particles) was used. The alpha particle penetrates the solid sample, is attenuated by the potential field in the solid and is then elastically backscattered by the nucleus of an atom in the solid. As it moves out of the solid it loses more energy due to interaction with the solid. The number of elastically backscattered alpha's as well as their energy can be detected by a solid state detector.

The energy of the backscattered alpha particle is proportional to the atomic mass of the atom from which it was scattered. The number of alpha's is proportional to the square of the atomic number of the scattering atom. The energy loss of the alpha as it moves through the solid gives depth information. The three basic concepts in RBS are therefore each responsible for one of its analytic capabilities:

- kinematic factor (mass analysis)
- differential scattering cross-section (quantitative analysis)
- energy loss (depth analysis).

3.2.2.1 The backscattering kinematic factor

When a projectile of mass m, energy E_0 and velocity v_0 collides with a stationary target atom of mass M, there is momentum transfer from the projectile to the target atom (see **Fig. 3.2**).

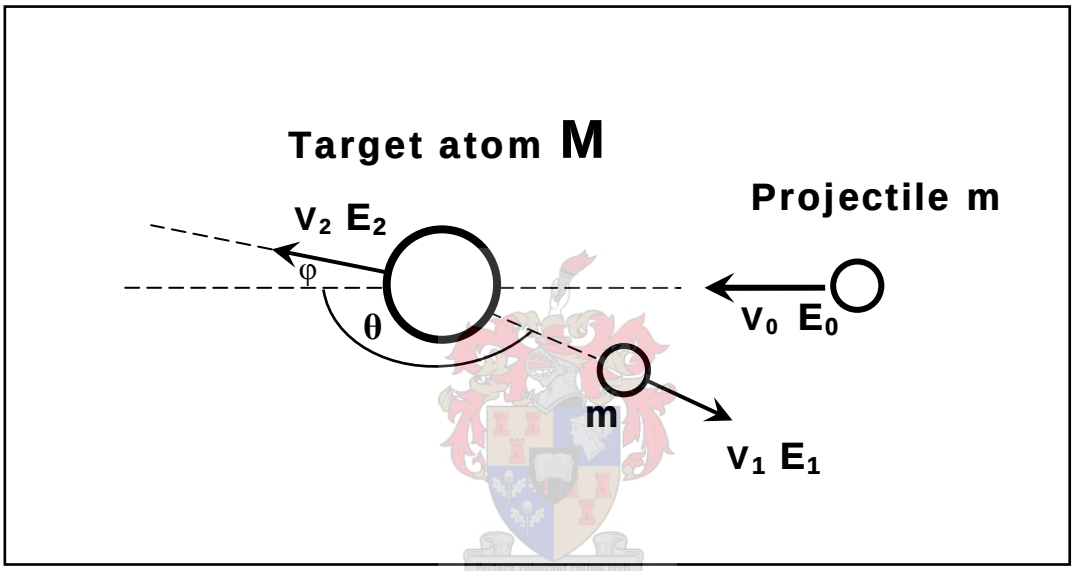

Figure 3.2. Diagrammatic representation of the elastic backscattering of a light projectile atom of mass m off a heavier target atom of mass M.

After the collision the target atom has an energy of E_2 and velocity v_2, while the projectile is scattered with energy E_1 and velocity v_1. The energies of the backscattered projectile and recoil particle can be calculated by using the laws of conservation of energy and momentum. The kinematic factor K is defined **[159,160]** as the ratio between the projectile energy E_1 after collision and E_0 before the elastic collision:

$$K = \frac{E_1}{E_0} \qquad \textbf{3. 2}$$

This factor depends on the scattering angle θ as well as the masses m and M. In a given backscattering experiment m and θ are predetermined and it can be shown that:

$$K = \frac{E_1}{E_0} = \left(\frac{v_1}{v_0}\right)^2 = \left[\frac{m\cos\theta + \left(M^2 - m^2\sin^2\theta\right)^{\frac{1}{2}}}{m+M}\right]^2 \qquad \textbf{3. 3}$$

Therefore, if the energy of the backscattered particle is measured, the mass **M** of the atom from which it was scattered can be calculated and the atom can thus be identified.

3.2.2.2 Differential scattering cross section

The identity of target atoms is established by the energy of the scattered particle after an elastic collision. The number N_s of target atoms per unit area is determined by the probability of a collision between the incident particles and target atoms as measured by the total number Q_D of detected particles for a given number Q of particles incident on the target. The connection between the number of target atoms N_s and detected particles is given by the scattering cross section **[159].** For a thin target of thickness t with N atoms/cm^3, N_s = Nt. The differential scattering cross section $d\sigma/d\Omega$ of a target atom for scattering an incident charged nuclear particle through and angle θ into a differential solid angle dΩ centered about θ is given by

$$\frac{d\sigma}{d\Omega}\cdot d\Omega \cdot N_s = \frac{\text{Number of charged particles scattered onto } d\Omega}{\text{Total number of incident particles}}$$

In backscattering spectrometry, the detector solid angle Ω is small and this leads to the definition of an average differential scattering cross section σ.

This is sometimes called the scattering cross section and is given by

$$\sigma = \frac{1}{\Omega}\int_{\Omega}\frac{d\sigma}{d\Omega}d\Omega \qquad \textbf{3. 4}$$

For very small detector solid angles Ω, it is clear that $\sigma \to d\sigma/d\Omega$.

The differential scattering cross section $d\sigma/d\Omega$ can be given **[160]** as follows:

$$\frac{d\sigma}{d\Omega} = \left(\frac{zZe^2}{4E_0}\right)^2 \frac{4}{\sin^4\theta}\frac{\left\{\cos\theta + \left[1-\left(\frac{m}{M}\right)^2\sin^2\theta\right]^{\frac{1}{2}}\right\}^2}{\left[1-\left(\frac{m}{M}\sin\theta\right)^2\right]^{\frac{1}{2}}} \qquad \textbf{3. 5}$$

where z is the atomic number of the projectile, Z is the atomic number of the target atom, E_0 is the energy of the projectile before scattering, θ the laboratory scattering angle and Ω the finite solid angle spanned by the detector. This definition implies that the solid angle of the detector dΩ is so small that the angle θ is well defined. This would mean that the number of particles measured at an angle θ in a solid angle dΩ would be proportional to the differential scattering cross section.

3.2.2.3 Energy loss

When a projectile penetrates a target, it loses energy throughout its trajectory to the electrons of the target atoms by ionization and excitation as well as by nuclear collisions. Such an elastic collision can change its trajectory into an outward direction (backscattering). By measuring the energy loss of the particle as it moves into the sample and is backscattered onto the detector it is possible to determine the depth to which it has penetrated.

The energy loss **[160]** is normally expressed as a stopping power dE/dx in units of eV/Å. The stopping cross section ε is given by:

$$\varepsilon = \frac{1}{N}\frac{dE}{dx} \qquad \textbf{3. 6}$$

where N is the atomic density of the target. Both stopping power and cross section are dependant on the target composition and incoming beam energy.

Consider an elemental target of atomic mass A and atomic density N. In **Fig. 3.3** the incident energy of the projectile is E_0, the scattered particles have energy KE_0 when scattered from the surface. When a particle is scattered at a depth t and emerges from the target to the detector, it will have lower energy because of the energy loss of the projectile in the target. The incident and scattered angles are θ_1 and θ_2 with respect to the normal of the target and this means that the scattering angle $\theta = 180^\circ - \theta_1 - \theta_2$.

The energy of the projectile at depth t just before scattering is E and can be related to E_0 as follows:

$$E = E_0 - \int_0^{\frac{t}{\cos\theta_1}} \frac{dE}{dx} dx \qquad \textbf{3. 7}$$

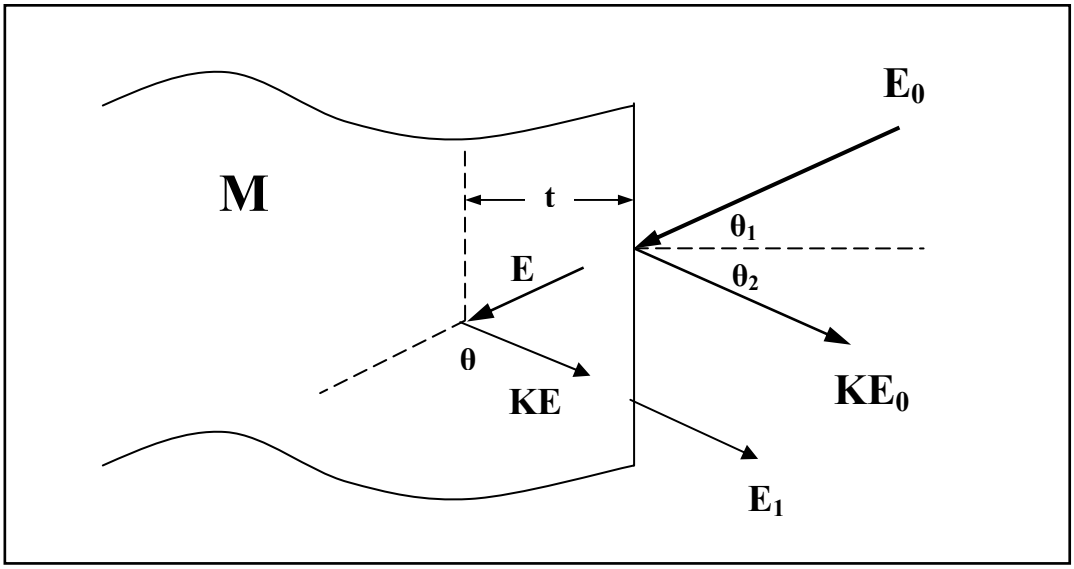

Figure 3. 3. Backscattering geometry to show energy loss.

It is clear from **Eq. 3.7** that the energy loss dE/dx depends on the energy of the projectile and the depth x.

After scattering at depth t the particle will lose energy on its outward path and it will have energy E_1 when emerging from the target, where

$$E_1 = KE - \int_0^{\frac{t}{\cos\theta_2}} \frac{dE}{dx} dx \qquad \textbf{3. 8}$$

The energy difference ΔE, between the particles scattered from atoms on the surface and those scattered at a certain depth t, can be defined from the spectrum in **Fig. 3.3** as follows:

$$\Delta E = KE_0 - E_1 \qquad \textbf{3. 9}$$

and when **Eq. 3.7** is substituted into **Eq. 3.8**, equation **Eq. 3.9** becomes:

$$\Delta E = K \int_0^{\frac{t}{\cos\theta_1}} \frac{dE}{dx} dx + \int_0^{\frac{t}{\cos\theta_2}} \frac{dE}{dx} dx \qquad \textbf{3. 10}$$

In general though, for small variations in energy, the stopping power dE/dx does not change much and energy loss ΔE can be expressed as:

$$\Delta E = [S]t \qquad \textbf{3. 11}$$

where [S] is the backscattering energy loss factor and it changes slowly as a function of E and depth t. For thin films the relative change in energy along the path of the

particle is small. In this case the surface energy approximation can be used and this means that $(dE/dx)_{in}$ is evaluated at E_0 and $(dE/dx)_{out}$ is evaluated at KE_0.

Thus from **Eq. 3.10** the energy loss of the projectile of mass m which was backscattered by an atom of mass M at depth Δt can be approximated **[160]** by:

$$\Delta E = [S]\Delta t = \left(\frac{K}{\cos\theta_1} \frac{dE}{dx}\bigg|_{E_0} + \frac{1}{\cos\theta_2} \frac{dE}{dx}\bigg|_{kE_0} \right) \Delta t \qquad \textbf{3. 12}$$

where θ_1 and θ_2 are the angles of the incoming and outgoing particle with respect to the normal.

The backscattering energy loss factor [S] at the surface can be defined from **Eq. 3.11** and **Eq. 3.12** as:

$$[S] = \frac{K}{\cos\theta_1} \frac{dE}{dx}\bigg|_{E_0} + \frac{1}{\cos\theta_2} \frac{dE}{dx}\bigg|_{kE_0} \qquad \textbf{3. 13}$$

For normal incidence, i.e. $\theta_1 = 0$ and $\theta_2 = 2\pi - \theta$, [S] then becomes:

$$[S] = K\frac{dE}{dx}\bigg|_{E_0} + \frac{1}{|\cos\theta|} \frac{dE}{dx}\bigg|_{kE_0} \qquad \textbf{3. 14}$$

3.2.2.4 Backscattering from compound targets

In a compound sample there will always be more than one element present. For instance consider a compound consisting of two elements A and B. The projectile scatters off only one atom and therefore only one of the elements is the target, but the stopping power of the material is however affected by both the elements in the sample. The energy loss of the particle backscattered off element A at a depth Δt in a compound A_mB_n using the surface energy approximation is given by:

$$\Delta E = [S]_A \Delta t = \left(\frac{K_A}{\cos\theta_1} \frac{dE}{dx}\bigg|_{E_0} + \frac{1}{\cos\theta_2} \frac{dE}{dx}\bigg|_{kE_0} \right) \Delta t \qquad \textbf{3. 15}$$

where K_A is the backscattering kinematic factor off element A.

Bragg's rule states that $\varepsilon^{A_mB_n} = m\varepsilon^A + n\varepsilon^B$, where ε^A and ε^B are the stopping cross sections of atoms A and B respectively.

The total energy loss **[160]** of the particle in the compound A_mB_n can therefore be given by:

$$\Delta E = [S]^{A_mB_n}\Delta t = \frac{M}{m+M}[S]_A^{A_mB_n} + \frac{n}{M+n}[S]_B^{A_mB_n} \qquad \textbf{3. 16}$$

3.2.2.5 The height of the energy spectrum

The shape and height of a Rutherford backscattering energy spectrum also contains quantitative information. The height H of the energy spectrum gives the number of backscattered particles with energy in a certain energy interval δE and (E + δE) and can be calculated as follows **[160]:**

$$H = n_0\Omega\left(\frac{d\sigma}{d\Omega}\right)N\frac{\delta E}{[S]\cos\theta_1} \qquad \textbf{3. 17}$$

where n_0 is the number of incident particles, Ω the solid angle of the detecting system and N the atomic density, while dσ/dΩ is given by **Eq. 3.5** and [S] is given by **Eq 3.13**.

Using **Eq 3.17** the height of the spectrum peak H_A for element A in the compound A_mB_n will then be:

$$H_A = n_0\Omega\left(\frac{d\sigma}{\Omega}\right)N_A\frac{\delta E}{[S]_{A_mN_n}\cos\theta_1} \qquad \textbf{3. 18}$$

where N_A is the atomic density of the A atoms in the compound A_mB_n.

A similar equation holds for the height H_B of the spectrum peak of element B in the same compound. As N_A and N_B must be proportional to m and n respectively, the height ratio can be given by:

$$\frac{H_A}{H_B} = \frac{\sigma_A}{\sigma_B}\frac{m}{n}\frac{[S]_B^{A_mB_n}}{[S]_A^{A_mB_n}} \qquad \textbf{3. 19}$$

The height ratio of the peaks can be used to ascertain the phase of the compound A_mB_n as it is possible to calculate the ratio m/n.

3.2.2.6 Channeling RBS

The arrangement of atoms in a solid determines the properties of the solid and in single crystals it also determines the magnitude of incident ion-target atom interactions **[159]**. The influence of the crystal lattice on the trajectories of ions penetrating into the crystal is known as channeling – under certain conditions of

incidence the atomic rows and planes form “channels” that steer the incident ions along through the crystal structure. The steering action is effective and can lead to hundredfold reductions in the yield of backscattered particles.

Channeling of incident particles or ions occur when the beam is carefully aligned with a major symmetry direction of a single crystal **[159]**. Channeled particles then can not get close enough to the atomic nuclei of the solid to undergo large angle Rutherford back scattering and thus the scattering from the crystal is drastically reduced, resulting in a marked decrease in the height of the signal from the crystal. Thus, if the channeling RBS spectrum of a sample of a silicide grown on a single crystal Si substrate shows a greatly reduced yield of backscattered ions, indicated by a noticeable decrease in the height of the silicide RBS signal, it means that the silicide formation has been epitaxial, i.e. the silicide has conformed to the exact single crystal lattice structure of the Si substrate. As mentioned in **paragraph 1.3**, epitaxial silicides are usually more uniform, stable and have better electrical properties. Channeling RBS is therefore a valuable technique to indicate the degree of epitaxiality of a silicide.

3.2.2.7 RUMP

To interpret the RBS spectra, do computer simulations and to produce hard copy RBS spectra, extensive use was made of the RUMP RBS data processing and simulation computer package **[161]**. RUMP is a series of FORTRAN subroutines designed for the analysis and simulation of RBS data. It was initially developed at Cornell University in Dr J. W. Mayer’s research group by L.R. Doolittle and M.O. Thompson with assistance from R.C. Cochran.

3.2.3 Dynamic RBS

A normal RBS spectrum gives the instantaneous composition of a compound as a function of depth. In order to obtain information on the phase changes as they occur during the annealing process, a series of RBS spectra needs to be taken and compared. This process is called in-situ real-time RBS or dynamic RBS **[156].** The dynamic RBS system used in this investigation made it possible for one sample to be annealed in the scattering chamber and the RBS data acquired during this one annealing process yielded all information about the growth of the different phases for this particular sample type.

Dynamic RBS was done by using an air cooled copper heating stage mounted into the RBS analysis chamber and mounting the sample onto the front plate of the heating stage with silver paste. Temperature measurements were done by a thermocouple touching the back surface of the front plate. A special detector was used to withstand the high temperatures in the chamber - a surface barrier detector with a thicker Au window that did not allow radiated photons from the sample to enter the active region.

A liquid nitrogen cold trap was used in addition to the standard fore pump and turbo pump to help keep the pressure in the chamber below 10^{-6} Torr. Similar to the normal RBS measurements, a 2 MeV He^{+} beam with a backscattering angle of 165° was used for the dynamic RBS and the sample was also tilted 10° towards the detector. The heating stage was controlled by a Eurotherm processor. RBS spectra were continuously acquired and stored at 10 second intervals, together with the corresponding acquired charge and sample temperature. The spectra were analyzed using the RUMP computer simulation package **[161]. Appendix B** gives some additional information about Dynamic RBS data acquisition.

Chapter 4

Ni-SILICIDE FORMATION THROUGH BARRIER LAYERS

4.1 Introduction

Nickel-silicide phase formation is discussed by considering firstly the nickel-silicon EHF and phase diagrams as shown in **Fig. 4.1**. On the Ni-Si phase diagram there are three congruent compound phases, i.e. NiSi, Ni_2Si and Ni_5Si_2, three non congruent phases, i.e. $NiSi_2$, Ni_3Si_2, and Ni_3Si. The EHF model states that the first phase to form will be the one that has the most negative heat of formation ($\Delta H'$) at the concentration of the liquidus minimum (47 at.% silicon). It can be seen from the EHF diagram in **Fig. 4.1** that at the concentration of the liquidus minimum the formation of Ni_3Si_2 will lead to the biggest free energy change. This is, however, a non congruent phase, which for silicides is difficult to nucleate and is usually skipped **[6,7].** This leaves the two congruent phases Ni_2Si and NiSi which have effective heats of formation of –37.6 and –39.4 kJ(mol.at)$^{-1}$, respectively, at an effective concentration of 47 at.% silicon. If it is kept in mind that thermodynamic data could have errors of up to 10 %, it is clear that from a thermodynamic point of view there is not much to choose between the formation of Ni_2Si and NiSi. Although entropy changes ΔS° are very small during solid state interaction **[10]** and can usually be ignored, this is not so when effective heats of formation are very close to each other, as in this case. Normally the first phase to form is Ni_2Si at about 300°C, followed by NiSi at about 400°C and then $NiSi_2$, which only starts to form at 750°C **[6].**

An example of concentration controlled phase selection (CCPS) in the Ni-Si binary system has been the formation of $NiSi_2$ at temperatures as low as 350°C in the presence of a NiZr diffusion barrier **[116].** In the case of Si<111>|NiZr|Ni structures **[116]**, the NiZr barrier apparently reduces the effective concentration of Ni at the growth interface to a region of less than 33 at.% Ni where $NiSi_2$ has the most negative $\Delta H'$ (see **Fig. 4.1)**.

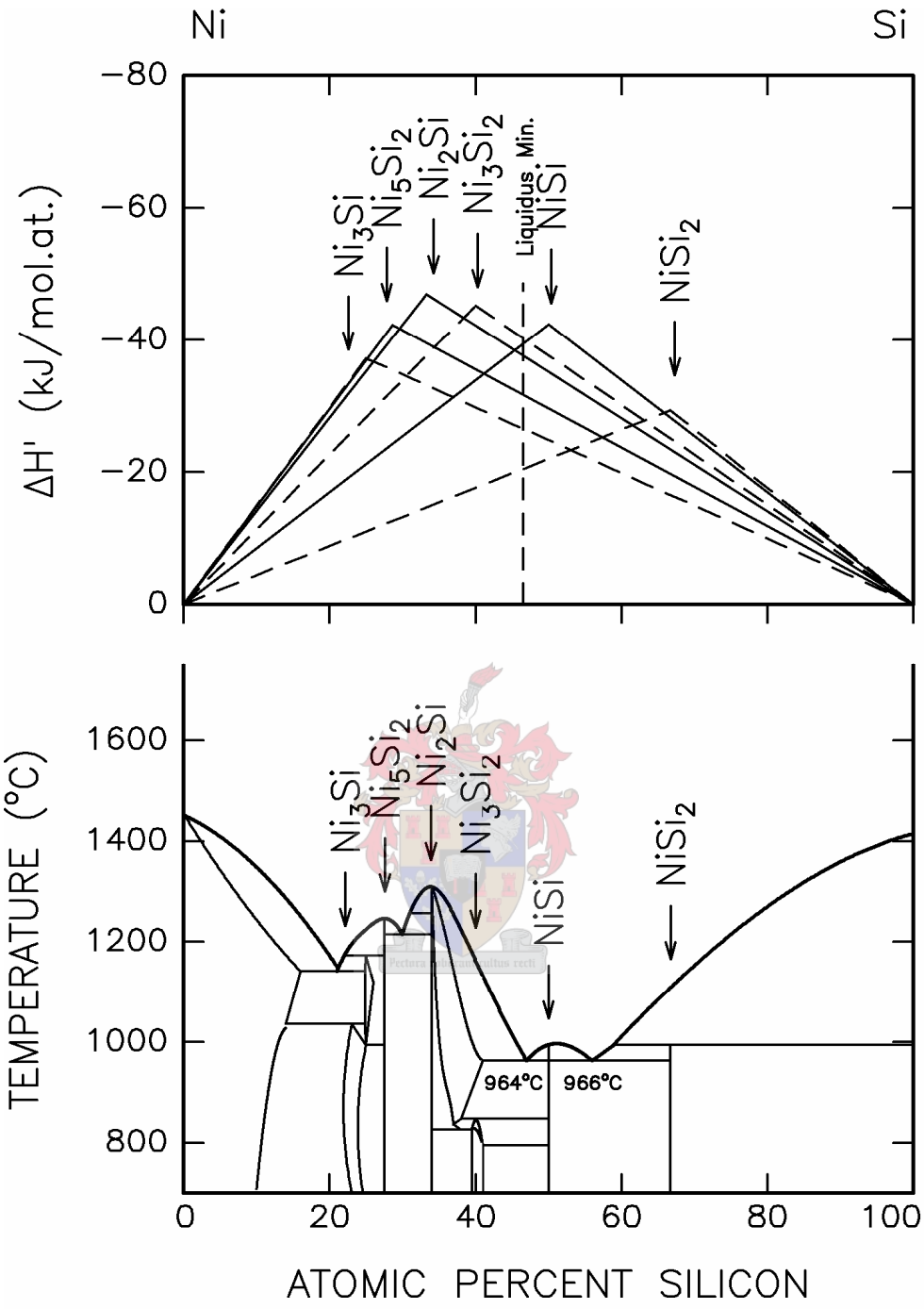

Figure 4. 1. EHF and phase diagram **[10]** of the Ni-Si system. Each triangle of the EHF diagram represents the energy released as a function of concentration during formation of a particular phase. The effective concentration at the interface of a binary system is chosen to be that of the liquidus minimum. Dashed triangles in the EHF diagram show the energy released during formation of the non congruent Ni_3Si, Ni_3Si_2 and $NiSi_2$ phases.

Thermodynamics can be used as follows to explain this seemingly anomalous behavior. In the case of normal $NiSi_2$ formation, NiSi reacts with single crystal silicon to form $NiSi_2$, whereas in Si|NiZr|Ni structures, $NiSi_2$ forms directly as the first

phase. The heats of reaction ΔH°_R for these two cases can be calculated from the ΔH° values as follows **[3]**:

Normal $NiSi_2$ formation (Si|Ni):

NiSi	+	Si	=	$NiSi_2$
2(–42.4)		1(0)		3(–29.3)
ΔH°_R	=	(–3.1)/3	=	-1.0 ± 4.4 kJ $(mol.at)^{-1}$

$NiSi_2$ formation with barrier (Si|NiZr|Ni):

Ni	+	2Si	=	$NiSi_2$
1(0)		2(0)		3(–29.3)
ΔH°_R	=	(–87.9)/3	=	-29.3 ± 2.9 kJ $(mol.at)^{-1}$

It is clear that the heat of reaction for $NiSi_2$ formation from the preceding NiSi phase, without a diffusion barrier, is for all practical purposes equal to zero (taking a 10 % error into account) and only at higher temperatures does the entropy term in the equation $\Delta G^\circ = \Delta H^\circ - T\Delta S^\circ$ make the free energy negative. In the case of $NiSi_2$ first phase formation in Si|NiZr|Ni structures **[116]**, the heat of reaction is seen to be very negative, as there is direct interaction between Ni that diffuses through the barrier and the Si substrate. A high temperature is therefore not needed to make the reaction thermodynamically possible **[2]**. This formation of $NiSi_2$ as first phase instead of the normal Ni_2Si is an excellent example of the successful application of concentration controlled phase selection (CCPS).

In this study of nickel-silicide formation we used three different metallic diffusion barrier interlayers in order to examine their successful application in CCPS, the aim being to possibly form NiSi or even $NiSi_2$ as first phase by controlling the Ni concentration at the growth interface. The metals used were Ta, Cr and Ti and the experimental results will be now be discussed in that order.

4.2 Si <111> | Ta | Ni system

As can be seen from **Table 2.6** in **Chapter 2** no previous research is known to have been done using tantalum as a diffusion barrier in the Si-Ni system. In this study

for investigating the effects of a tantalum diffusion barrier on the formation of nickel-silicides, the following types of samples were prepared:

- 20 Å Ta barrier layer
- 100 Å Ta barrier layer

All anneals were carried out in vacuum at times ranging from 10 to 30 min (sometimes more) and at temperatures ranging from about 350 to 800˚C. For obvious reasons not all of the RBS spectra are shown in this thesis, but only a representative selection is given for each system. On all the RBS spectra shown in this thesis, the vertical arrows on the RBS spectra indicate the surface energy positions of alpha particles scattered from the atoms under discussion. The horizontal lines on some of the RBS spectra indicate the expected height of the Ni signal for Ni-metal, Ni_2Si, NiSi and $NiSi_2$.

4.2.1 20 Å Ta barrier layer

4.2.1.1 RBS results and discussion

RBS spectra of Si<111>|Ta(20Å)|Ni(1100Å) samples that were vacuum annealed at 400, 500, 600, 700 and 800˚C are shown in **Fig. 4.2.**

These RBS measurements showed that, because the Ta interlayer acts as a diffusion barrier between the Si substrate and the Ni, there was still no reaction after 10 min annealing at 400˚C (sample E8 **Fig. 4.2**). After 15 min at 400˚C, however, uniform NiSi was found to form very suddenly as first phase instead of the usual first phase formation of Ni_2Si. The Ta RBS signal had moved to the surface (sample G2), indicating that the Ni atoms diffuse through the Ta barrier interlayer to react with the Si substrate at the growth interface. Annealing for longer times at 400˚C only very slightly improved the uniformity of the NiSi.

Heating for 30 min at 500, 600 or 700˚C (samples E3, E10 and E5 **Fig. 4.2**) also yielded spectra showing uniform NiSi formation. At 700˚C the slight broadening of the Ta signal indicates that the Ta is beginning to diffuse back into the silicide. The formation of $NiSi_2$ is nearly complete after 30 min at 800˚C, but the $NiSi_2$ is not uniform and a small amount of NiSi still remains unreacted. The Ta is not at the surface anymore, but has diffused through the silicide at this temperature.

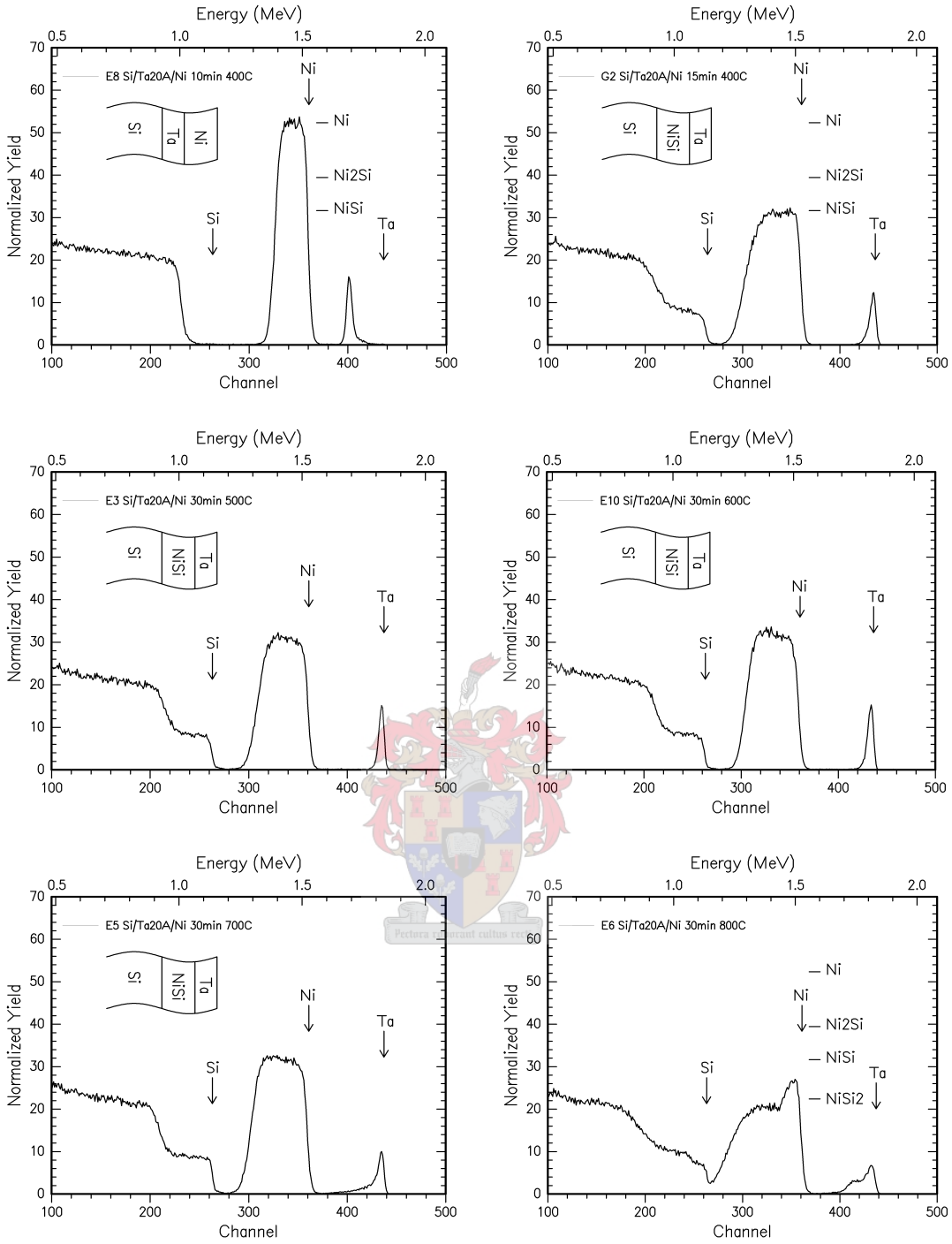

Figure 4. 2. RBS spectra of similar Si<111>|Ta(20Å)|Ni(1100Å) samples annealed at 400, 500, 600, 700 and 800˚C. At 400˚C there was still no reaction after 10 min annealing (sample E8), however after 15 min at 400˚C NiSi was found to form very suddenly as first phase instead of the usual first phase formation of Ni_2Si. Uniform NiSi first phase formation also occurred at 500, 600 and 700˚C. At 800˚C the $NiSi_2$ formation is not yet complete after a 30 min anneal.

4.2.1.2 XRD analysis

The RBS and corresponding XRD spectra of two Si<111>|Ta(20Å)|Ni(1100Å) samples annealed for 10 and 15 min respectively at 400˚C are shown in **Fig. 4.3**. The

sudden phase change, discussed in **paragraph 4.2.1.1**, that occurred between 10 and 15 min at 400˚C is very interesting. From the height of the Ni signal in **Fig. 4.3(b)** it can clearly be seen that NiSi, instead of Ni_2Si, is the first phase to form. This is confirmed by the X-ray diffraction measurements, which show only NiSi peaks. [ICDD: Ni = 04-0850 ; Si = 27-1402 ; NiSi = 38-0844]

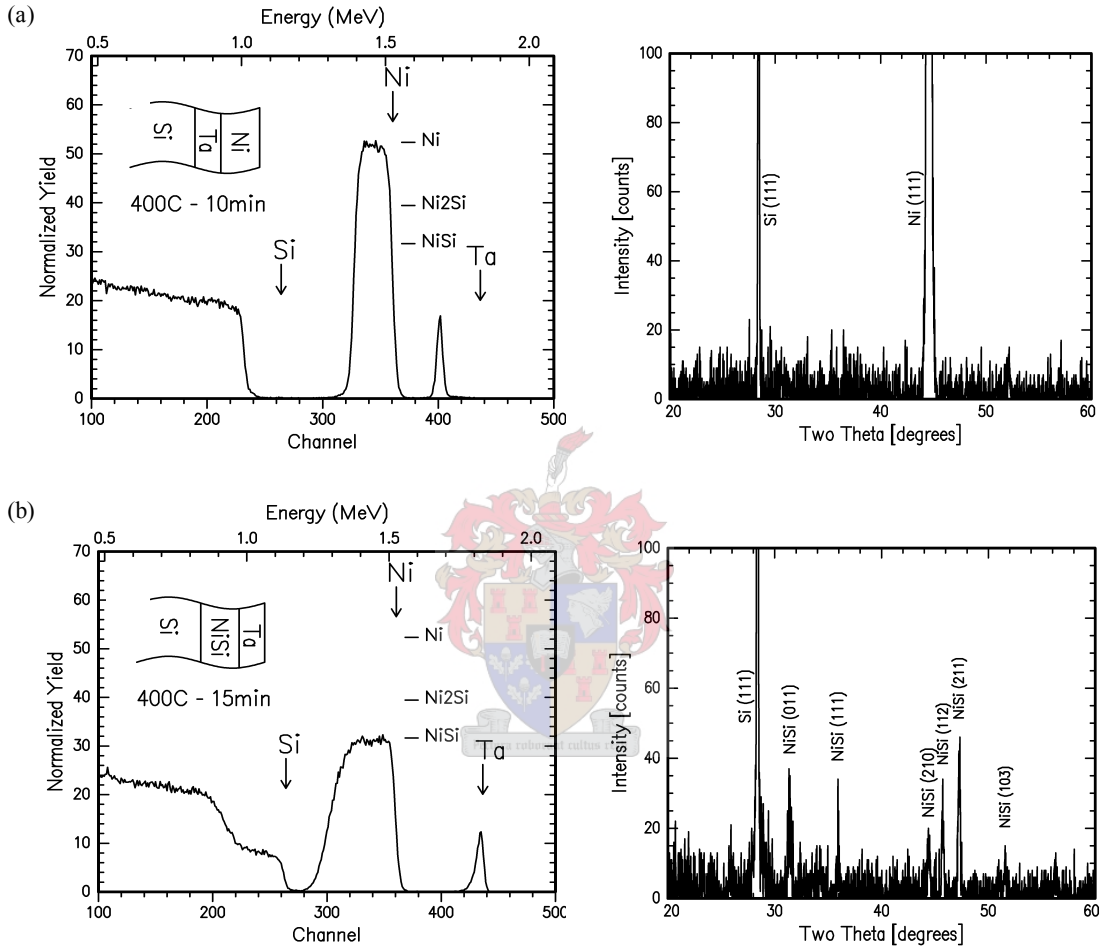

Figure 4. 3. RBS and corresponding XRD spectra of identical Si<111>|Ta(20Å)|Ni(1100Å) samples annealed at 400˚C for (a) 10 minutes and (b) 15 minutes. The XRD spectra confirm the sudden first phase formation of NiSi between 10 and 15 min at 400˚C.

More RBS and corresponding XRD spectra of Si<111>|Ta(20Å)|Ni(1100Å) samples are shown in **Fig. 4.4.** The RBS and XRD spectra of a sample annealed for 30 min at 500˚C confirms the formation of uniform NiSi (sample E3) and the sample heated for 30 min at 600˚C also yielded an RBS spectrum showing uniform NiSi formation. The XRD measurements show only NiSi peaks and it is interesting to note that different NiSi reflections occur at the higher temperatures.

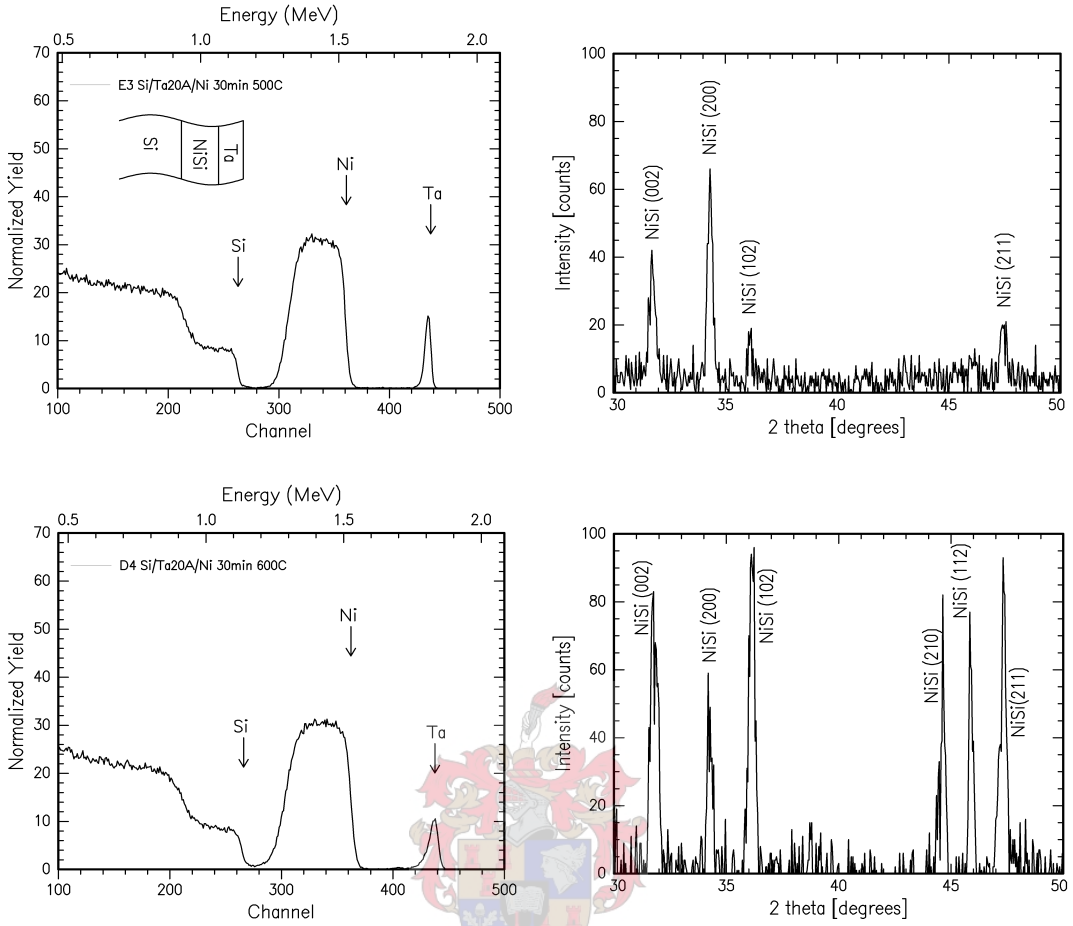

Figure 4. 4. RBS and corresponding XRD spectra of similar Si<111>|Ta(20Å)|Ni(1100Å) samples annealed for 30 minutes at temperatures of 500 and 600˚C. The XRD spectra show only NiSi peaks, indicating uniform formation of NiSi. [ICDD: NiSi = 38-0844].

4.2.1.3 Dynamic RBS measurements

Consider again the two Si|Ta(20Å)|Ni samples shown in **Fig. 4.3** that were annealed for 10 and 15 min at 400˚C. It can be argued that in the period between 10 and 15 minutes, Ni_2Si could have formed first, followed by NiSi. It was therefore decided to carry out dynamic real-time RBS measurements **[156]** during the heating of a similar Si|Ta(20Å)|Ni sample. The temperature of this sample was ramped from 375 to 500˚C at a rate of 2˚C per minute and the resulting dynamic RBS spectrum, that clearly shows the abrupt formation of good quality uniform first phase NiSi, can be seen in **Fig. 4.5**.

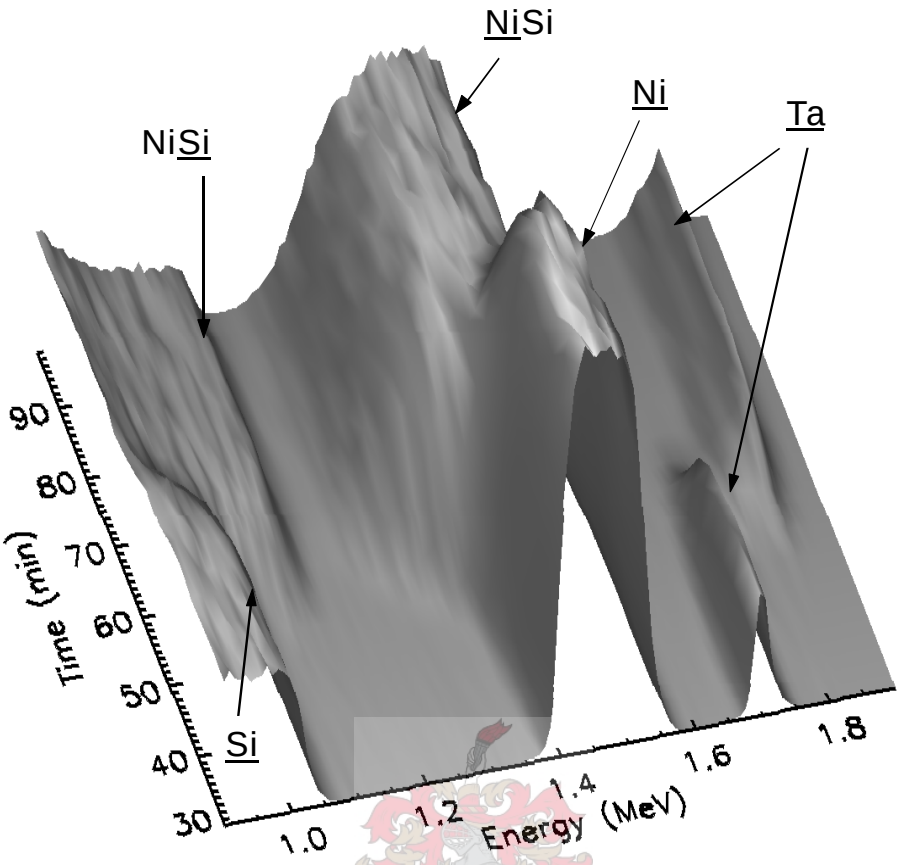

Figure 4. 5. Dynamic RBS spectrum of a Si<111>|Ta(20Å)|Ni(1100Å) sample ramped from 375 to 500˚C at a rate of 2˚C per minute. The abrupt formation of uniform NiSi can clearly be seen, as well as the Ta marker moving to the surface of the sample. The underlined element is that from which backscattering has taken place.

These continuous measurements show without any doubt the abrupt formation of NiSi and therefore skipping of the normal first phase Ni_2Si. At exactly the same time that the NiSi starts to form, the Ta RBS signal moves to the surface of the sample, indicating that the Ni atoms diffuse through the Ta barrier interlayer to directly form NiSi as the first phase. This is direct evidence that the barrier layer reduces the flux (concentration) of the Ni atoms to a value where the effective heat of formation **[3,51]** of NiSi is more negative than that of Ni_2Si. First phase formation of NiSi is thus thermodynamically favoured. This is a good example of concentration controlled phase selection **[2]** and the thin (20Å) Ta diffusion barrier has proven very effective as a diffusion barrier in the Si-Ni system in promoting the growth of uniform first phase NiSi and the skipping of the usual first phase formation of Ni_2Si.

4.2.1.4 Channeling RBS

Fig. 4.6 shows the channeling RBS spectra of a Si|Ta|Ni sample and a Si|Ni sample after two consecutive anneals.

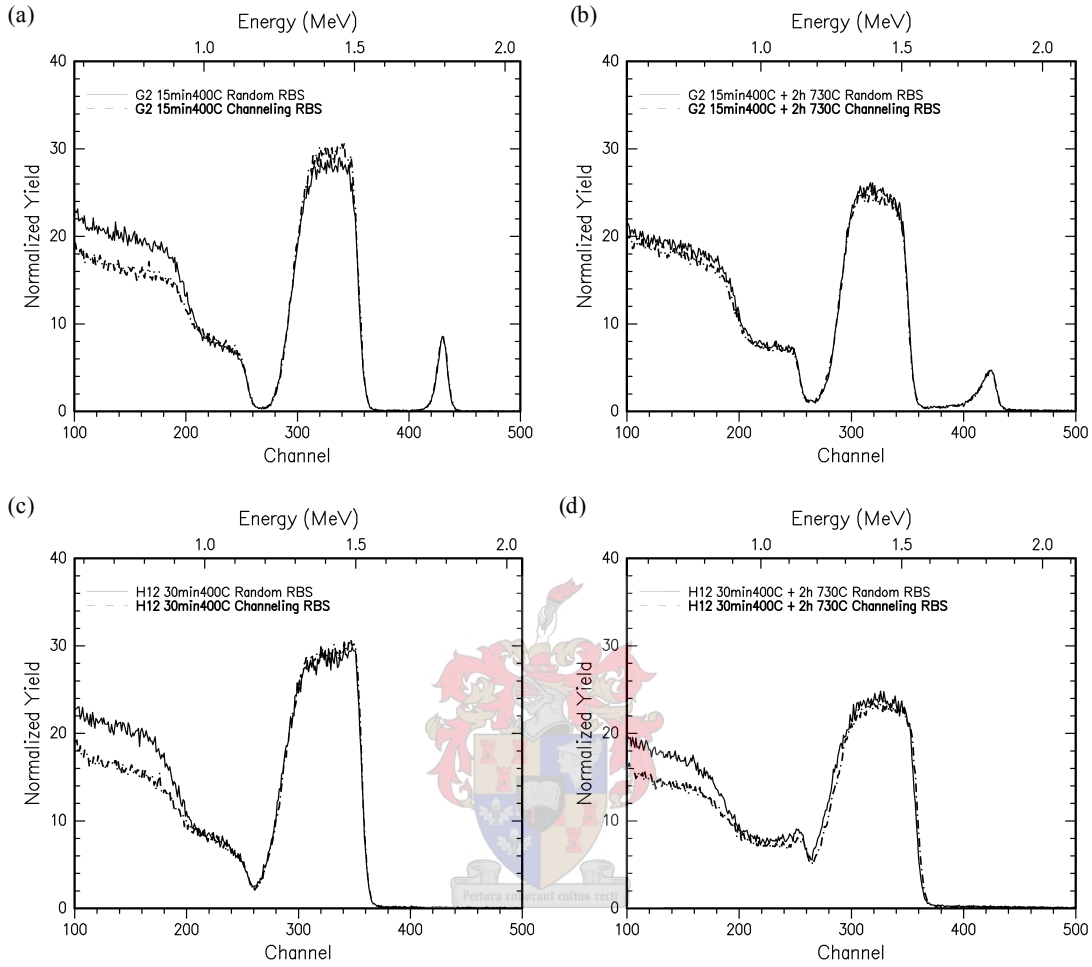

Figure 4. 6. Random and channeling RBS spectra of (a) a Si<111>|Ta(20Å)|Ni(1100Å) sample annealed for 15 min at 400˚C forming first phase NiSi, (b) the same sample annealed for an additional 2 hours at 730˚C, (c) a Si<111>|Ni(1100Å) sample annealed for 30 min at 400˚C forming NiSi in the normal phase sequence and (d) the same sample annealed for an additional 2 hours at 730˚C.

These channeling RBS measurements were done to determine if the uniform first phase NiSi that abruptly formed after heating for 15 min at 400˚C (sample G2 first shown in **Fig 4.2** and above in **Fig 4.6(a)**) is epitaxial. To compare this degree of epitaxy with that of the NiSi formed during the normal phase sequence, channeling RBS was also done on a Si-Ni sample that had no Ta interlayer and was annealed for 30 min at 400˚C (sample H12 **Fig. 4.6(c)**). After this, both samples were annealed for a further 2 hours at 730˚C to try and improve the epitaxy of the NiSi. The temperature was kept below 750˚C to prevent the formation of any $NiSi_2$.

The sample G2 (**Fig. 4.6(a)**) with the 20Å Ta barrier, annealed for 15 min at 400˚C, showed channeling in the Si part of the RBS spectrum, as expected, because of the crystal <111> orientation of the Si substrate. However, no channeling was present in the Ni peak area, indicating that the formed NiSi was not epitaxial. When this sample was reheated for 2 hours at 730˚C (**Fig. 4.6(b)**) there was slight channeling in the Ni part of the spectrum, indicating that the epitaxiality of the NiSi had not really improved. These results indicate that, although the NiSi that formed suddenly as first phase after a 15 min anneal at 400˚C was uniform, it was not epitaxial to any marked degree.

The sample H12 without the Ta barrier (**Fig 4.6(c)**) showed similar results: channeling in the Si part after a 30 min anneal at 400˚C; after an additional 2 h anneal at 730˚C (**Fig. 4.6(d)**) a slight degree of channeling in the NiSi part of the spectrum.

4.2.1.5 Double or split Ta RBS peaks

Some of the samples of the Si|Ta|Ni system that were annealed showed the presence of a "double" or "split" Ta peak on the RBS spectrum and also the sloping shoulders indicative of non-uniform silicide formation. Improving the sample washing procedure prevented double Ta peaks from re-occurring (for the thin (20Å) Ta barrier) and the silicide formation was uniform. **Fig. 4.7** compares the RBS spectra of two similar samples, annealed for 30 min at 500˚C, before and after improved washing.

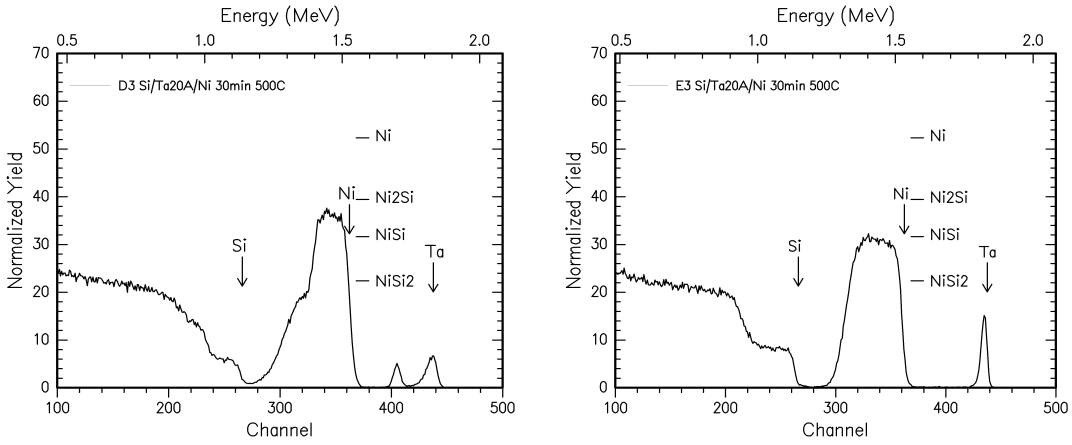

Figure 4. 7. RBS spectra of two similar Si<111>|Ta(20Å)|Ni(1100Å) samples, both annealed for 30 min at 500˚C. The one on the left shows non-uniform silicide formation and two Ta peaks and the one on the right shows uniform NiSi formation and a single Ta peak at the surface position, after an improved sample washing procedure.

The samples that had double Ta peaks also appeared slightly "mottled" or "blotchy" with alternating shiny and dark areas. The shiny areas were thought to be Ni metal remaining unreacted and the darker areas were ascribed to NiSi formation.

It must be mentioned that these double Ta RBS peaks could also perhaps have been caused by "peeling" of the Ni or formed Ni-silicide on the surface, thus exposing part of the remaining interlayer of Ta at the growth interface. However, integration of counts for the Ni and Ta signals in the RBS spectra indicated that no peeling had occurred and so this phenomenon does seem to be due to interface impurity effects that inhibit uniform phase formation.

The RBS spectra showing double (or split) Ta peaks as shown in **Fig. 4.7**, imply the presence of Ta at the surface of the sample and also some Ta at the interface, indicating Ni diffusion through the Ta barrier at certain places leading to NiSi formation and no Ni diffusion at other places and therefore no silicide formed. This situation is represented schematically in **Fig. 4.8**.

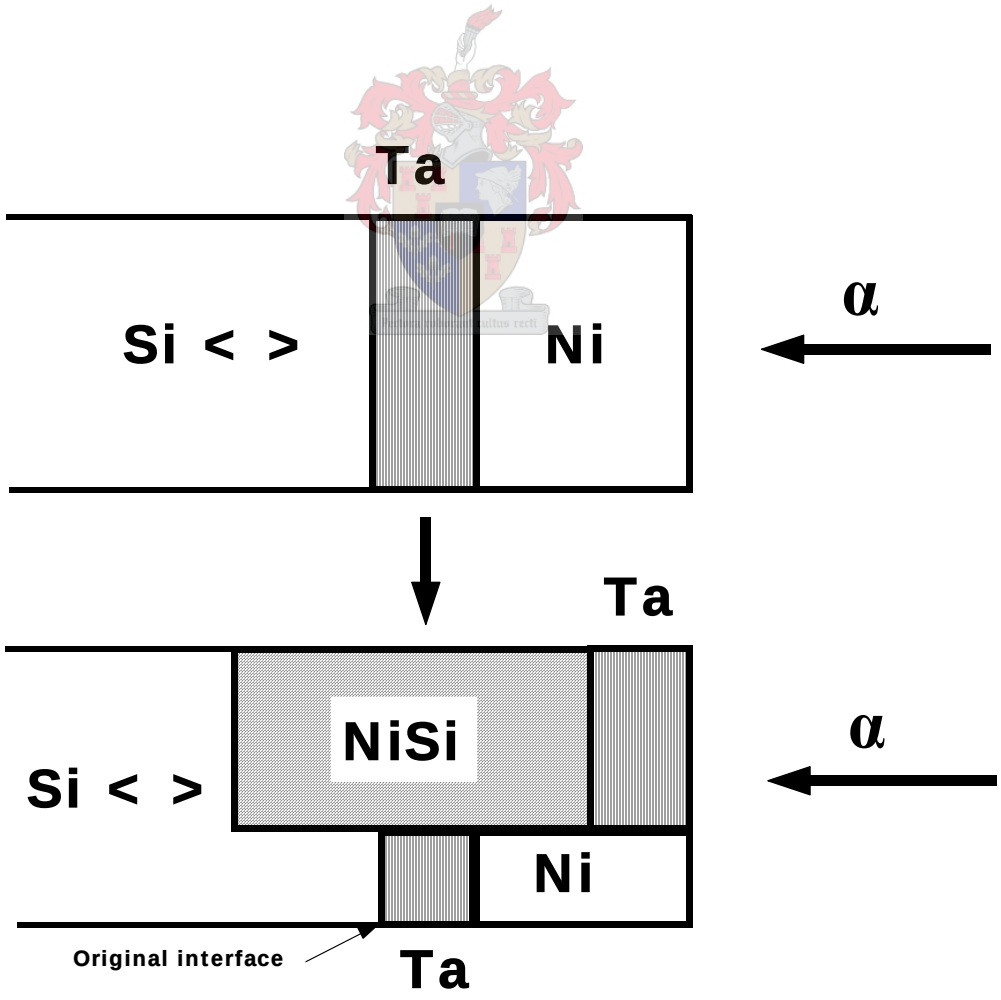

Figure 4. 8. Schematic illustration of a sample showing a double Ta peak on the RBS spectrum.

In **Fig 4.9** the RBS spectrum (of the simulated sample shown in **Fig. 4.8**) showing a double Ta peak is overlaid on the RBS spectrum of the actual sample. It is clear from **Fig. 4.9** that the simulated structure represents the actual sample structure quite well. This implies that the double Ta peak effect did indeed occur because only some of the Ta moved to the surface and thus allowed the Ni diffusion and silicide formation, while the rest of the Ta remained at the interface, preventing the Ni atoms from reaching the Si substrate and preventing any silicide formation from occurring in that area. The RUMP computer program **[161]** used for the simulation is given in **Appendix C.**

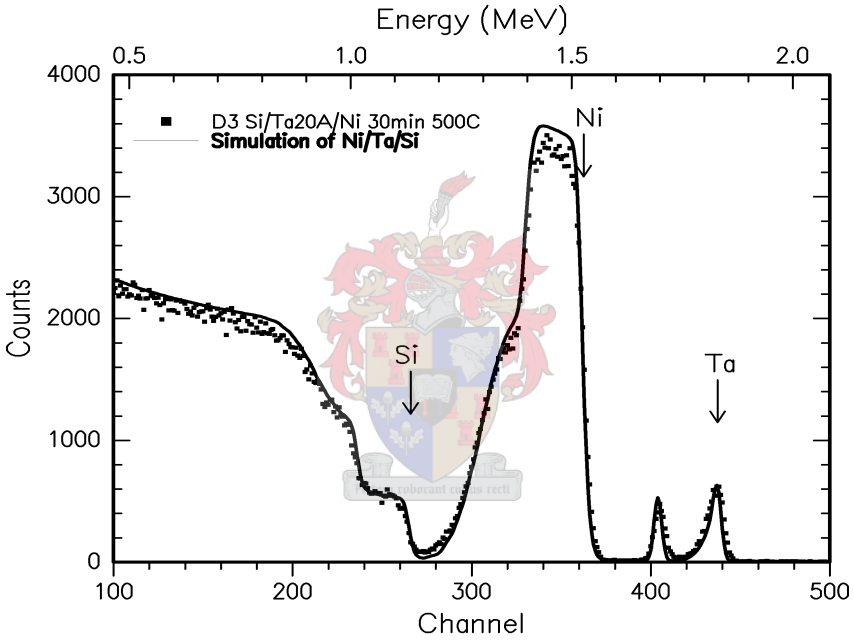

Figure 4. 9. RBS spectrum of a Si|Ta(20Å)|Ni sample annealed at 500˚C showing a double Ta peak, with an overlay of the simulated RBS spectrum of the sample structure shown in **Fig. 4.8**.

4.2.2 100 Å Ta barrier layer

4.2.2.1 RBS results and discussion

RBS spectra of Si<111>|Ta(100Å)|Ni(1100Å) samples annealed at 400, 500, 600 and 800˚C are shown in **Fig. 4.10.** In the case of the thicker (~100 Å) Ta interlayer there was no reaction even after 30 min annealing at 400˚C. The first reaction was found at 500˚C after 10 min annealing and the sloping shoulders of the RBS spectrum indicates the non-uniform nature of the silicide that was formed. This

sample also exhibits a double Ta peak, showing some of the Ta has moved to the surface, while some has remained in the as-deposited position.

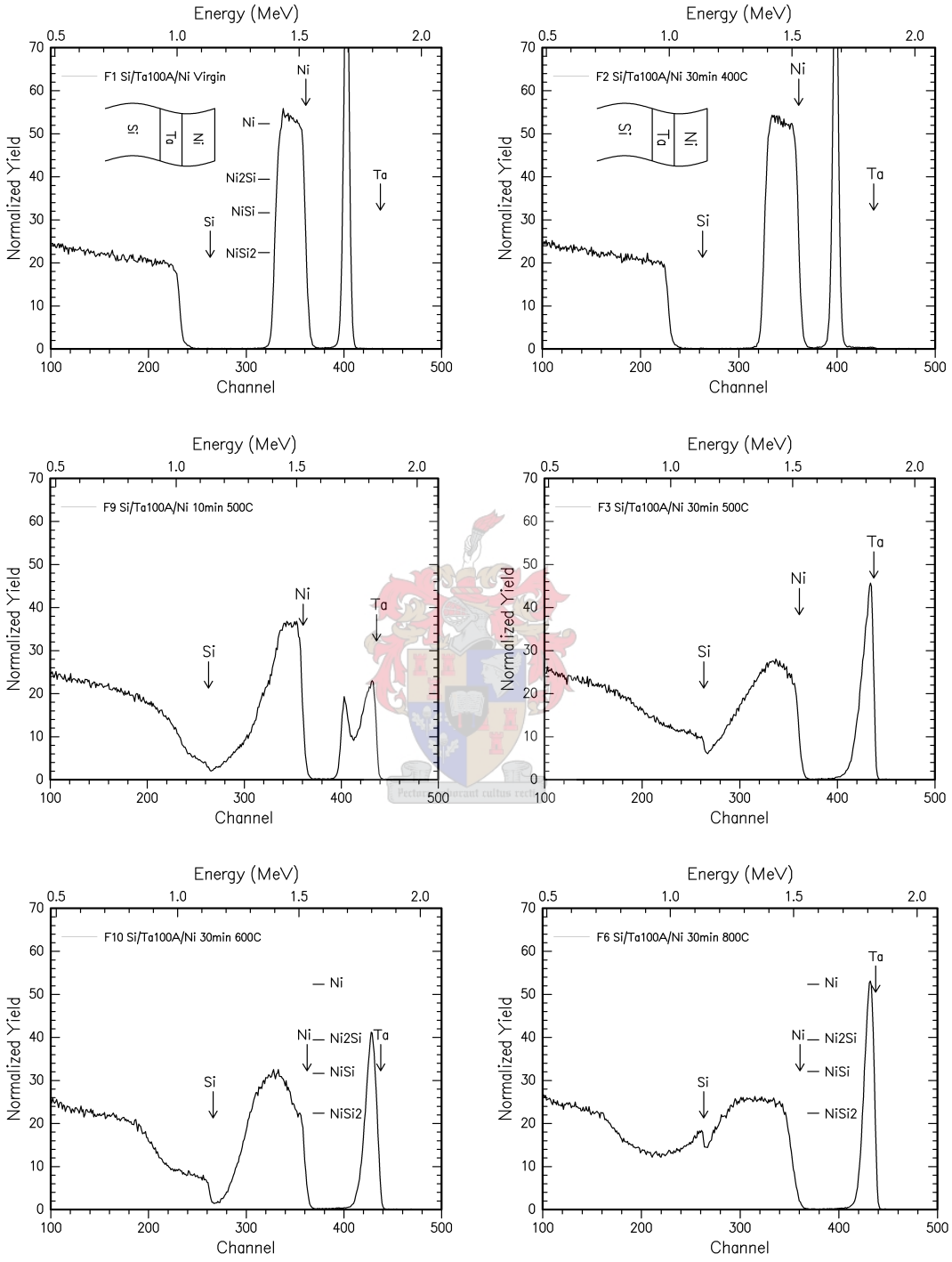

Figure 4. 10. RBS spectra of identical Si<111>|Ta(100Å)|Ni(1100Å) samples annealed at 400, 500, 600 and 800˚C. There was no reaction at 400˚C, even after a 30 min anneal. The first reaction was found at 500˚C and annealing at 500 and 600˚C formed non-uniform NiSi. Annealing at 800˚C for 30 min completely formed non-uniform $NiSi_2$.

Annealings of these samples with the 100 Å Ta barrier layer, carried out in the 500 to 600˚C temperature range, initially yielded many blotchy samples having a "split" Ta peak. As already discussed in **paragraph 4.2.1**, in the case of the thin Ta barrier layer this phenomenon was corrected by an improved washing procedure. In the case of the thicker (~100 Å) barrier layer, however, this phenomenon was only partially corrected by the improved washing procedure and as can be seen in **Fig 4.10** sample F9 still displays such a split or double Ta peak. This sample also has a mottled appearance, indicating the presence of unreacted surface Ni metal. It is interesting to note that no splitting of the Ta peak occurs at temperatures above 500˚C (**Fig. 4.10**). This is understandable because impurities at the growth interface are expected to have less effect at higher temperatures. The Si|Ta|Ni system seems to be quite sensitive to the presence of impurities at the growth interface and great care needs to be taken during the washing procedure.

Heating for 30 min at 500˚C (sample F3) yielded NiSi that was very non-uniform, as can be seen by the sloping shoulders in the RBS spectrum. When samples having a 100 Å Ta barrier were annealed at 600˚C (sample F10 **Fig. 4.10**) or 700˚C (see sample F5 in **Fig. 4.11**) the NiSi formation was complete although not very uniform. Furthermore it was found that after a 30 min anneal at 800˚C the formation of $NiSi_2$, though complete, was non-uniform (sample F6 **Fig. 4.10**).

The presence of the 100 Å Ta diffusion barrier does not seem to improve the uniformity of NiSi or $NiSi_2$ to any significant degree. Although the barrier caused the normal first phase formation of Ni_2Si to be skipped in favour of NiSi first phase formation at the elevated temperature of 500˚C, the non-uniform nature of the formed silicide is disappointing. In contrast, the 20 Å Ta barrier was very successful in completely forming uniform first phase NiSi after only 15 min annealing at 400˚C.

4.2.2.2 XRD analysis

RBS and corresponding XRD spectra of two Si<111>|Ta(100Å)|Ni(1100Å) samples are shown in **Fig. 4.11**. Sample F3 that was heated for 30 min at 500˚C yielded non-uniform NiSi as indicated by the sloping shoulders of the RBS spectrum. Corresponding XRD measurements show the presence of only NiSi peaks (**Fig. 4.11)**. The XRD spectrum of a sample annealed for 30 min at 700˚C also confirms the

formation of NiSi (sample F5 **Fig. 4.11**) by showing only NiSi reflections. [ICDD: NiSi = 38-0844]

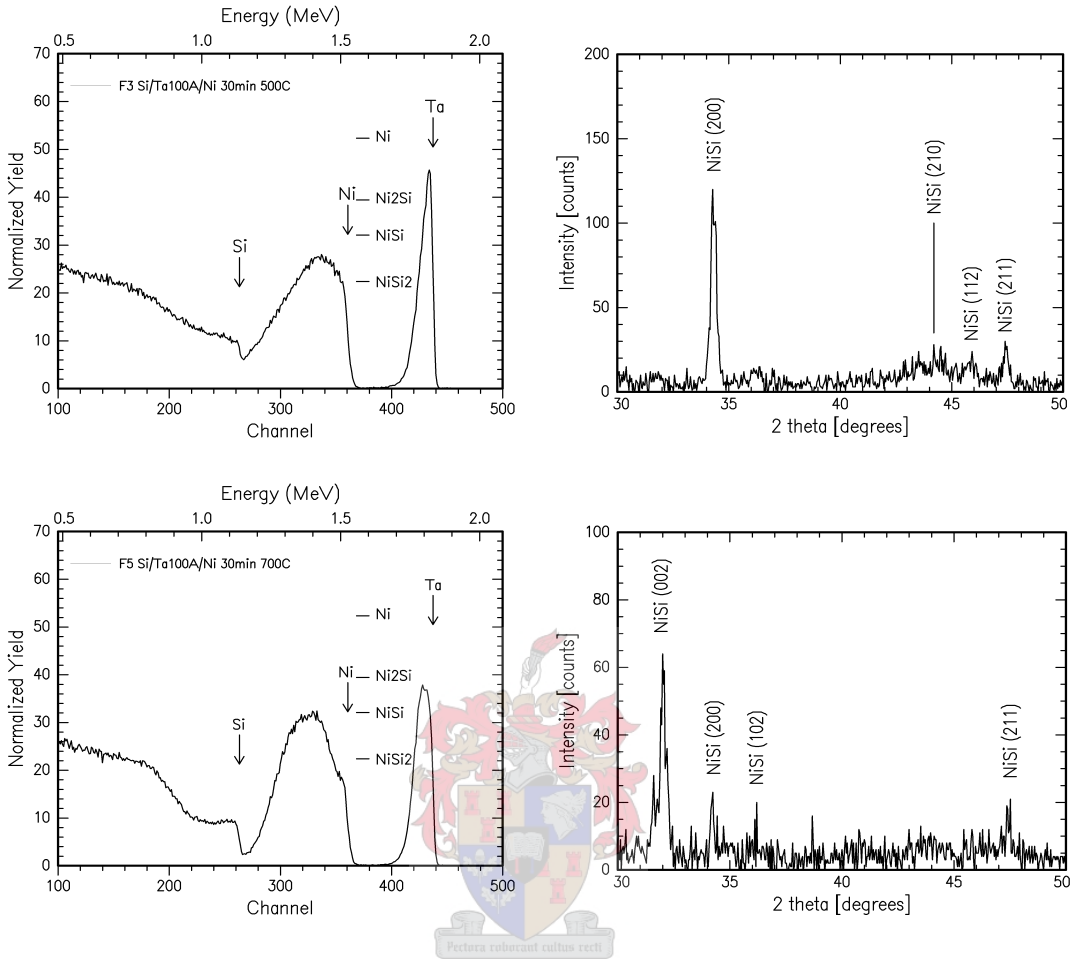

Figure 4. 11. RBS and corresponding XRD spectra of two Si<111>|Ta(100Å)|Ni(1100Å) samples annealed for 30 minutes at temperatures of 500 and 700˚C. The height of the Ni signal on the RBS spectra indicate NiSi formation and the XRD spectra only shows NiSi peaks.

4.3 Si <100> | Cr | Ni system

No previous research is known to have been done using a Cr metal interlayer as a diffusion barrier. However, Lee *et al.* **[120]** reported the formation of NiSi as first phase in samples formed by sputter-deposited Ni80Cr20 alloy films on Si substrates annealed at 300˚C. In this study for investigating the effects of a Cr diffusion barrier on the formation of nickel-silicides the following types of samples were prepared:

- 30 Å - 50 Å Cr barrier layer
- $CrSi_2$ (Cr = 50 Å) barrier layer
- 100 Å Cr barrier layer

4.3.1 30 - 50 Å Cr barrier layer

4.3.1.1 RBS results and discussion

RBS spectra of Si<100>|Cr(30Å)|Ni(1200Å) samples annealed at temperatures ranging from 340 to 800°C are shown in **Fig. 4.12.**

These RBS measurements show that in the case of the 30 Å Cr barrier slight reaction occurred at 340°C (sample E8 **Fig. 4.12**). The Cr RBS signal has moved to the right and is overlapped by the signal from the formed nickel-silicide. This indicates the diffusion of Ni atoms through the Cr barrier towards the Si substrate. The sloping shoulders of these RBS spectra show that the silicide is non-uniform.

Annealing for 20 min at 400°C completely forms non-uniform first phase NiSi and all the Cr has now moved to the surface because the Cr signal is clearly visible at the surface energy position (sample E3 **Fig 4.12**). Sample E5 that was annealed for 20 min at 500°C formed quite uniform first phase NiSi and at 600°C the uniformity of the NiSi is even more improved (sample E6). A 20 min anneal at 800°C formed complete, quite uniform $NiSi_2$ (sample E7). The fact that the Cr signal has now disappeared indicates that the Cr is no longer at the surface, but has dispersed throughout the $NiSi_2$. This intermixing also explains why the $NiSi_2$ RBS peak is slightly higher than the expected Ni height for $NiSi_2$.

From these RBS measurements it can be said that the use of the thin (30 Å) Cr diffusion barrier successfully formed first phase NiSi at 400°C and the uniformity of the NiSi increased with increasing heating temperature up to 700°C. Although we are stating that NiSi forms as first phase instead of Ni_2Si, it would really only be possible to prove this by doing dynamic RBS measurements. However it was decided not to do so in this instance as the uniformity of the NiSi did not seem good enough and dynamic RBS measurements are time consuming.

The RBS spectra of Si<100>|Cr(50Å)|Ni(900Å) samples annealed at the same temperatures showed very similar results to the Si<100>|Cr(30Å)|Ni(1200Å) samples and a selection of these is shown in **Fig. 4. 13.** However, these RBS results are not discussed again here, because of the obvious similarities between the RBS results of the 30 and the 50 Å Cr diffusion barriers.

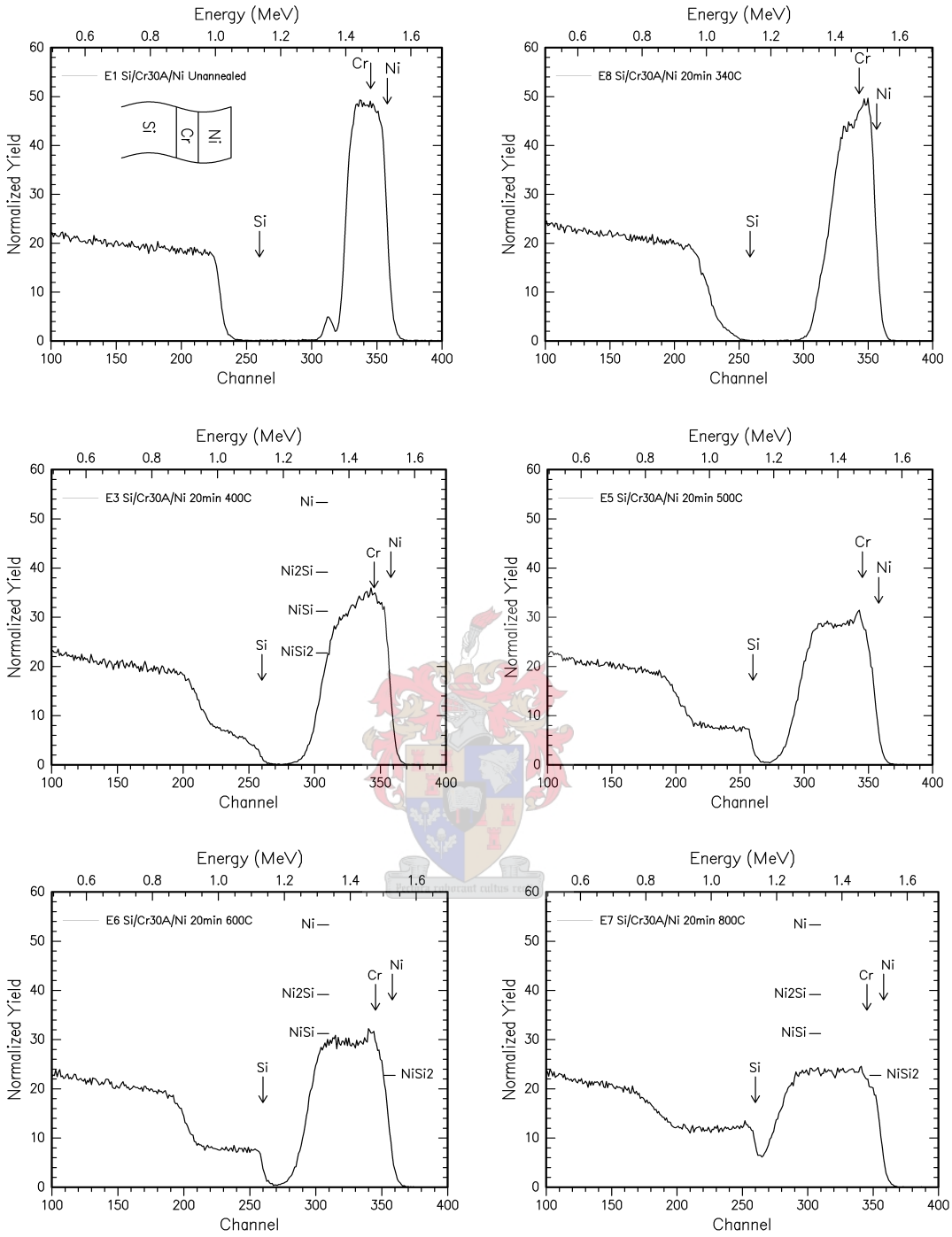

Figure 4. 12. RBS spectra of identical Si<100>|Cr(30Å)|Ni(1200Å) samples annealed in a temperature range of 340 to 800˚C. Annealing for 20 min at 400, 500 or 600˚C forms NiSi and the Cr signal is clearly present at the surface position. Heating for 20 min at 800˚C forms complete, quite uniform $NiSi_2$ and now the Cr is no longer at the surface, but has dispersed throughout the $NiSi_2$.

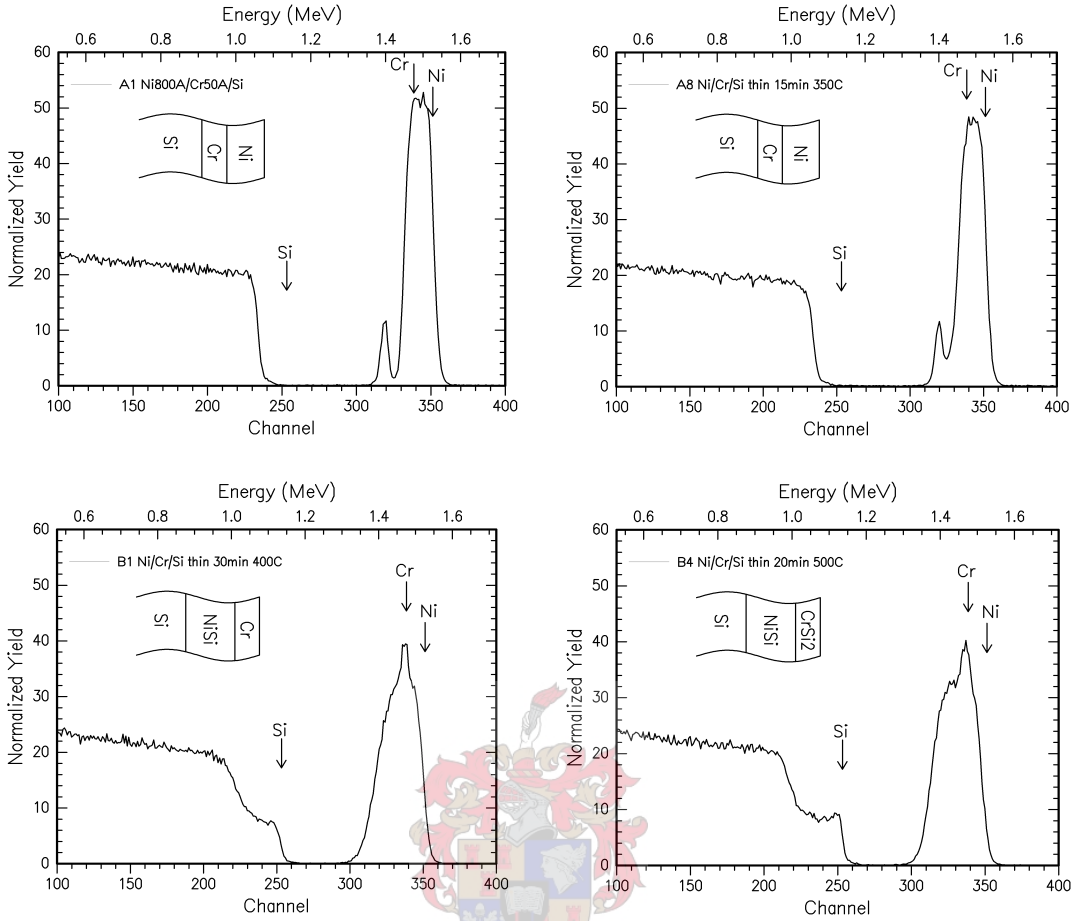

Figure 4. 13. RBS spectra of similar Si<100>|Cr(50Å)|Ni(900Å) samples annealed at 350, 400 and 500˚C. Annealing for 20 min at 400˚C forms NiSi as first phase and the Cr signal is at the surface position and heating for 20 min at 500˚C leads to the complete formation of quite uniform NiSi.

4.3.1.2 XRD analysis

The RBS and corresponding XRD spectra of a Si<100>|Cr(30Å)|Ni(1200Å) sample that was annealed for only 10 min at 400˚C are shown in **Fig. 4.14**. The heating resulted in the formation of non-uniform NiSi and this is confirmed by the XRD spectrum that shows mainly NiSi reflections, although the presence of the Ni_2Si (203) peak does indicate the formation of some Ni_2Si. [ICDD: Ni_2Si = 03-0943 NiSi = 38-0844]

The RBS and corresponding XRD spectra of two Si<100>|Cr(50Å)|Ni(900Å) samples annealed for (a) 30 minutes at 400˚C and (b) 20 minutes at 500˚C are shown in **Fig. 4.15**. [ICDD: Ni_2Si = 03-0943 NiSi = 38-0844]

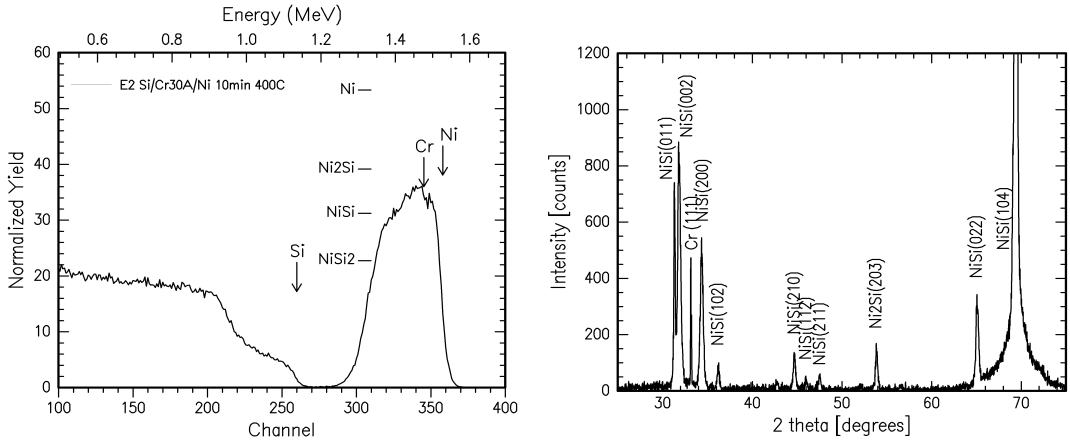

Figure 4. 14. RBS and corresponding XRD spectra of a Si<100>|Cr(30Å)|Ni(1200Å) sample that was annealed for 10 min at 400˚C. The formation of first phase NiSi is confirmed by the XRD spectrum, but the presence of some Ni_2Si is also indicated.

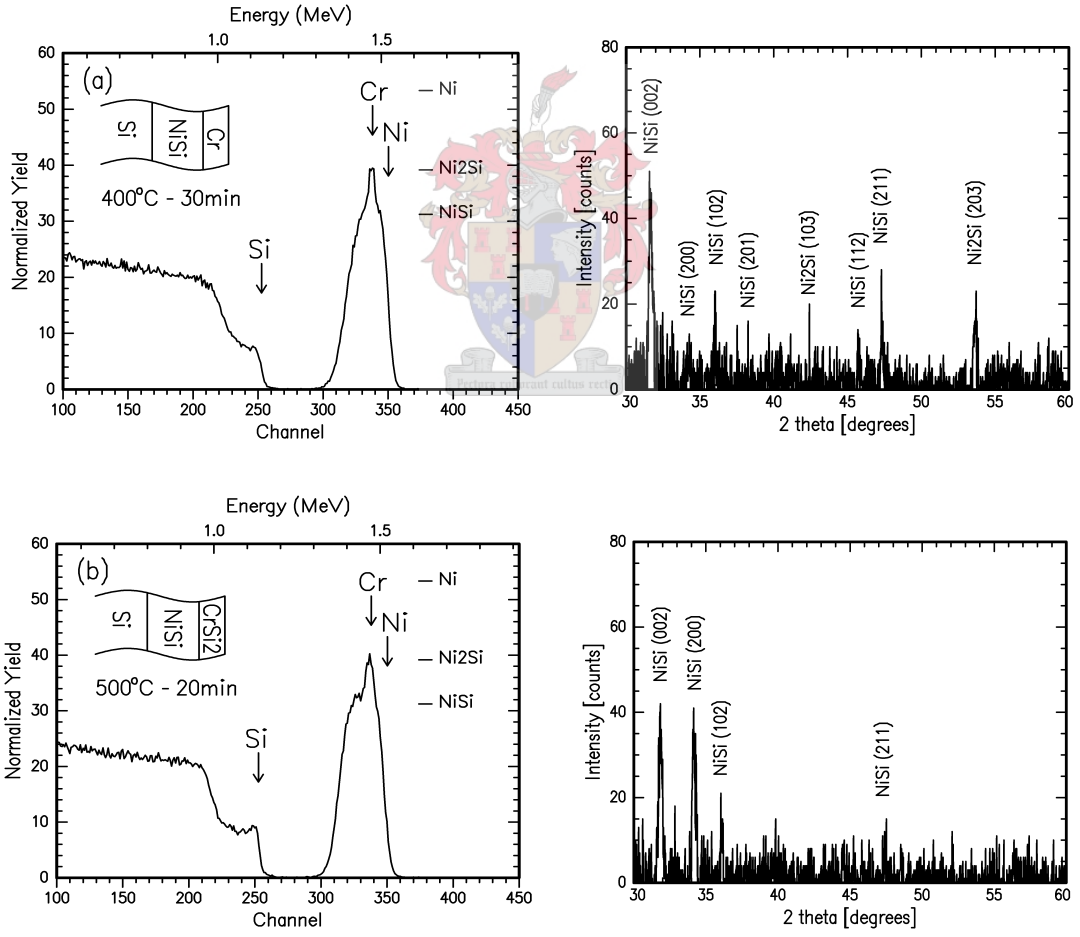

Figure 4. 15. RBS and corresponding XRD spectra of identical Si<100>|Cr(50Å)|Ni(900Å) samples annealed for (a) 30 minutes at 400˚C and (b) 20 minutes at 500˚C. The XRD spectrum in (a) confirms the presence of NiSi but also shows a reflection from Ni_2Si, similar to the 30 Å case. The complete formation of quite uniform first phase NiSi is confirmed by the XRD spectrum in (b).

Annealing a sample with a 50 Å Cr barrier at 400˚C for 30 min forms quite uniform first phase NiSi. The XRD spectrum in **Fig. 4.15(a)** confirms the presence of NiSi but also shows a reflection from Ni_2Si, similar to the 30 Å case mentioned earlier in **paragraph 4.3.1.2** and shown in **Fig. 4.14**. The complete formation of quite uniform first phase NiSi that was obtained by annealing for 20 min at 500˚C is also confirmed by XRD measurements shown in **Fig 4.15(b)**. In **Fig. 4.15(a)** and **(b)** the height of the Ni signal indicates that NiSi has formed and in **Fig. 4.15(b)** it is clear that the Cr at the surface has now formed $CrSi_2$ (this is indicated by the slight upward curve at the surface of the RBS Si signal, showing that additional Si has reached the surface). The barrier originally moved to the surface as Cr.

4.3.2 $CrSi_2$ (= 50 Å Cr) barrier layer

4.3.2.1 RBS results and discussion

In a comparative study, use was made of a substrate heater to keep the Si<100> substrate at 520˚C while depositing the Cr layer. This created a fully formed $CrSi_2$ diffusion barrier layer (formation temperature of $CrSi_2$ is 450˚C) and the Si<100>|$CrSi_2$ |Ni system was then formed by subsequent deposition of Ni without breaking vacuum. The deposited $CrSi_2$ barrier had an effective thickness of Cr of about 50 Å. The RBS spectra of Si<100>|$CrSi_2$(Cr=50Å)|Ni(900Å) samples annealed at temperatures ranging from 350 to 800˚C are shown in **Fig. 4.16**.

No reaction between the Ni and the Si occurred below 400˚C. Because the $CrSi_2$ barrier retarded the diffusion of Ni atoms, thereby lowering the effective concentration of Ni at the growth interface, this allowed the skipping of the formation of Ni_2Si and the formation of first phase NiSi, the non-uniformity shown by the sloping shoulders in the RBS spectrum (sample G8 **Fig. 4.16**). The Cr ($CrSi_2$) signal has moved completely to the surface and from the RBS spectrum the height of the Ni signal indicates that mainly NiSi has formed.

Annealing at 500 and 600˚C improves the uniformity of the first phase NiSi (samples G10 and G11 **Fig. 4.16**). The presence of the $CrSi_2$ at the surface is indicated by the slight upward curve at the surface of the RBS Si signal, showing that some more Si has reached the surface. After a 20 min anneal at 800˚C (sample G14) only non-uniform $NiSi_2$ exists and most of the $CrSi_2$ is still present at the surface (sample G14 **Fig. 4.16**).

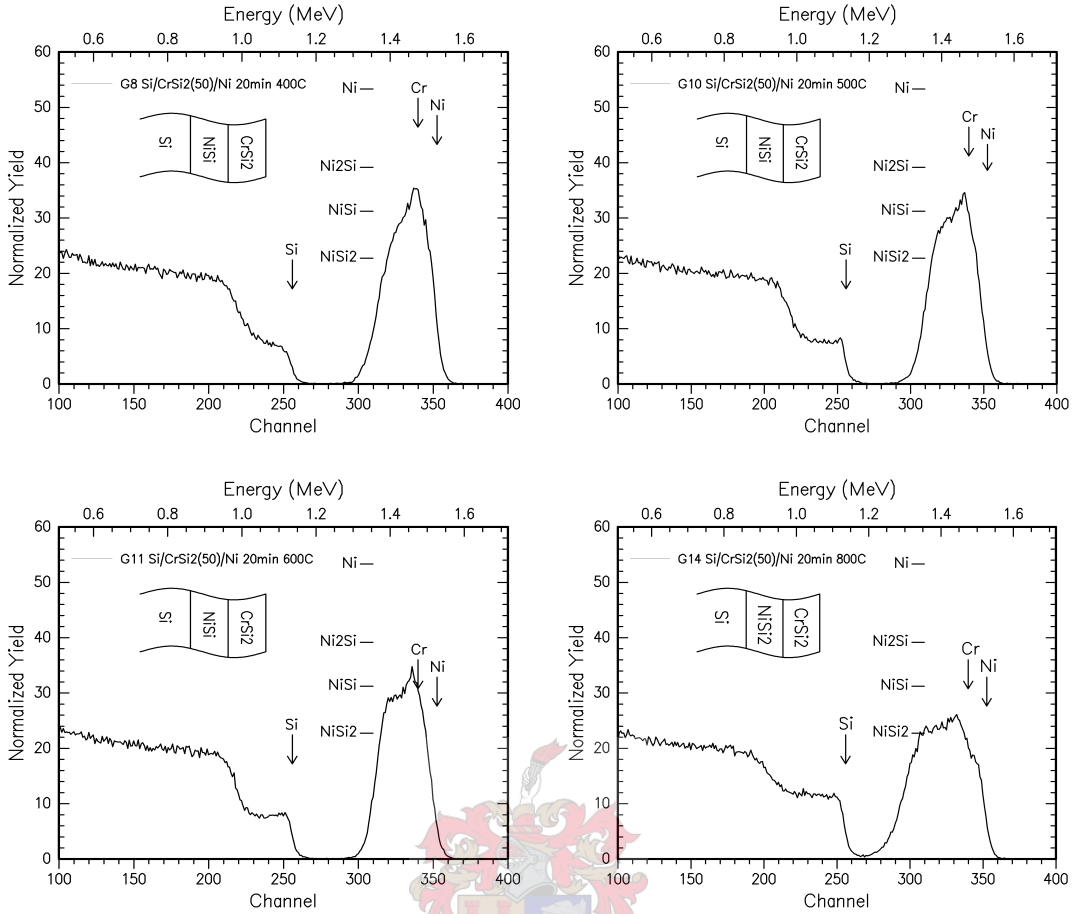

Figure 4. 16. RBS spectra of samples of the Si<100>|$CrSi_2$(Cr=50Å)|Ni(900Å) system annealed at 400 to 800˚C. A 20 min anneal at 400˚C forms non-uniform NiSi as first phase and the $CrSi_2$ is at the surface. Annealing at 500 and 600˚C improves the uniformity of NiSi. At 800˚C only non-uniform $NiSi_2$ exists and the $CrSi_2$ is spread throughout the silicide.

4.3.2.2 Comparison of Cr and $CrSi_2$ barriers

The RBS spectra of two samples having the Cr (50 Å) diffusion barrier are compared in **Fig. 4.17** with that of two samples having the $CrSi_2$ (Cr = 50Å) diffusion barrier. The samples were annealed at 400 and 500˚C respectively.

For both barriers complete non-uniform first phase NiSi formation occurred after heating for 30 min at 400˚C (**Fig. 4.17(a)**). Both the Cr and the $CrSi_2$ signals are at the surface energy position, indicating that all the Ni has diffused through the barrier to react with the Si substrate. For both systems the first phase NiSi formed at 500˚C is more uniform than the NiSi formed at 400˚C (compare **Fig. 4.17 (a)** and **(b)**). It is clear from **(b)** that there is hardly any difference between the impact of the Cr and the Cr_2Si barriers on NiSi formation for temperatures above 450˚C, because the Cr barrier changes to a $CrSi_2$ barrier at that temperature.

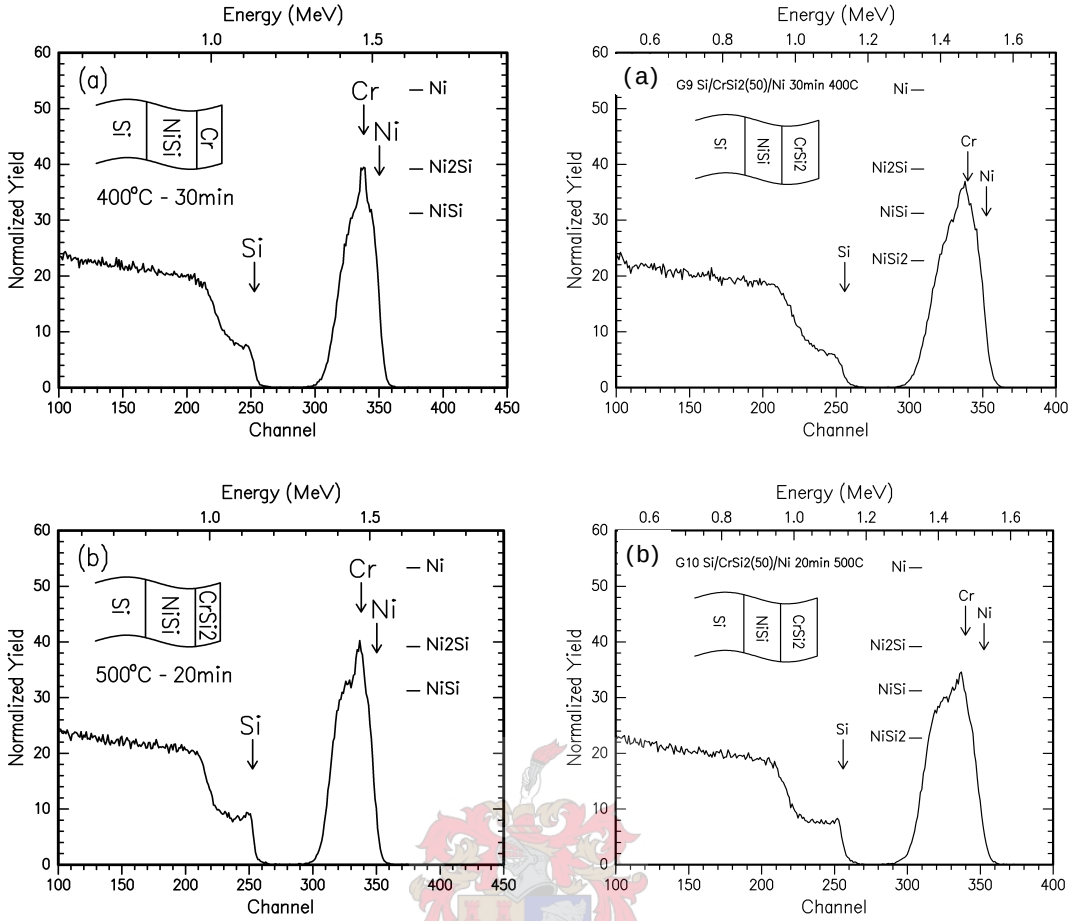

Figure 4. 17. Comparison of RBS spectra of samples having a 50 Å Cr barrier (the two spectra on the left) and having a $CrSi_2$ diffusion barrier (the two spectra on the right) annealed (a) for 30 min at 400˚C and (b) for 20 min at 500˚C. This comparison shows that for NiSi formation we found little or no difference between the use of a Cr or a $CrSi_2$ barrier, particularly at temperatures higher than the formation temperature of $CrSi_2$.

4.3.3 100 Å Cr barrier layer

Some RBS spectra of Si<100>|Cr(100Å)|Ni(1200Å) samples annealed at temperatures ranging from 350 to 800˚C are shown in **Fig. 4.18**.

In the case of the thicker (~100 Å) Cr interlayer the first signs of movement of the Cr signal occurs after 15 minutes at 350˚C (sample C8 **Fig. 4.18**). This reaction is indicated by the slight shift to the right of the Cr peak on the RBS spectrum, which shows that the Ni atoms have started to diffuse through the Cr diffusion barrier, causing the Cr to move towards the surface of the sample. For both the thin (~50 Å) and the thicker (~100 Å) barriers complete (although non-uniform) silicide formation is found after 20 minutes at 400˚C. The thick Cr barrier thus behaves the same as the thin Cr barrier for low temperatures (up to 400˚C).

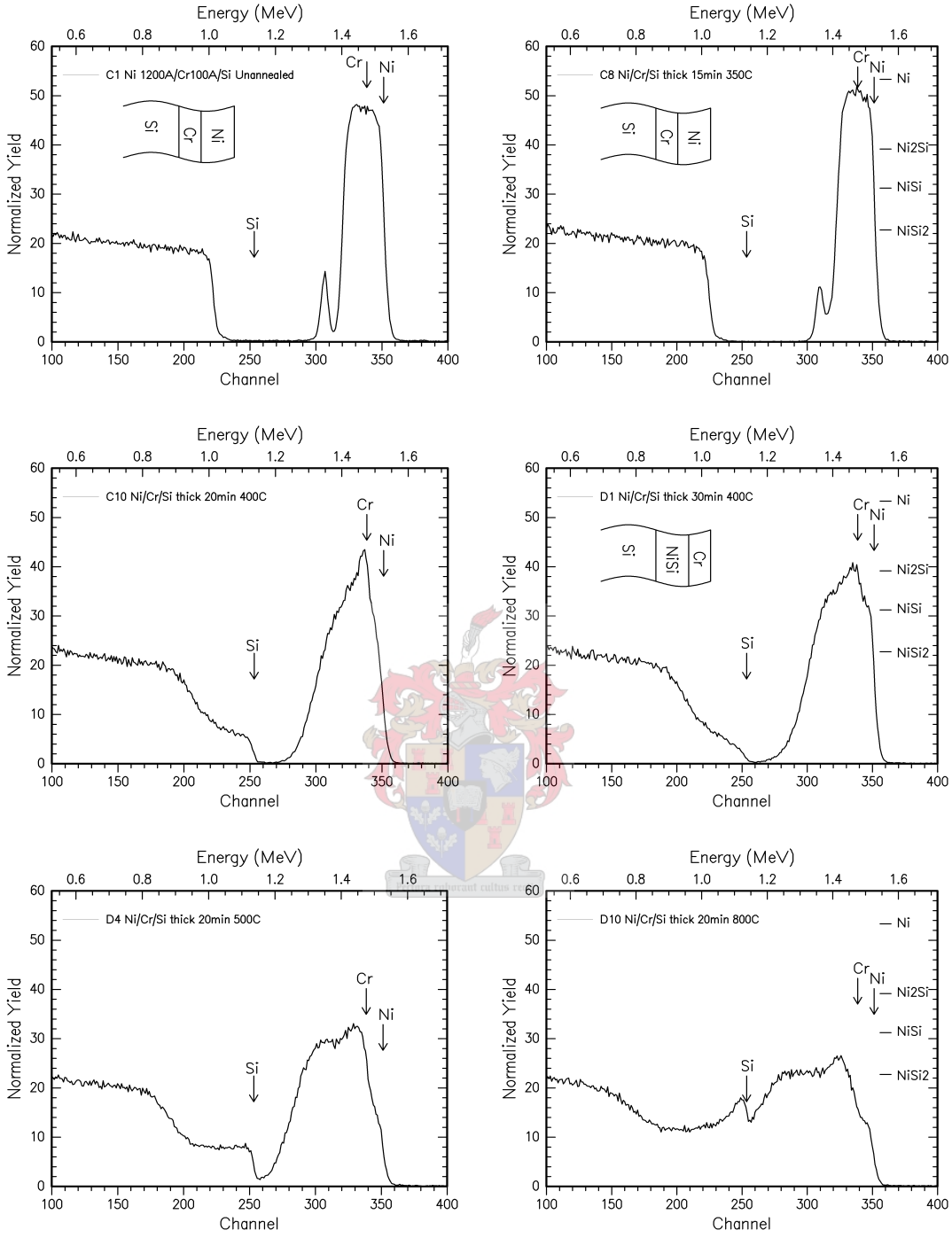

Figure 4. 18. RBS spectra of similar Si<100>|Cr(100Å)|Ni(1200Å) samples annealed in a temperature range of 350 to 800˚C. First reaction occurred at 400˚C and a 30 min anneal at 400˚C formed quite uniform first phase NiSi with the Cr signal at the surface position. Annealing at 500 forms non-uniform NiSi and at 800˚C non-uniform $NiSi_2$ formation is complete.

Annealing at 500 for 20 min forms non-uniform NiSi, with the RBS spectrum showing the Cr peak at it's surface position. At 800˚C after a 20 min anneal, the

$NiSi_2$ formation is complete but non-uniform. These results indicate that although the thicker Cr barrier also prevents diffusion of Ni atoms for temperatures up to 400˚C, at higher temperatures the thicker Cr barrier seems less effective than the thinner Cr barriers in obtaining uniform NiSi or $NiSi_2$ formation.

4.4 Si <100> | Ti | Ni system

As can be seen from **Table 2.6** in **Chapter 2** some research has been done on the use of Ti as a diffusion barrier interlayer for the Ni|Si system. This research was discussed in **paragraph 2.3.4**. In this investigation the Si<100>|Ti|Ni system was also studied, using the following sample types:

- 30 Å - 50 Å Ti barrier layer
- 100 Å Ti barrier layer

4.4.1 30 Å - 50 Å Ti barrier layer

4.4.1.1 RBS results and discussion

RBS spectra of Si<100>|Ti(30Å)|Ni(1100Å) samples annealed at temperatures ranging from 380 to 800˚C are shown in **Fig. 4.19**.

For this system no reaction between Ni and Si occurred up to 380˚C due to the Ti acting as a diffusion barrier between the substrate and the Ni. There was, however some movement of the Ti signal to the right of the RBS spectrum, indicating that some Ni atoms have started to diffuse through the Ti diffusion barrier after 20 min at 380˚C (sample F1 **Fig. 4.19**). The first reaction was found at 400 °C which formed non-uniform NiSi as first phase (sloping shoulders indicating non-uniformity).

Annealing at 500 and 600˚C quite significantly improves the uniformity of the first phase NiSi (samples E6 and E7 **Fig. 4.19**) and the Ti signal can clearly be seen at the surface energy position, showing that all of the Ti in the barrier has diffused to the surface of the sample. A 20 min anneal at 800˚C (sample E8) leads to the complete formation of quite uniform $NiSi_2$ and some Ti is still visible at the surface position, although most of the Ti has intermixed with the Ni-disilicide (the formation temperature of $TiSi_2$ is usually about 600˚C **[6]**).

These results indicate that a 30 Å Ti barrier reduces the effective Ni concentration at the growth interface and so thermodynamically favors the formation

of NiSi at 400˚C. It also greatly improves the uniformity of the first phase NiSi that forms at 500 and 600˚C.

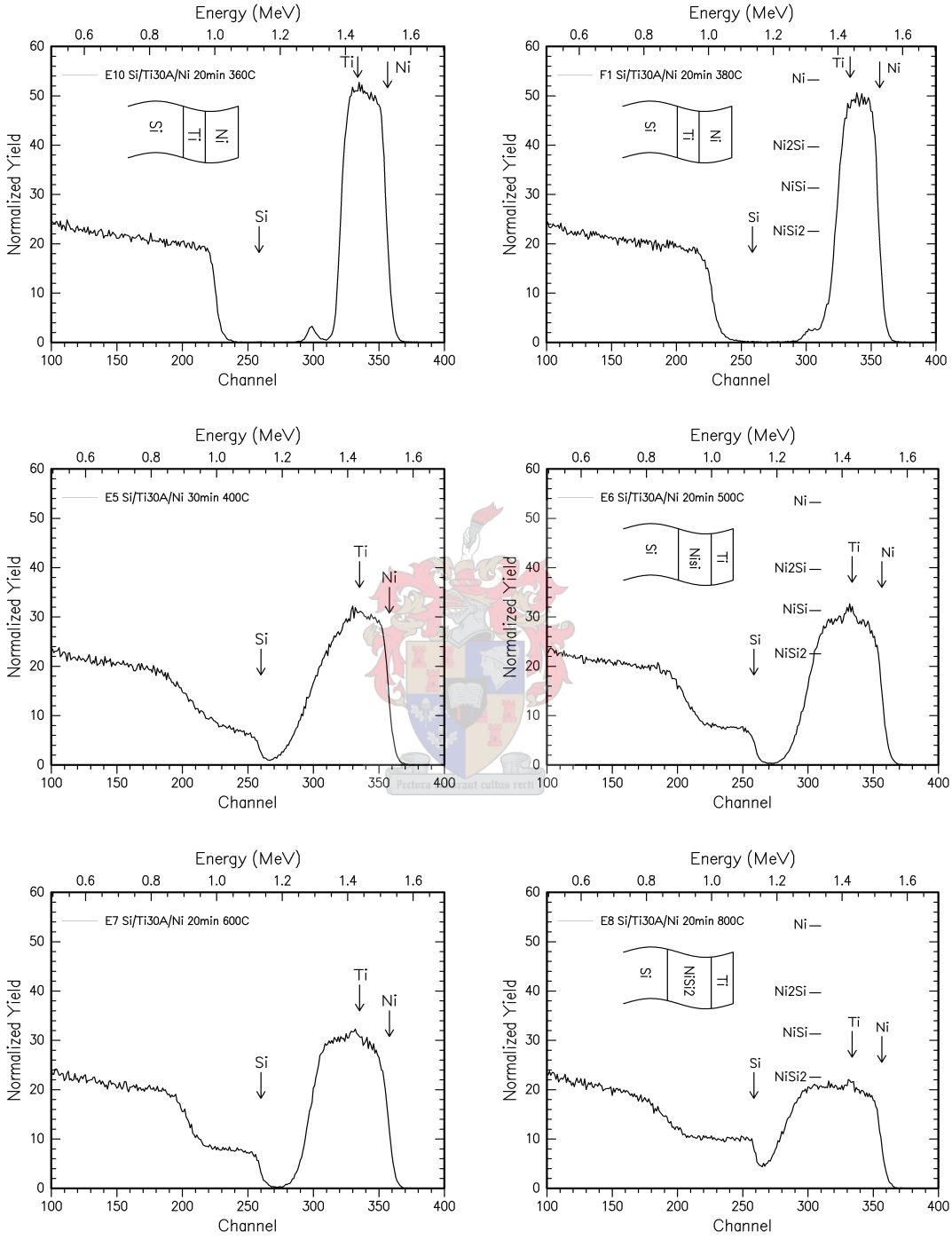

Figure 4. 19. RBS spectra of similar Si<100>|Ti(30Å)|Ni(1100Å) samples annealed at 380 to 800˚C. Annealing at 400˚C formed non-uniform NiSi. At 500 and 600˚C the uniformity of the NiSi improved and the Ti signal is clearly visible at the surface position (samples E6 and E7). At 800˚C complete uniform $NiSi_2$ formation was found.

The use of a 50 Å Ti barrier showed very similar results and a few RBS spectra of Si<100>|Ti(50Å)|Ni(800Å) samples annealed at temperatures ranging from 350 - 800˚C are shown in **Fig. 4.20**.

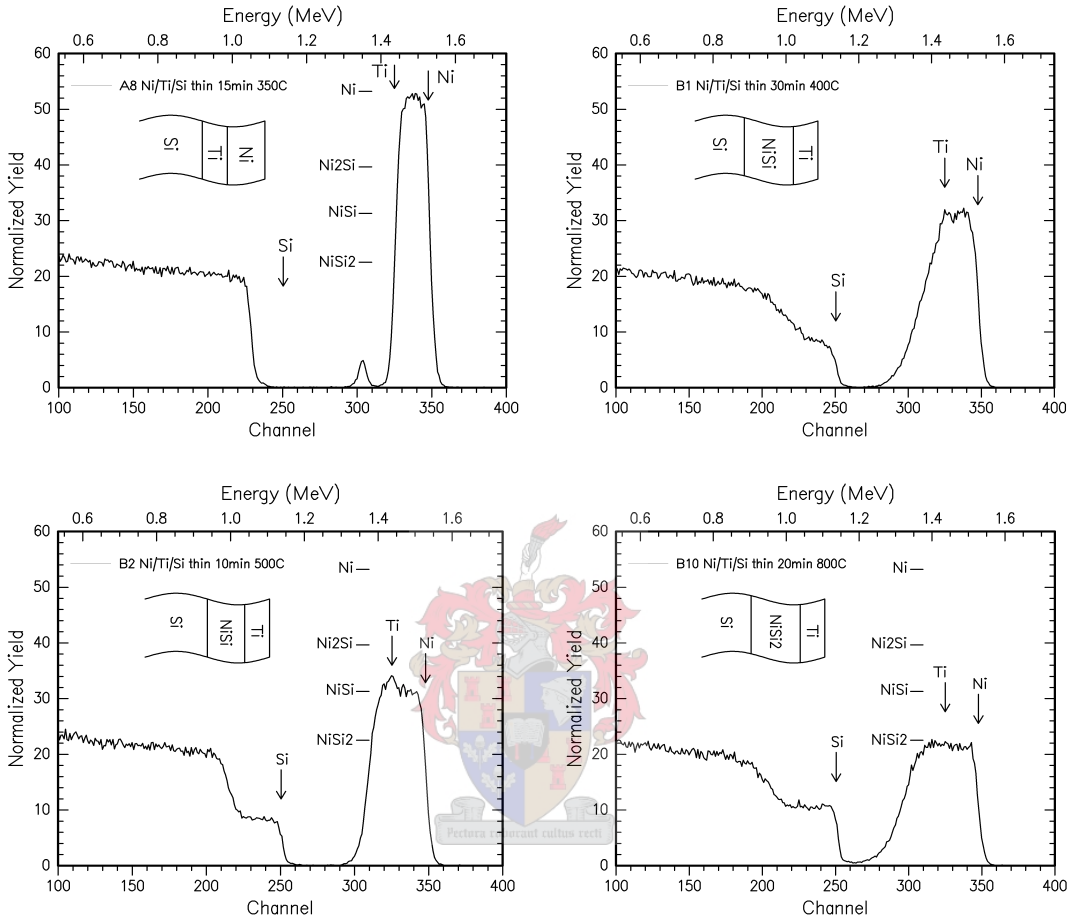

Figure 4. 20. RBS spectra of similar Si<100>|Ti(50Å)|Ni(900Å) samples annealed at 350, 400, 500 and 800˚C. No reaction occurred below 400˚C and non-uniform NiSi formed as first phase after heating at 400˚C for 30 min. After heating for 10 min at 500˚C uniform first phase NiSi (sample B2) is formed and after 20 min at 800˚C only uniform $NiSi_2$ exists.

As these RBS results are so very similar to those obtained using the 30 Å Ti barrier, no further discussion is given here, exept for two remarks: firstly, that the 50 Å Ti barrier formed more uniform first phase NiSi in less time (10 min, sample B2 **Fig. 4.20**) at 500˚C than the 30 Å Ti barrier and, secondly that at 800˚C the 50 Å Ti barrier was not present anymore at the surface position like the 30 Å Ti barrier, but the Ti had dispersed throughout the di-silicide (sample B10).

4.4.1.2 XRD analysis

The RBS and corresponding XRD spectra of a Si|Ti(30Å)|Ni sample heated for 10 min at 400˚C as well as a Si|Ti(50Å)|Ni sample heated for 10 min at 500˚C are shown in **Fig. 4.21.**

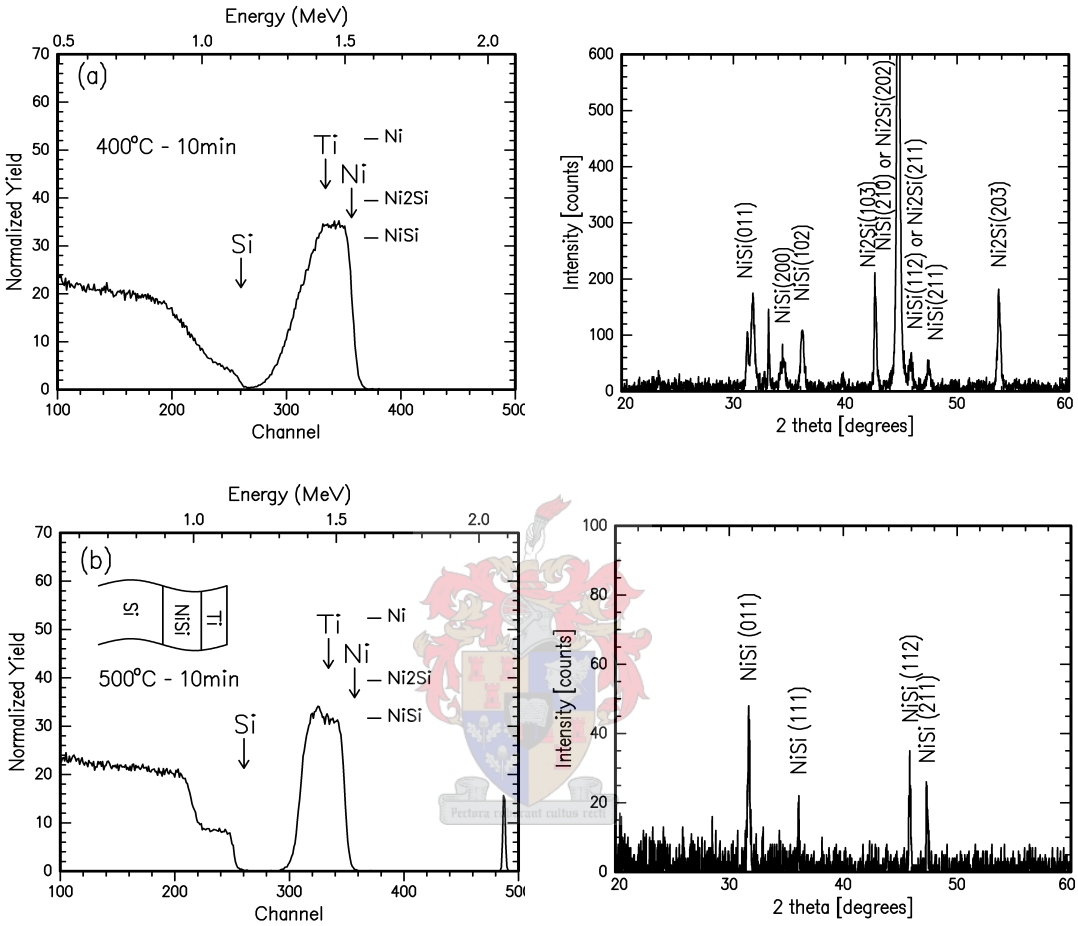

Figure 4. 21. RBS and corresponding XRD spectra of (a) a Si<100>|Ti(30Å)|Ni(1100Å) sample annealed for 10 minutes at 400˚C showing the formation of a mixture of NiSi and Ni_2Si and (b) of a Si<100>|Ti(50Å)|Ni(900Å) sample annealed for 10 minutes at 500˚C showing the complete formation of NiSi as first phase. (The peak near channel 500 on the RBS spectrum in (b) was used to make sure that no channel drift occurred.)

In **Fig. 4.21(a)** the height of the RBS spectrum indicates mainly NiSi formation but with some Ni_2Si also present in a sample with a 30 Å Ti barrier layer annealed for 10 min at 400˚C. The XRD spectrum shows reflections of both NiSi and Ni_2Si, confirming the presence of some Ni_2Si. [ICDD: Ni_2Si = 03-0943 ; NiSi = 38-0844]

However, annealing at 500˚C, the use of the 50 Å Ti barrier layer forms uniform first phase NiSi after only 10 min of annealing. In the RBS and

corresponding XRD spectra of a Si<100>|Ti(50Å)|Ni(900Å) sample heated for 10 min at 500˚C shown in **Fig. 4.21(b)** there is no sign of Ni_2Si formation. This is due to the fact that, according to the EHF model, the Ti barrier reduces the effective Ni concentration at the growth interface, thereby thermodynamically favouring the formation of NiSi instead of Ni_2Si as first phase.

4.4.2 100 Å Ti barrier layer

Some RBS spectra of Si<100>|Ti(100Å)|Ni(1200Å) samples annealed at temperatures ranging from 400 - 800˚C are shown in **Fig. 4.22.**

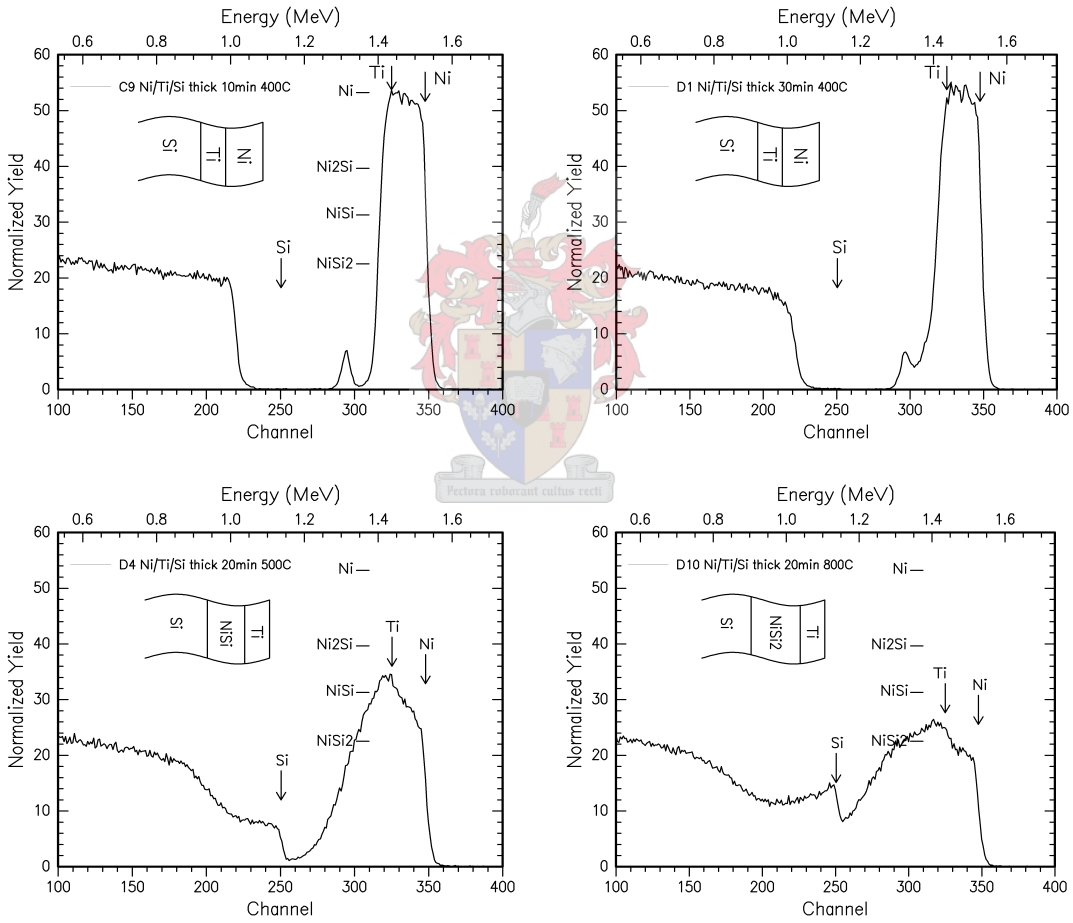

Figure 4. 22. RBS spectra of similar Si<100>|Ti(100Å)|Ni(1200Å) samples annealed in a temperature range of 400 to 800˚C. It is clear that the 100 Å Ti barrier prevents diffusion of Ni atoms even at 400˚C. First reaction was found after heating at 500˚C for 20 min and this yielded non-uniform NiSi (sample D4). Annealing at 800˚C formed non-uniform $NiSi_2$.

When a 100 Å Ti barrier was used no reaction occured even after annealing for 30 min 400˚C (sample D1 **Fig. 4.22**), showing that this thicker Ti barrier layer

acts more effectively as a diffusion barrier for the Ni atoms. The first reaction was found at 500˚C after heating for 20 min and this yielded non-uniform NiSi with the Ti signal at the surface position. Annealing at 800˚C (sampleD10, **Fig. 4.22**) showed similar results as in the case of the thinner Ti barriers, namely the complete formation of non-uniform $NiSi_2$, with the Ti signal still visible at the surface energy position, although slightly broadened (probably due to the formation of $TiSi_2$).

These results show that in this study no indication was found of the formation of $NiSi_2$ as first phase by using a Ti diffusion barrier layer as other groups have reported **[117-119].** However, it must be kept in mind that our experimental conditions differed significantly from those of Fenske *et al*. **[117-119]**:

- The Ti barriers used in this investigation were a lot thinner (100 Å or less Ti was used compared to the 500 Å Ti barriers used by Fenske *et al*.);
- the Ni layers used in this investigation were a lot thinner (1000 Å Ni compared to 2000 Å Ni used by Fenske *et al*.);
- no Ag capping layer was used in this study (as was used by Fenske *et al.)* and
- no ambient nitrogen atmosphere was used (as was used by Fenske *et al*.) during annealing, as all depositions and annealing were done in vacuum.

4.5 Summary and conclusions

In **Chapter 4** the experimental results of the investigation of Ni-silicide formation through Ta, Cr and Ti diffusion barrier interlayers was reported and a summary of these results is given in **Table 4.1.**

The use of a thin (20 Å) Ta diffusion barrier in the Ni-Si system allowed no reaction even after annealing for 10 min at 400˚C, but RBS measurements showed that after annealing for 15 min at 400˚C uniform NiSi formed suddenly as first phase and XRD measurements confirmed this. Dynamic RBS measurements also confirmed the abrupt formation of NiSi instead of the normal first phase Ni_2Si. According to the EHF model this shows that the diffusion barrier interlayer reduces the effective concentration of the Ni atoms to a value where the effective heat of formation of NiSi is more negative than that of Ni_2Si and first phase formation of NiSi is thus thermodynamically favoured. The thickness uniformity of the first phase NiSi that formed through the 20 Å Ta barrier improved at higher temperature anneals (500 to 700˚C). Non-uniform $NiSi_2$ formed through the thin Ta barrier at 800˚C.

Table 4. 1. Ni-silicide formation through Ta, Cr and Ti diffusion barrier layers.

NICKEL-SILICIDE FORMATION THROUGH BARRIER LAYERS			
BARRIER	**TEMP (˚C)**	**SILICIDE FORMATION**	**THICKNESS UNIFORMITY**
Ta 20 Å	350	no reaction	
	400	10 min no reaction 15 min first phase NiSi	uniform
	500	first phase NiSi	uniform
	600	first phase NiSi	uniform
	700	first phase NiSi	uniform
	800	$NiSi_2$	uniform
Ta 100 Å	400	no reaction	
	500	10 min NiSi and unreacted Ni 30 min first phase NiSi	non-uniform
	600	first phase NiSi	more uniform
	700	first phase NiSi	more uniform
	800	$NiSi_2$	non-uniform
Cr 30 - 50 Å	350	slight diffusion of Ni	
	400	NiSi and some Ni_2Si	non-uniform
	500	first phase NiSi	uniform
	600	first phase NiSi	more uniform
	800	$NiSi_2$	uniform
$CrSi_2$ (Cr = 50 Å)	350	no reaction	
	400	first phase NiSi	non-uniform
	500	first phase NiSi	uniform
	600	first phase NiSi	uniform
	800	$NiSi_2$	non-uniform
Cr 100 Å	350	slight diffusion of Ni	
	400	mixture NiSi and Ni_2Si	very non-uniform
	500	first phase NiSi	non-uniform
	600	first phase NiSi	non-uniform
	800	$NiSi_2$	non-uniform
Ti 30 - 50 Å	380	slight diffusion of Ni	
	400	NiSi and some $NiSi_2$	non-uniform
	500	10 min first phase NiSi	uniform
	600	first phase NiSi	uniform
	800	$NiSi_2$	uniform
Ti 100 Å	400	no reaction	
	500	first phase NiSi	non-uniform
	800	$NiSi_2$	non-uniform

A thicker (100 Å) Ta diffusion barrier layer prevented any reaction between the Si substrate and the Ni from occurring up to about 480˚C and yielded, as first reaction, non-uniform NiSi at 500˚C. The uniformity of the first phase NiSi that formed through the 100 Å Ta barrier improved with increasing temperature up to

700˚C, but the thin Ta barrier produced more uniform first phase NiSi in the 400 to 700˚C temperature range. At 800˚C non-uniform $NiSi_2$ formed. It must also be mentioned here that in the RBS spectra of all annealed samples of the Si|Ta|Ni system, the Ta signal is clearly visible at the surface energy position, indicating that the Ni diffused through the Ta barrier and the barrier moved to the surface of the sample. No spreading of the Ta signal occurs, even at 800˚C, showing that the Ta does not diffuse back into the $NiSi_2$.

A thin (30 - 50 Å) Cr barrier allowed the formation of mainly NiSi at 400˚C, although XRD spectra also indicated the presence of some Ni_2Si. The complete formation of more uniform NiSi, as confirmed by the XRD measurements, was obtained by annealing at 500˚C and the uniformity was improved by heating at 600˚C. The $NiSi_2$ formation at 800˚C was complete and quite uniform. The results were very similar when a $CrSi_2$ (Cr = 50Å) barrier was used, the only difference being that the $NiSi_2$ that formed at 800˚C was non-uniform. The use of a thicker (100 Å) Cr barrier layer resulted in the formation of very non-uniform NiSi at 400˚C and even after heating at temperatures of up to 600˚C the NiSi was still non-uniform. The thicker Cr barriers were a lot less effective than the thinner Cr barriers at delivering a NiSi layer of uniform thickness in the 500 to 700˚C temperature range and at 800˚C the $NiSi_2$ that formed was non-uniform. In the RBS spectra of all samples of the Si|Cr|Ni system annealed in the 400 to 700˚C temperature range, the Cr signal is clearly visible at the surface energy position, indicating that the Ni diffused through the Cr barrier and the barrier moved to the surface of the sample. However, at 800˚C the Cr signal becomes less visible or disappears, particularly for the thinner Cr barriers, showing the intermixing of the Cr into the $NiSi_2$.

The use of a thin (30 - 50 Å) Ti barrier produced mostly non-uniform NiSi as first reaction at 400˚C as confirmed by RBS and XRD measurements. The uniformity of the NiSi improved with an increase in annealing temperature, up to 700˚C. At 800˚C complete uniform $NiSi_2$ formation occurred. The thicker (100 Å) Ti interlayer allowed no reaction below 500˚C, showing that it retards Ni diffusion more effectively. Non-uniform first phase NiSi formed at 500˚C and at temperatures above 750˚C the $NiSi_2$ that formed was non-uniform. In the RBS spectra of all samples of the Si|Ti|Ni system annealed in the 400 to 700˚C temperature range, the Ti signal is

clearly visible at the surface energy position, indicating that the Ni has diffused through the Ti barrier. However, at 800˚C the Ti signal becomes less visible, showing the spreading or intermixing of the Ti into the $NiSi_2$.

From these experimental results it can be concluded that the presence of a *thinner* diffusion barrier layer of either Ta, Cr or Ti lowers the effective concentration of Ni at the growth interface and this results in the skipping of the formation of Ni_2Si as first phase in favour of the formation of NiSi. The thin Ta barrier seems most effective as it allows a sudden phase change to form the desired uniform NiSi as first phase after annealing for only 15 min at 400˚C. The thin Cr barrier was less effective than Ta at 400˚C because, although it also formed mainly NiSi, a little Ni_2Si was also detected by XRD measurements. The thin Ti barrier formed a mixture Ni_2Si and NiSi at 400˚C. At temperatures ranging from 500 to 700˚C the thin barriers all completely formed first phase uniform NiSi, with the uniformity improving with increased annealing temperature. All three thin barriers formed $NiSi_2$ at temperatures of 750˚C and above, but the thin Ti barrier formed the most uniform di-silicide.

The *thicker* Ta and Ti barriers were more effective in retarding the diffusion of the Ni atoms than the thinner barriers, as both prevented any reaction from occurring below 500˚C. However, the thicker Cr barrier allowed the formation of very non-uniform NiSi at 400˚C. Furthermore, the thicker Ta and Ti barriers formed first phase NiSi at higher temperatures (500 to 700˚C), although less uniform than the thinner barriers. The NiSi uniformity also improved with increased annealing temperature. The thicker Cr barrier did not perform as well at higher temperatures, not at retarding diffusion, nor at promoting the growth of first phase NiSi of uniform thickness. The $NiSi_2$ that formed at 800˚C through all three of the thicker barriers was non-uniform.

In general it can be stated that only the thin (20 Å) Ta barrier led to the abrupt formation of uniform first phase NiSi. In all the other cases either some Ni_2Si was present and/or the layer was non-uniform. Furthermore, the Ni-silicide formation was more uniform at higher annealing temperatures and when thinner barriers were used. In all cases $NiSi_2$ formed at 800˚C, which is similar to the situation without a diffusion barrier. This is because the barrier moves to the surface of the sample during the formation of NiSi and it does not act as a diffusion barrier any more when $NiSi_2$ starts to form. Finally, it was generally found that, the thicker the barrier, the higher the temperature of Ni-silicide formation.

Chapter 5

Co-SILICIDE FORMATION THROUGH BARRIER LAYERS

5.1 Introduction

The discussion of cobalt-silicide phase formation begins by considering once more the cobalt-silicon EHF and phase diagram as shown in **Chapter 1**, **Fig. 1.2**. On the Co-Si phase diagram there are three congruent compound phases, i.e. CoSi, Co_2Si and $CoSi_2$. The EHF model states that the first phase to form will be the one that has the most negative heat of formation ($\Delta H'$) at the concentration of the liquidus minimum. It can be seen from the EHF diagram in **Fig. 1.2** that at the concentration of the liquidus minimum the formation of Co_2Si will lead to the biggest free energy change. It follows that Co_2Si will normally be the first phase to form at a temperature of about 450˚C, followed by CoSi formation at about 500˚C and then $CoSi_2$ forms at about 550˚C **[6].**

By using Concentration Controlled Phase Selection or CCPS, it is possible to control or influence phase formation so that only phases with suitable physical and electrical properties are formed. As was discussed in **paragraph 2.2.1**, a Ti diffusion barrier has been used in the presence of different ambient atmospheres and / or different capping layers to successfully form uniform, epitaxial $CoSi_2$ directly as first phase **[14,18-20]** instead of Co_2Si which is usually found as first phase.

In this study of cobalt-silicide formation all depositions and annealing were done in vacuum. Two different metallic diffusion barrier interlayers, i.e. Ta and Ti were used in different thicknesses to determine the possible successful application in concentration controlled phase selection, the aim being to possibly form uniform, epitaxial CoSi or $CoSi_2$ as first phase, instead of the normal Co_2Si by controlling the Co concentration at the growth interface. A comparative study was done by adding a Ta capping layer, thus forming the Si<100>|Ta|Co|Ta_{cap} system. The experimental results of this research on Co-silicide formation through Ta and Ti diffusion barriers will now be discussed.

5.2 Si <100> | Ta | Co system

As can be seen from **Table 2.6** in **Chapter 2** a fair amount of research has been done during the past decade or so using tantalum as a diffusion barrier in the Si-Co system. The results of this research was discussed in **paragraph 2.2.3.** In this investigation of the effects of a tantalum diffusion barrier on the formation of cobalt-silicides the following Ta barriers were used:

- 10 - 30 Å Ta barrier layer
- 100 Å Ta barrier layer

The experiments on samples with 20 and 100 Å Ta barrier layers were carried out first by annealing for 30 min at 400, 500, 600 700 and 800˚C. These results had indicated that it could be beneficial to keep the Ta barrier quite thin (10 - 30 Å), as the 20 Å barrier seemed to lead to more uniform silicide formation than the 100 Å barrier. It would also be better to anneal more specifically in the temperature range between 500 and 640˚C, as it had been found that the 20 Å Ta diffusion barrier prevented all Co diffusion for temperatures up to 500˚C.

5.2.1 10 - 30 Å Ta barrier layer

5.2.1.1 RBS results and discussion

RBS spectra of Si<100>|Ta(10Å)|Co(1200Å) samples annealed at 560, 600 and 640˚C are shown in **Fig. 5.1.** These results show that even after annealing for 30 min at 560˚C (sample H8 **Fig. 5.1**) the 10 Å Ta diffusion barrier allowed no Co diffusion and this meant that no silicide could form, although the normal formation temperature of CoSi is 500˚C. However, the height of the Co signal indicates that a mixture of CoSi and $CoSi_2$ formed after heating for 60 min at 560˚C (sample H9). The non-homogeneous nature of the formed silicide is also indicated by the sloping shoulders of the RBS spectrum. Annealing for one hour at 600˚C (sample H13 **Fig. 5.1**) resulted in practically complete $CoSi_2$ formation, but complete uniform $CoSi_2$ (sample H17) was only formed after heating for 60 min at 640˚C, which is a higher temperature than the normal formation temperature of $CoSi_2$ (~550˚C). These results are very similar to those reported by J. Pelleg *et al*. **[80,81]** discussed in **paragraph 2.2.3**. They found that, when annealing in vacuum, a Ta barrier raised the formation temperature of both CoSi and $CoSi_2$.

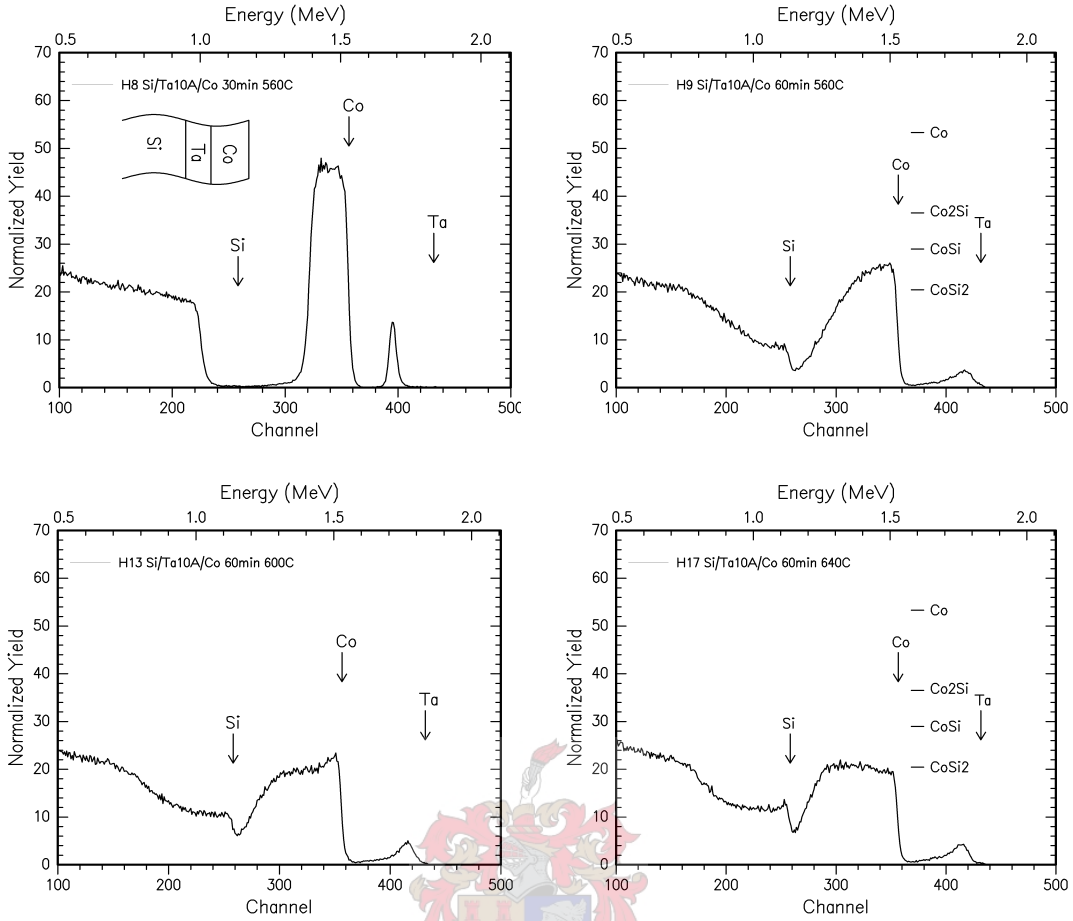

Figure 5. 1. RBS spectra of identical Si<100>|Ta(10Å)|Co(1000Å) samples annealed at 560, 600 and 640˚C. No silicide was formed even after annealing for 30 min at 560˚C and after 1h at 600˚C the $CoSi_2$ formation was still incomplete. Complete uniform $CoSi_2$ formation only occurred after heating for 60 min at 640˚C.

RBS spectra of Si<100>|Ta(20Å)|Co(1200Å) samples annealed for 30 min at temperatures from 400 to 800˚C are shown in **Fig. 5.2**. A thermal anneal of 30 min at 500˚C (sample D3 **Fig. 5.2**) still showed no silicide formation. This is due to the diffusion barrier action of the Ta barrier, which lowers the effective concentration of the Co at the growth interface so that no silicide is formed. The formation of $CoSi_2$ was incomplete after annealing for 30 min at 600˚C and the height of the Co signal indicates the presence of some CoSi formation. (sample D4 **Fig. 5.2**) The Ta signal has not moved completely to the surface energy position (sample D5), but the Ta seems to be dispersed throughout the $CoSi_2$. Complete non-uniform $CoSi_2$ formation occurred at 700 or 800˚C. The $CoSi_2$ RBS peak is overlapping the Si peak (samples D4, D5 and D6 **Fig. 5.2**), because the deposited Co layer was thick (>1200Å).

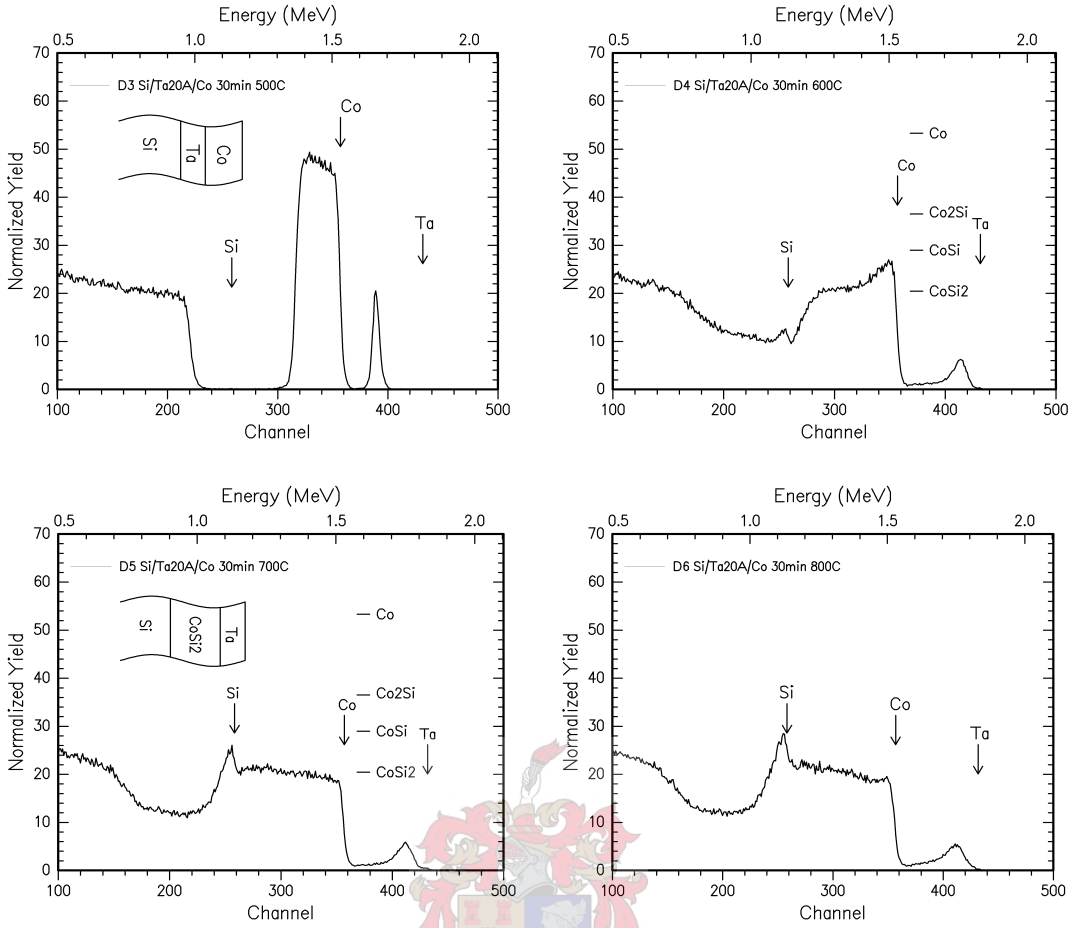

Figure 5.2. RBS spectra of identical Si<100>|Ta(20Å)|Co(1200Å) samples annealed at temperatures ranging from 500 to 800˚C. Heating for 30 min at 500˚C (sample D3) formed no silicide, but annealing at 600˚C formed mostly $CoSi_2$ with some CoSi also present. At 700 and 800˚C complete uniform $CoSi_2$ formation occurred.

A few RBS spectra of Si<100>|Ta(30Å)|Co(1200Å) samples annealed between 520 to 640˚C are shown in **Fig. 5.3.**

These RBS spectra show that even after heating for 30 min at 560˚C (sample G8 **Fig. 5.3**) the 30 Å Ta barrier allowed no diffusion of Co atoms and therefore no silicide formation occurred. After annealing at 560˚C for 60 min (sample G9) the height of the Co signal indicates that a mixture of CoSi and $CoSi_2$ formed, the sloping shoulders of the spectrum showing the non-uniformity of the silicide. Nearly complete $CoSi_2$ formation was found after heating for 60 min at 600˚C (sample G13 **Fig. 5.3**), although the height of the Co signal indicates the presence of some CoSi. The $CoSi_2$ formation was practically complete after a 60 min anneal at 640˚C (sample G17) and the $CoSi_2$ thickness uniformity was better at this temperature.

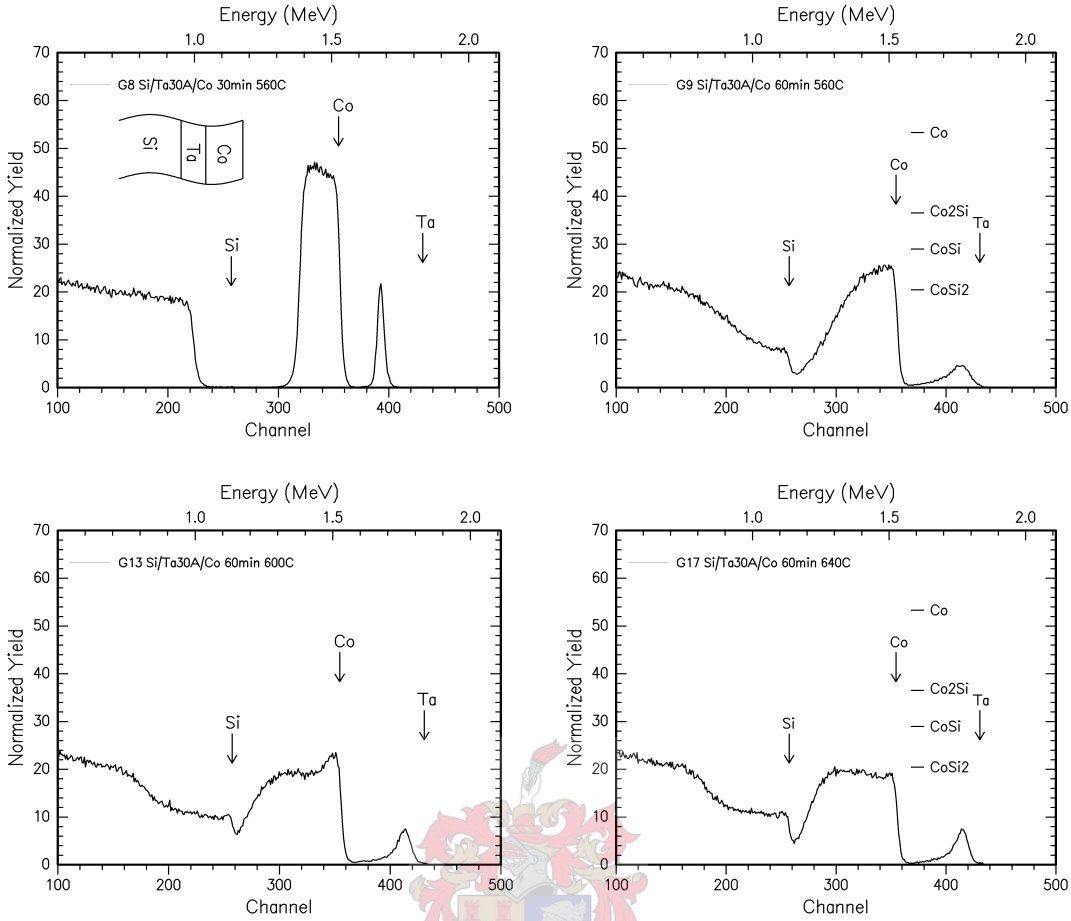

Figure 5. 3. RBS spectra of identical Si<100>|Ta(30Å)|Co(1000Å) samples annealed at 560, 600 and 640˚C. Even after heating for 30 min at 560˚C no silicide formation occurred. Nearly complete $CoSi_2$ formation was found after heating for 60 min at 600˚C (sample G13) but complete uniform $CoSi_2$ only formed after 60 min at 640˚C.

In **Fig. 5.1**, **5.2** and **5.3** the shape and position of the Ta peak in the RBS spectra after the reaction started taking place indicate that, either all of the Ta has not reached the surface, or that the Ta reached the surface and then re-diffused throughout the cobalt-disilicide. At these annealing temperatures some Ta-silicide could be present, because the normal formation temperature of $TaSi_2$ is 650˚C **[6].**

In conclusion it can be said that the thin (10, 20 and 30 Å) Ta barriers deliver very similar Co-silicide formation, i.e. prevents Co diffusion (up to about 560˚C), lowers the effective concentration of Co at the growth interface, allows the skipping of the precursor Co_2Si phase to form first phase non-uniform CoSi and aids the complete formation of uniform $CoSi_2$ after heating for 30 min at 800˚C. The barrier efficiency in preventing Co diffusion slightly improves with an increase in barrier thickness.

5.2.1.2 XRD analysis

The RBS and corresponding XRD spectra of two identical Si<100>|Ta(30Å)|Co(1000Å) samples annealed for one hour at 560 and 640˚C respectively are shown in **Fig. 5.4**. The XRD spectrum in **Fig. 5.4(a)** confirms the formation of a non-uniform mixture of CoSi and $CoSi_2$, that was indicated by the height of the Co signal in the RBS spectrum, as well as by the sloping shoulders of the RBS spectrum. From the height of the Co RBS signal in **Fig. 5.4(b)** it can clearly be seen that mostly $CoSi_2$ has formed and the thickness uniformity seems improved at this temperature. However, the XRD spectrum in (b) shows that there is some CoSi present as well. [ICDD: Si = 27-1426 ; Co_2Si = 38-1449 ; CoSi = 72-1328]

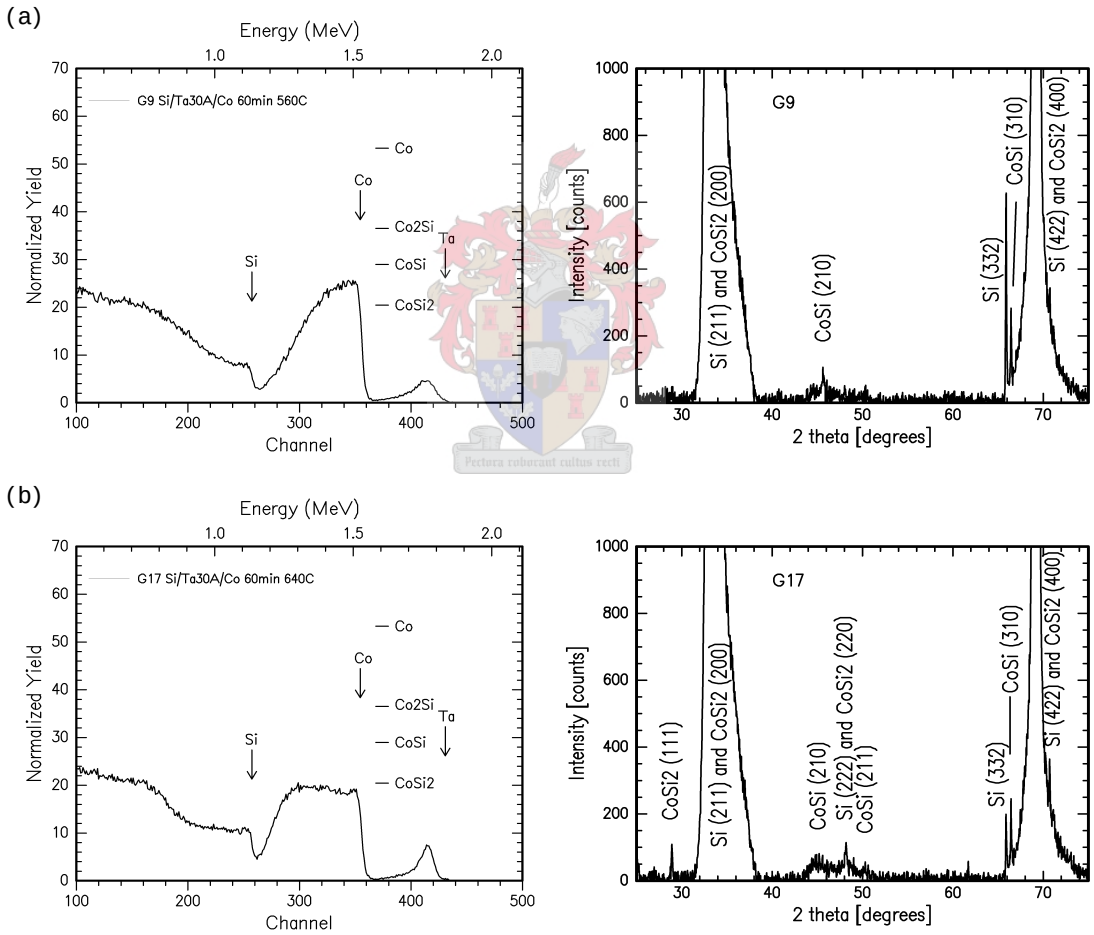

Figure 5. 4. RBS and corresponding XRD spectra of identical Si<100>|Ta(30Å)|Co(1000Å) samples annealed for one hour respectively at (a) 560˚C and (b) 640˚C. The XRD spectra confirm the presence of both CoSi and $CoSi_2$.

5.2.2 100 Å Ta barrier layer

RBS spectra of Si<100>|Ta(100Å)|Co(1200Å) samples annealed for 30 min at 600, 700 and 800˚C are shown in **Fig. 5.5.**

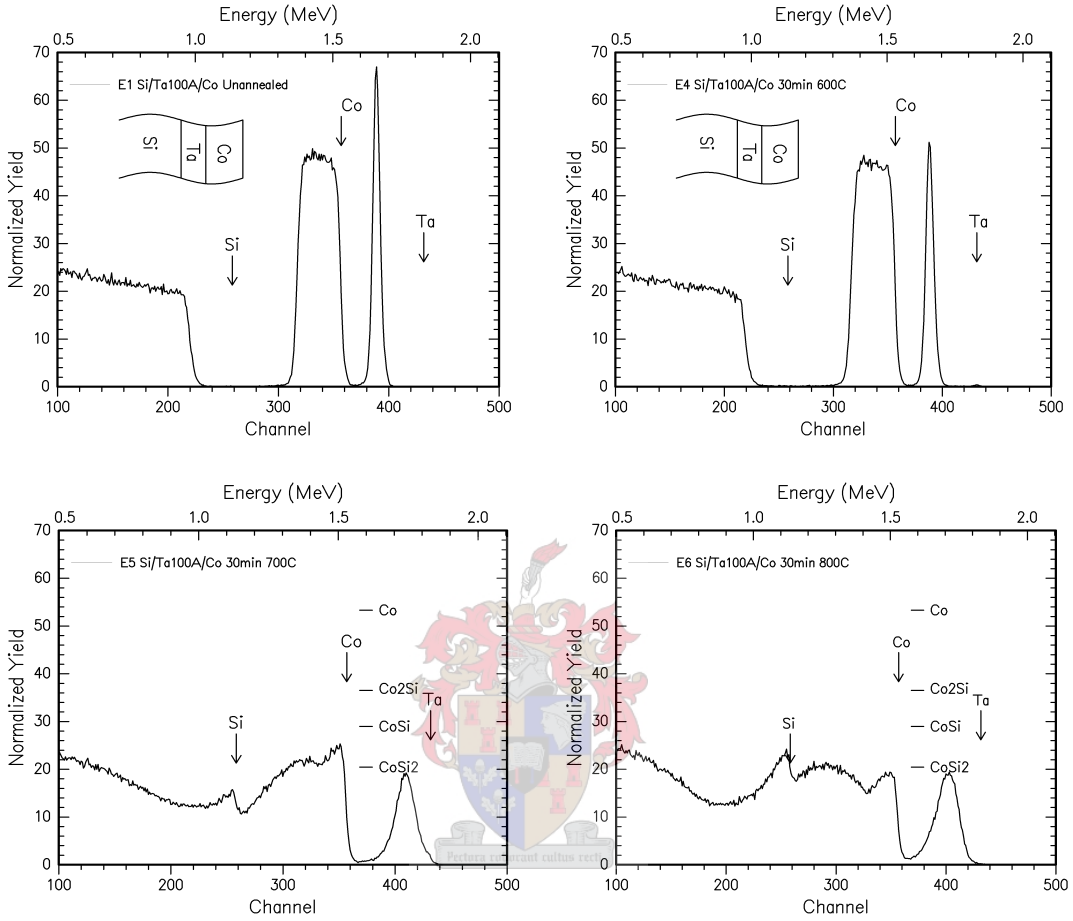

Figure 5. 5. RBS spectra of identical Si<100>|Ta(100Å)|Co(1200Å) samples annealed for 30 min at temperatures ranging from 600 to 800˚C. No reaction occurred even after annealing for 30 min at 600˚C. At 800˚C (sample E6) non-uniform $CoSi_2$ formed.

In the case of the thicker (100 Å) Ta diffusion barrier no diffusion of Co atoms through the barrier layer occurred for temperatures of up to 600˚C (sample E4 **Fig. 5.5**). At 700˚C a 30 min anneal formed mostly first phase $CoSi_2$, but the height of the Co RBS signal indicates the presence of some CoSi as well. Heating at 800˚C (sample E6 **Fig. 5.5**) completely formed non-uniform $CoSi_2$. In the spectra of samples E5 and E6 the Ta seems to be dispersed throughout the $CoSi_2$ like in the case of the thinner Ta barriers. This is confirmed by the position of the Ta signal in the RBS spectra which is not at the Ta surface energy position.

5.3 Si<100> | Ta (30Å) | Co | Ta $_{cap}$ system

As can be seen from **Table 2.6** in **Chapter 2** no research has previously been done using a Ta capping layer in conjunction with a Ta barrier layer in the Si-Co system. In this study the effect of a 30 Å Ta diffusion barrier and a Ta capping layer *combination* on the formation of Co-silicides was investigated and the following Ta capping layers were used:

- 30 Å Ta capping layer
- 60 Å Ta capping layer
- 100 Å Ta capping layer
- 150 Å Ta capping layer

As the 30 Å Ta diffusion barrier had previously prevented any reaction between the Co and the Si for temperatures up to 500˚C, it was decided to keep the annealing temperatures between 500 and 640˚C for these experiments with the added Ta capping layers of varying thicknesses.

5.3.1 30 Å Ta capping layer

RBS spectra of Si<100>|Ta(30Å)|Co(1000Å)|Ta$_{cap}$(30Å) samples annealed for 30 min at 560, 600 and 640˚C are shown in **Fig. 5.6.**

The presence of both a Ta 30 Å barrier layer and a Ta 30 Å capping layer yielded results that were very similar to those with only the Ta barrier layer present. No reaction occurred even after heating at temperatures of up to 560˚C (sample B5 **Fig. 5.6**). First reaction occurred after heating for 30 min at 600˚C (sample B6) and formed mainly CoSi, with the presence of some $CoSi_2$ indicated by the height of the Co RBS signal and non-uniformity shown by the sloping shoulders of the spectrum. A 30 min anneal at 640 ˚C resulted in $CoSi_2$ formation that was still incomplete (some CoSi present) and non-uniform (sample B7) and the Ta barrier is dispersed through the cobalt-silicide (samples B6 and B7).

The Ta capping layer remained unreacted at the surface in the as-deposited position throughout all heating as can be seen by signal at the Ta surface position on all the RBS spectra in **Fig. 5.6.** The diffusion of the Co through the Ta diffusion barrier is indicated by the motion of the Ta barrier signal towards the Ta surface position. An interesting aspect of the diffusion was that all the Ta of the barrier layer

did not move completely to the surface position, but the Ta of the barrier seemed to end up being dispersed through the top part of the silicide layer, close to the surface of the sample, probably because of the formation of $TaSi_2$.

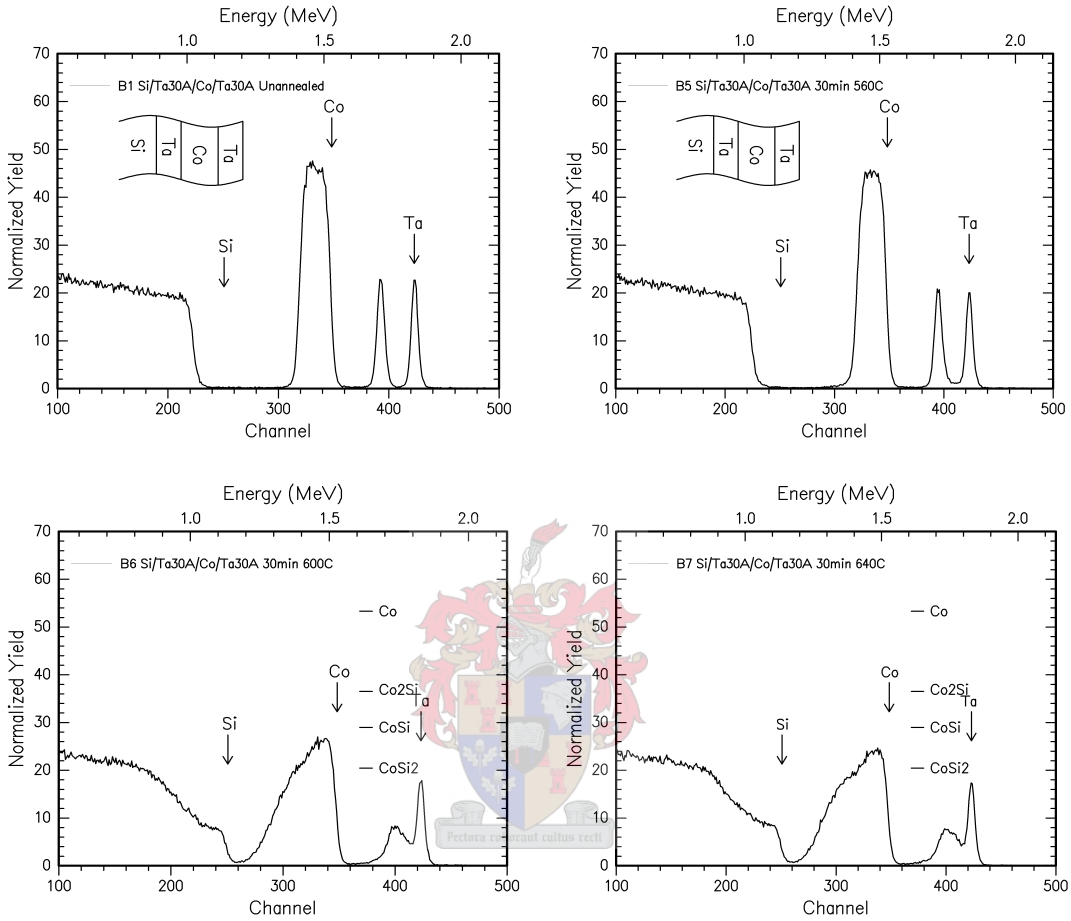

Figure 5. 6. RBS spectra of identical Si<100>|Ta(30Å)|Co(1200Å)|Ta_{cap}(30Å) samples annealed for 30 min at 560, 600 and 640˚C. No reaction was found at 560˚C and heating at 600 formed a non-uniform mixture of CoSi and $CoSi_2$. At 640˚C mostly $CoSi_2$ formed, but also some CoSi.

5.3.2 60 Å Ta capping layer

RBS spectra of Si<100>|Ta(30Å)|Co(1000Å)|Ta_{cap}(60Å) samples annealed for 30 min at temperatures from 500 to 640˚C are shown in **Fig. 5.7.**

The use of the 60 Å Ta capping layer slightly lowered the temperature at which first reaction occurred from 600 to 540˚C (**Fig. 5.7** sample C4), completely forming first phase CoSi, as can be seen from the height of the Co RBS signal, but the sloping shoulders of the spectrum indicates that the CoSi is non-uniform. This skipping of the usual first phase formation of Co_2Si occurs due to the lowering of the

effective concentration of Co at the growth interface caused by the Ta barrier. This formation temperature of 540˚C for CoSi is slightly higher than the normal formation temperature of 500˚C.

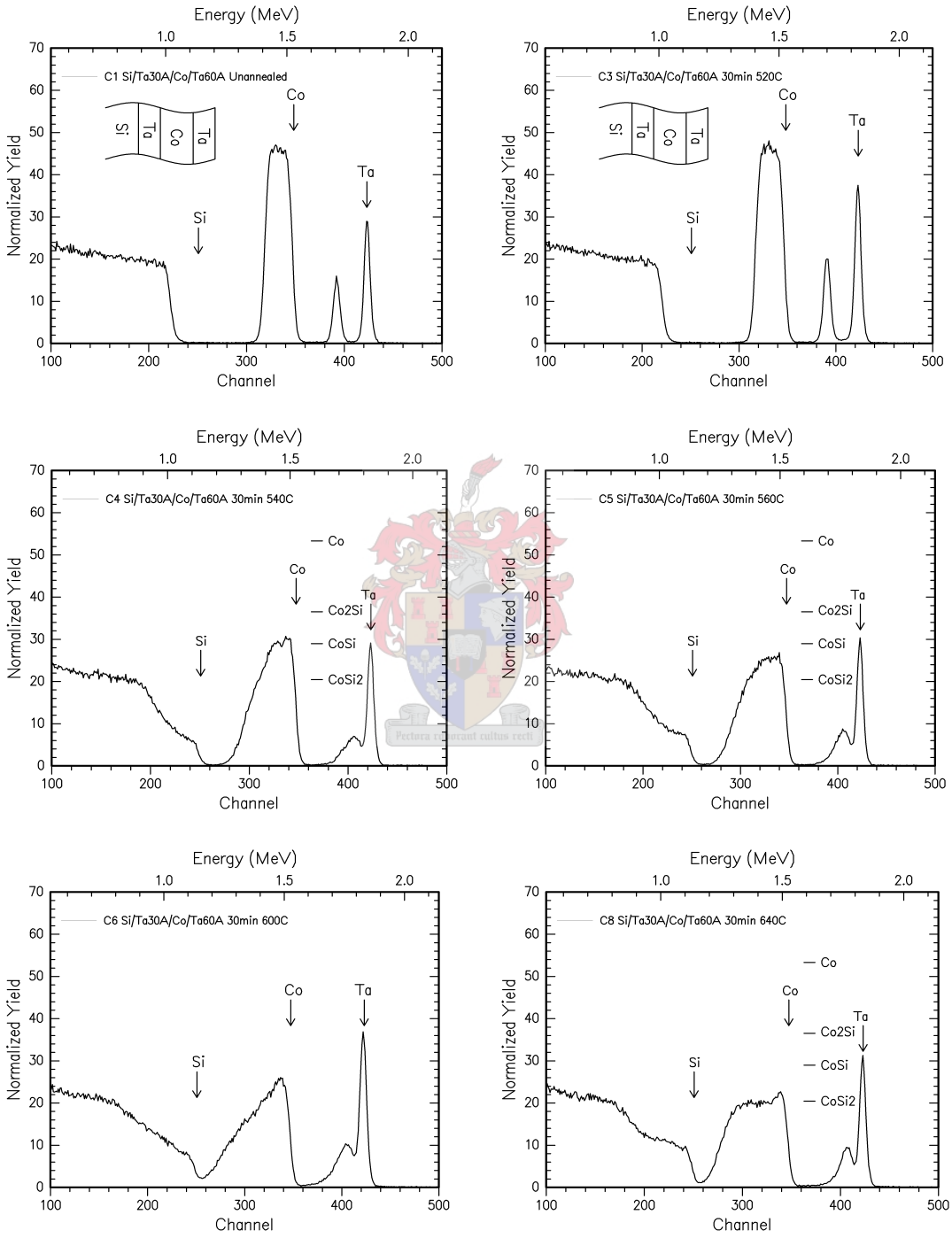

Figure 5. 7. RBS spectra of identical Si<100>|Ta(30Å)|Co(1000Å)|Ta_{cap}(60Å) samples annealed at temperatures ranging from 500 to 640˚C. At 540˚C non-uniform first phase CoSi formed and heating at 640˚C resulted in the nearly complete formation of uniform $CoSi_2$ (sample C8).

A 30 min anneal at 560˚C formed a non-uniform mixture of CoSi and $CoSi_2$ (sample C5) and at 600˚C the silicide is very non-uniform. However, heating for 30 min at 640˚C resulted in the nearly complete formation of uniform $CoSi_2$. (sample C8). The Ta from the barrier is again dispersed throughout the cobalt-disilicide while the Ta capping layer stayed completely in the surface position, as can be seen on all the RBS spectra in **Fig. 5.7**.

5.3.3 100 Å Ta capping layer

RBS spectra of Si<100>|Ta(30Å)|Co(1000Å)|Ta_{cap}(100Å) samples annealed for 30 min at 560, 600 and 640˚C are shown in **Fig. 5.8**.

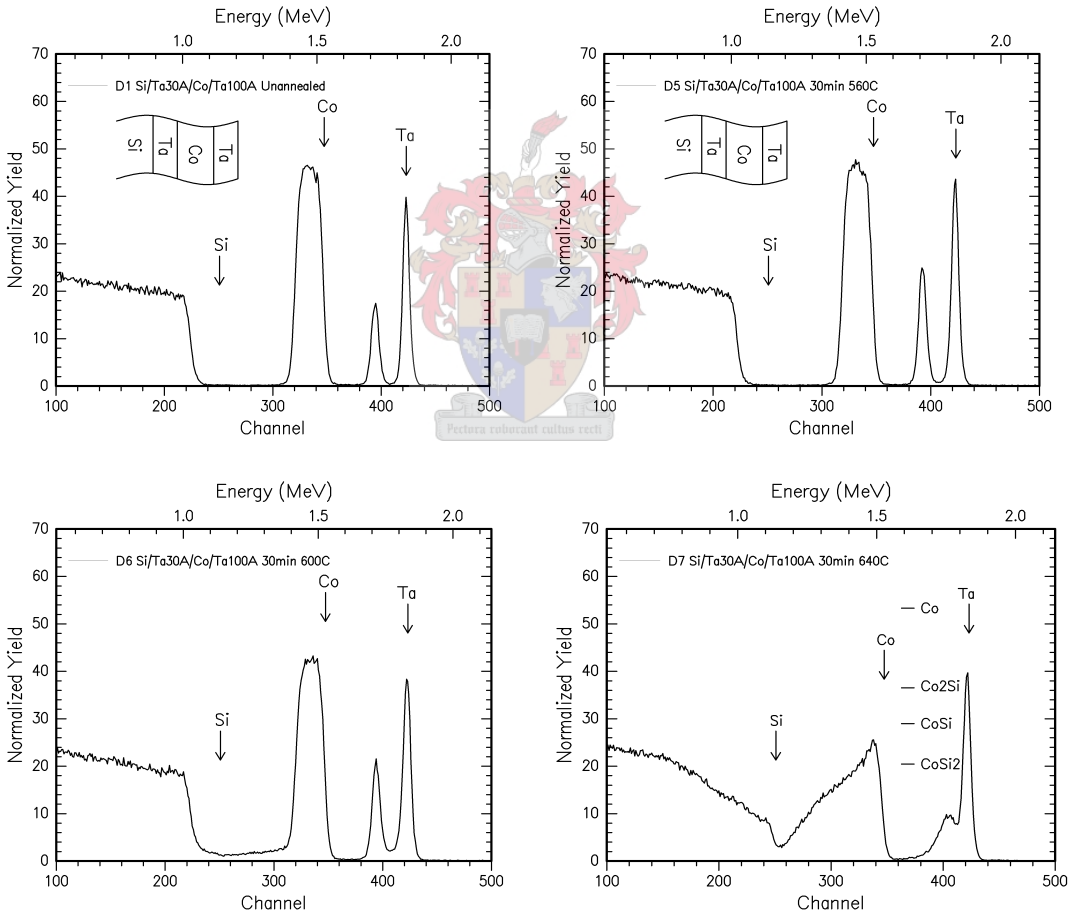

Figure 5. 8. RBS spectra of identical Si<100>|Ta(30Å)|Co(1000Å)|Ta_{cap}(100Å) samples annealed at 560, 600 and 640˚C. No reaction occurred up to 600˚C, but at 640˚C non-uniform $CoSi_2$ formed.

The presence of both the Ta barrier and the thicker (100 Å) Ta capping layer resulted in no reaction occurring between the Co and the Si even after annealing for

30 min at 600˚C (sample D6 **Fig. 5.8**). However, after heating for 30 min at 640˚C the height of the Co RBS signal indicates the first phase formation of very non-uniform $CoSi_2$ (the non-uniformity indicated by the sloping shoulders of the RBS spectrum). The Ta barrier moved closer to the surface as the Co diffused through it, while the Ta cap remained in the as-deposited position at the surface of the sample.

5.3.4 150 Å Ta capping layer

RBS spectra of Si<100>|Ta(30Å)|Co(1000Å)|Ta_{cap}(150Å) samples annealed for 30 min at 560, 600 and 640˚C are shown in **Fig. 5.9.**

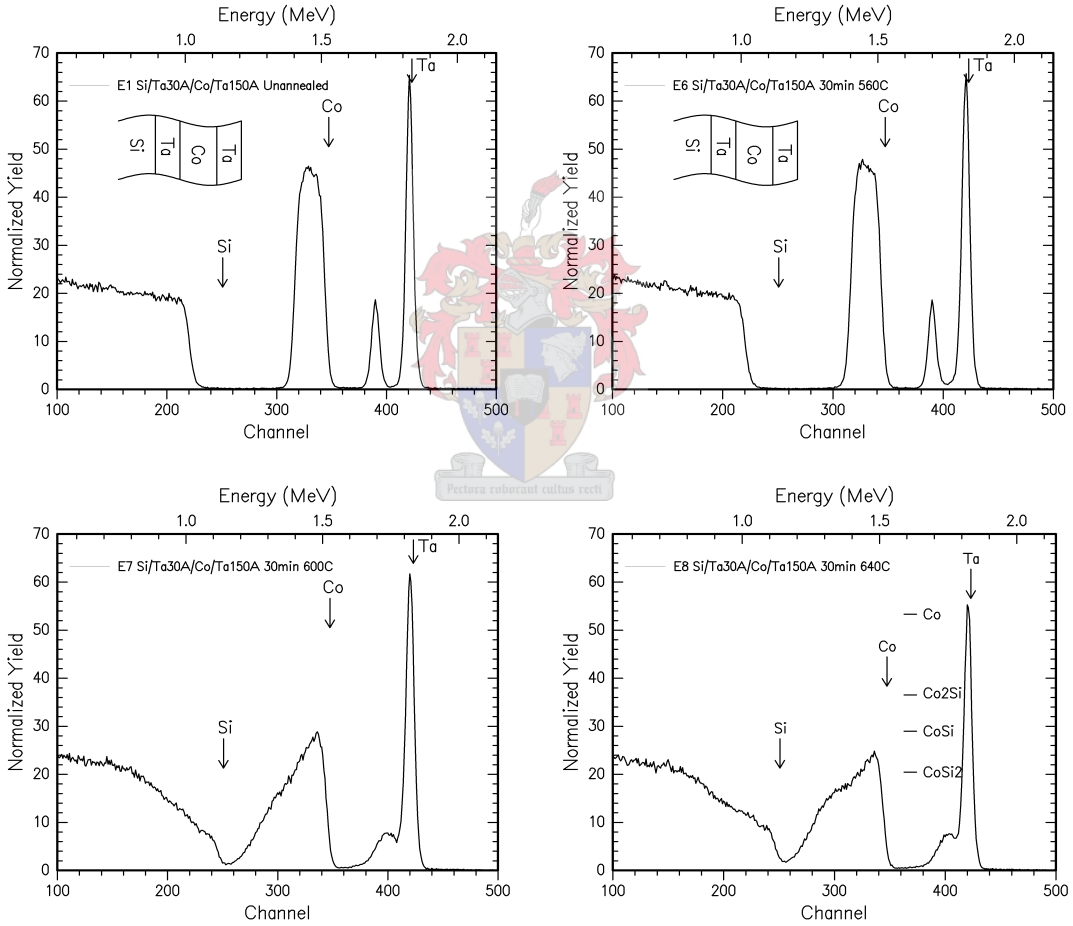

Figure 5. 9. RBS spectra of identical Si<100>|Ta(30Å)|Co(1000Å)|Ta_{cap}(150Å) samples annealed at 560, 600 and 640˚C. Heating for 30 min at 600˚C formed a non-uniform mixture of CoSi and $CoSi_2$ (sample E7) and annealing for 30 min at 640˚C formed more $CoSi_2$ than CoSi.

The presence of both the Ta barrier and the thick (150 Å) Ta capping layer resulted in no reaction occurring even after heating for 30 min at 560˚C (sample E6

Fig. 5.9). However, after heating for 30 min at 600˚C the height of the Co RBS signal indicated the formation of a non-uniform mixture of CoSi and $CoSi_2$ (the non-uniformity indicated by the sloping shoulders of the RBS spectrum). More $CoSi_2$ formed at 640˚C, but there was still some CoSi present as indicated by the height of the Co signal.

In conclusion it seems that the Ta barrier and cap combination does not significantly change the silicide formation of the Si|Ta(30Å)|Co system. Only the 60Å Ta capping layer had two beneficial effects: it allowed the complete formation of first phase CoSi (non-uniform) at 540˚C and it improved the uniformity of the $CoSi_2$ formed at 640˚C as can be seen in **Fig. 5.10** which compares the RBS spectra of samples having different Ta caps heated for 30 min at 640˚C.

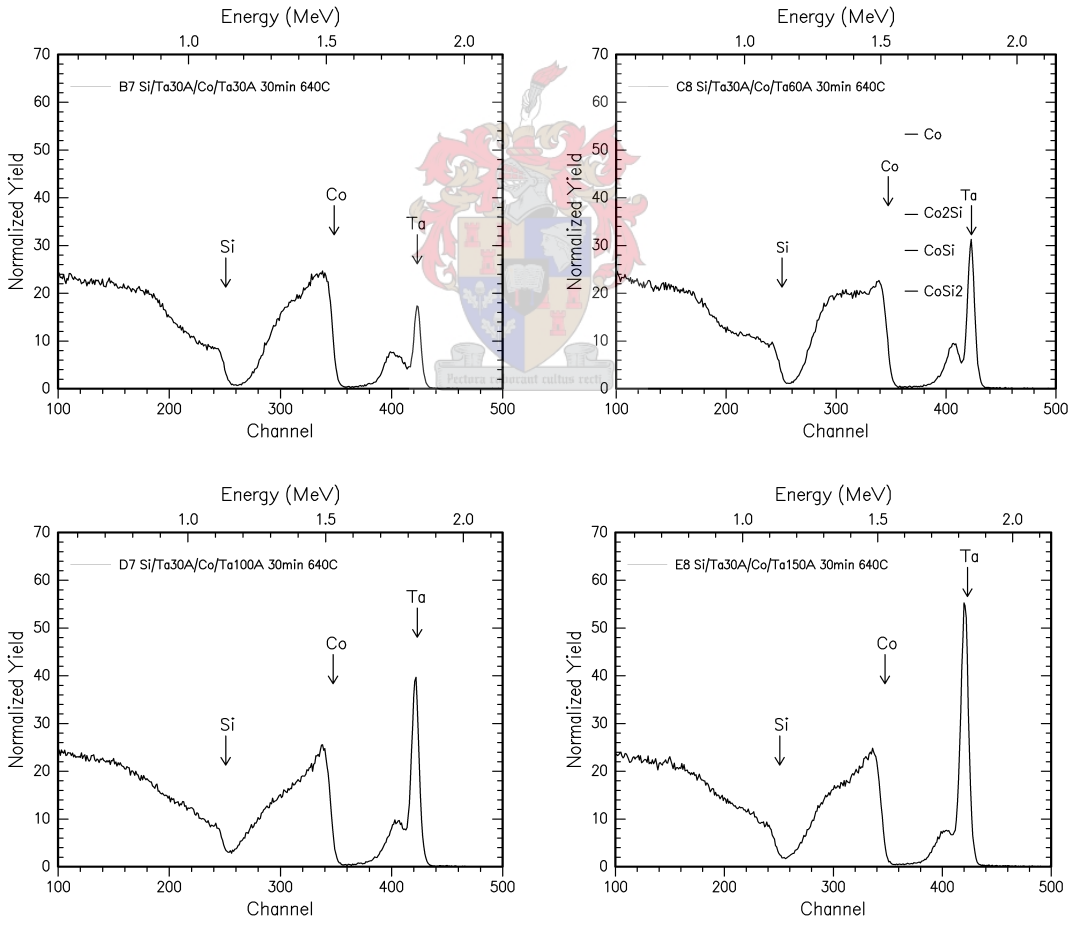

Figure 5. 10. RBS spectra of Si|Ta(30Å)|Co|Ta_{cap} samples having different thickness Ta caps, all annealed at 640˚C. Only the 60 Å Ta cap (sample C8) improved the uniformity of the $CoSi_2$.

5.4 Si <100> | Ti | Co system

As can be seen from **Table 2.6** in **Chapter 2** the use of Ti as a diffusion barrier in the Si/Co system has been very intensively researched. The results of this research was discussed in detail in **paragraph 2.2.1.** In this investigation of the effects of a titanium diffusion barrier on the formation of cobalt-silicides the following Ti barriers were used:

- 10 – 30 Å Ti barrier layer
- 100 Å Ti barrier layer

5.4.1 10 - 30 Å Ti barrier layer

The RBS spectra of Si<100>|Ti(10Å)|Co(1200Å) samples annealed at temperatures from 520 to 640˚C are shown in **Fig. 5.11.**

Using a 10 Å Ti diffusion barrier layer we found quite uniform first phase formation of CoSi after annealing for 20 min at 520˚C (sample D3 **Fig. 5.11**). This again is an example of a successful application of CCPS, because the presence of the 10 Å Ti diffusion barrier lowered the effective concentration of Co at the growth interface, resulting in the skipping of the usual first phase formation of Co_2Si in favour of the first phase formation of CoSi.

This skipping of the Co_2Si precursor phase in the ordinary Co-Si reaction was also reported by other groups **[12,19,26,51]** as discussed in **paragraph 2.2.1**. However, most of the other research using Ti barriers in non-reactive ambient (vacuum) showed the formation of epitaxial first phase $CoSi_2$ **[14,28-36].** The difference in our results could be due to the fact that the Ti layer used was very thin and could therefore not successfully lower the effective concentration of the Co to enable the formation of $CoSi_2$ as first phase.

The so-called “layer-reversal of the Ti and Co” (also mentioned in **paragraph 2.2.1**) was not visible here on the RBS spectra, as the movement of the very small Ti RBS signal to the right as the Co diffused through it was completely overlaid by the Co-silicide signal. (The Ti peak on the RBS spectrum is so small because, obviously, the Ti layer is physically very thin, but also because of the relatively low atomic number of Ti, which results in a weaker backscattered signal from it). In this case the formation temperature of 520 or 560˚C for CoSi is higher than the normal formation temperature (500˚C). This result is similar to the case of the Ta barrier, where an

increased formation temperature was also reported **[80,81],** but the only other groups using Ti barriers who found this increased formation temperature for CoSi were those annealing in an N_2 ambient **[18,53-56]**.

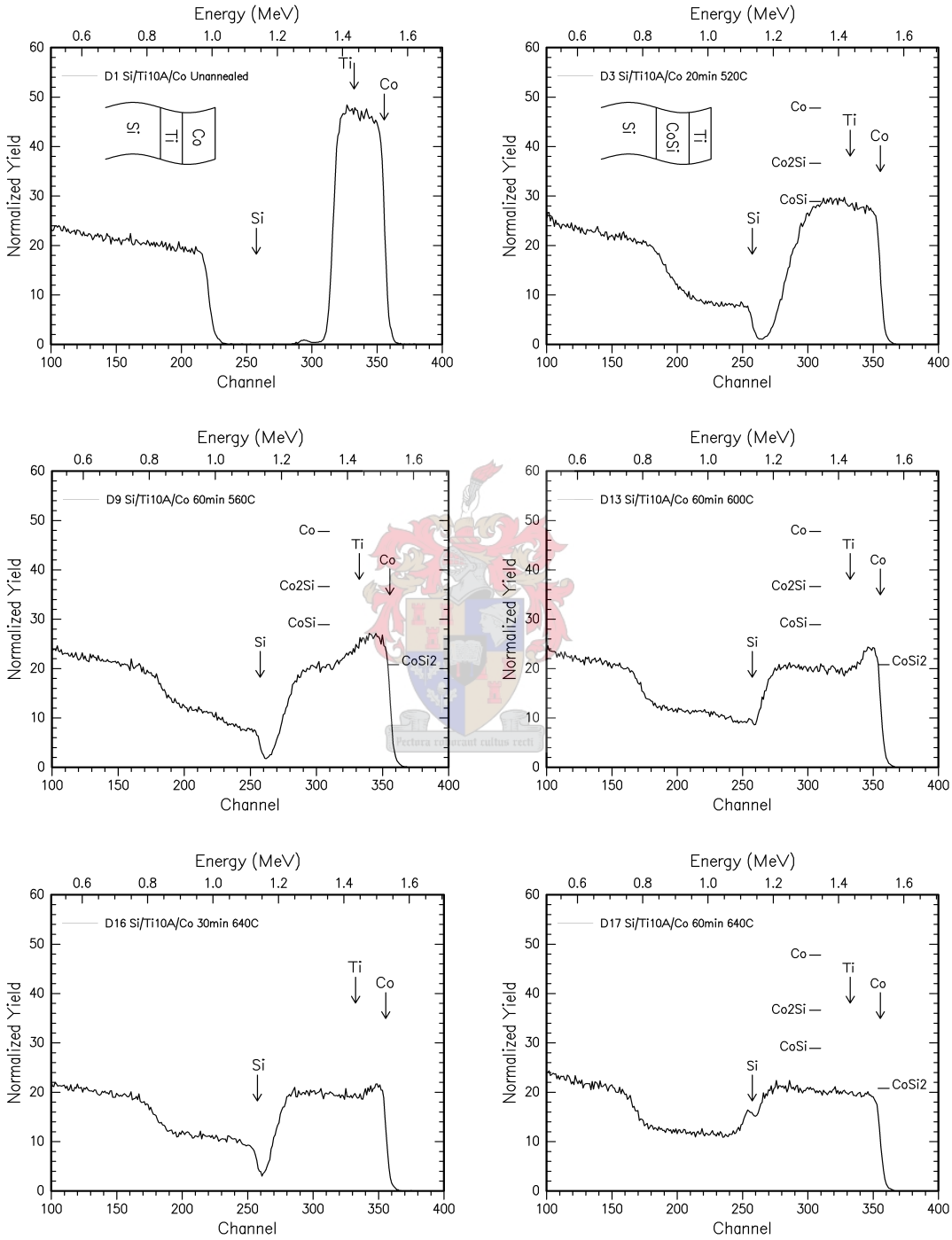

Figure 5. 11. RBS spectra of identical Si<100>|Ti(10Å)|Co(1200Å) samples annealed at temperatures ranging from 520 to 640˚C. Sample D3 shows uniform first phase formation of CoSi after annealing for 20 min at 520˚C. Heating at 560˚ started the formation of $CoSi_2$ and at 600˚C the $CoSi_2$ formation is nearly complete. Complete uniform $CoSi_2$ formed at 640˚C (sample D17).

Heating at 560˚C started the formation of $CoSi_2$ and resulted in a non-uniform mixture of CoSi and $CoSi_2$ (sample D9 **Fig. 5.11**). The sample annealed at 600˚C shows nearly complete $CoSi_2$ formation, although the height of the Co signal indicates the formation of some CoSi as well. Annealing for 30 min at 640˚C (sample D16) has nearly completed the formation of quite uniform $CoSi_2$, with only a little CoSi present. In all the spectra it is impossible to see if the thin Ti barrier signal is at the surface position or not, because it is such a small amount of Ti that it is completely overlaid by the broad Co-silicide signal (1200 Å Co layer). A one hour thermal anneal at 640˚C resulted in the complete formation of uniform $CoSi_2$ (sample D17 **Fig. 5.11**).

The 20 Å Ti diffusion barrier also retarded the diffusion of Co atoms up to 500˚C like the 10 Å Ti barrier did. RBS spectra of Si<100>|Ti(20Å)|Co(1200Å) samples annealed for 30 min at 600 and 800˚C are shown in **Fig. 5.12.** A thermal anneal of 30 min at 600˚C (sample B4) formed uniform $CoSi_2$, but the height of the Co RBS signal also indicates the presence of some CoSi. Uniform $CoSi_2$ formed at 800˚C (sample B7).

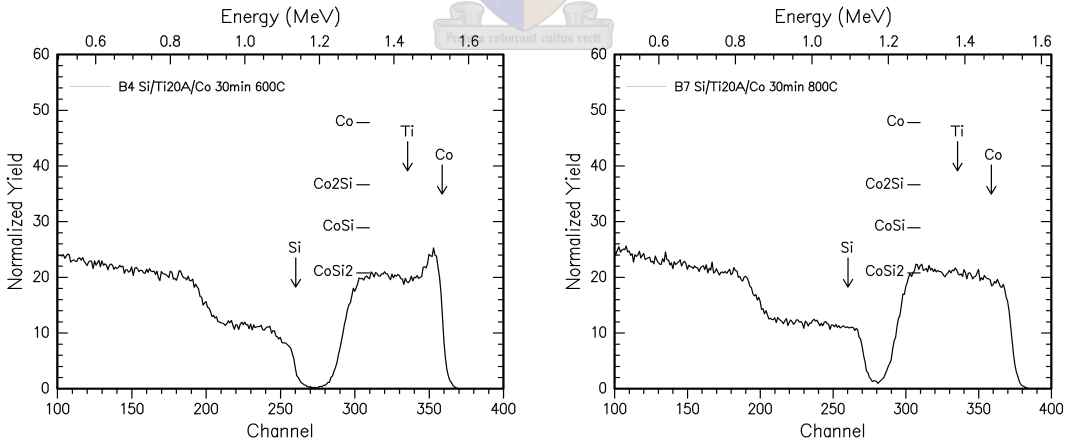

Figure 5. 12. RBS spectra of identical Si<100>|Ti(20Å)|Co(1200Å) samples annealed for 30 min at 600 and 800˚C. At 600˚C mostly Co_2Si formed, but some CoSi was also present. Uniform $CoSi_2$ formed after annealing for 30 min at 800˚C (sample B7).

RBS spectra of samples of the Si<100>|Ti(30Å)|Co(1200Å) system annealed from 520 to 640˚C are shown in **Fig. 5.13.** When this slightly thicker (30 Å) Ti barrier layer was used, the first signs of Co diffusion occurred after annealing for 10

min at 520˚C (sample C2 **Fig. 5.13**), whereas in the case of the thin (10Å) Ta barrier complete CoSi formation had occurred after a 20 min anneal at 520˚C (sample D3 **Fig. 5.11**). It seems that the thicker the Ti diffusion barrier, the better it retards the diffusion of Co atoms towards the Si substrate. This is in keeping with the findings of other groups who reported that increasing the Ti interlayer thickness increases its efficiency as a diffusion barrier **[33-36]**.

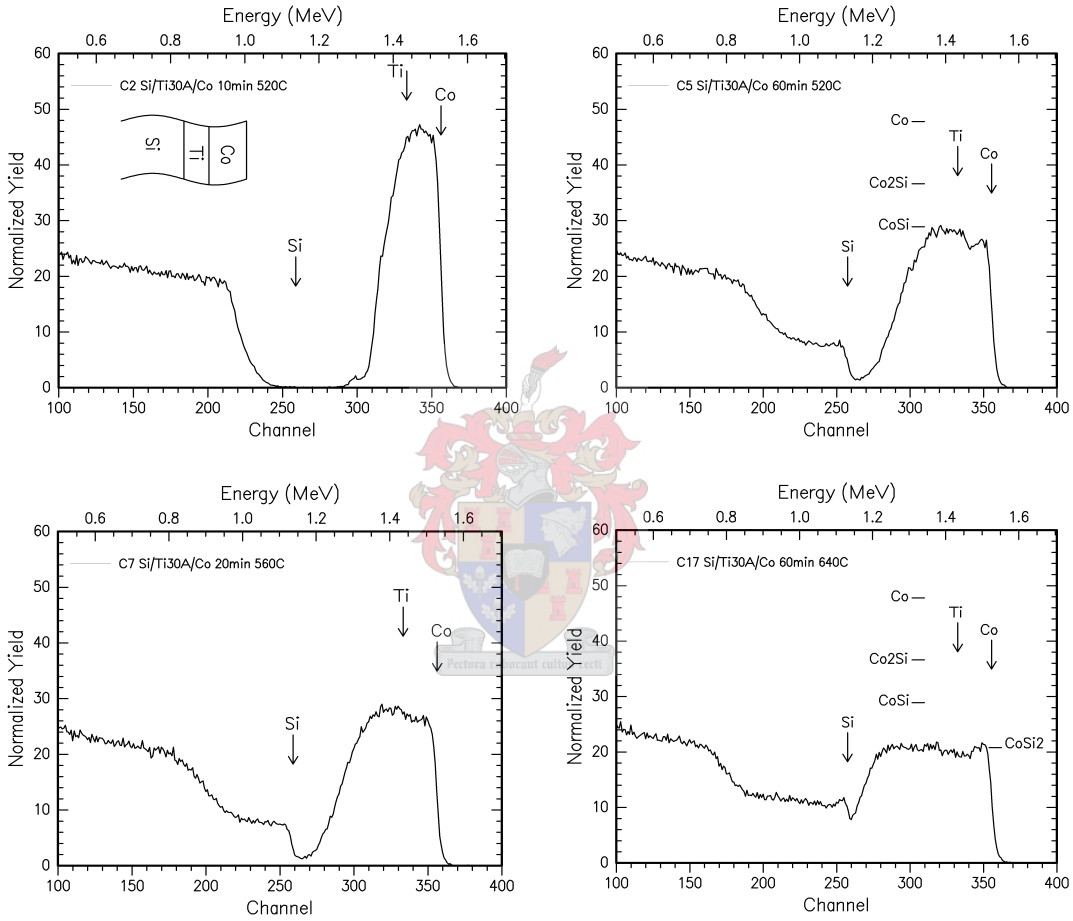

Figure 5. 13. RBS spectra of identical Si<100>|Ti(30Å)|Co(1200Å) samples annealed at 520 to 640˚C. The first reaction between the Co and the Si only occurred at 520˚C. At 640˚C the formation of quite uniform $CoSi_2$ is practically complete (sample C17).

A thermal anneal of one hour at 520˚C (sample C5) formed first phase CoSi, that was slightly non-uniform as indicated by the sloping shoulders of the RBS spectrum. Annealing for 20 min at 560˚C completely formed quite uniform first phase CoSi (sample C7). After heating for one hour at 640˚C the formation of

uniform $CoSi_2$ is practically complete (sample C17 **Fig. 5.13**), but the height of the Co RBS signal indicates the presence of some CoSi as well.

5.4.2 100 Å Ti barrier layer

The RBS spectra of samples of the Si<100>|Ti(100Å)|Co(1200Å) system annealed for 30 min at temperatures from 520 to 640˚C are shown in **Fig. 5.14.**

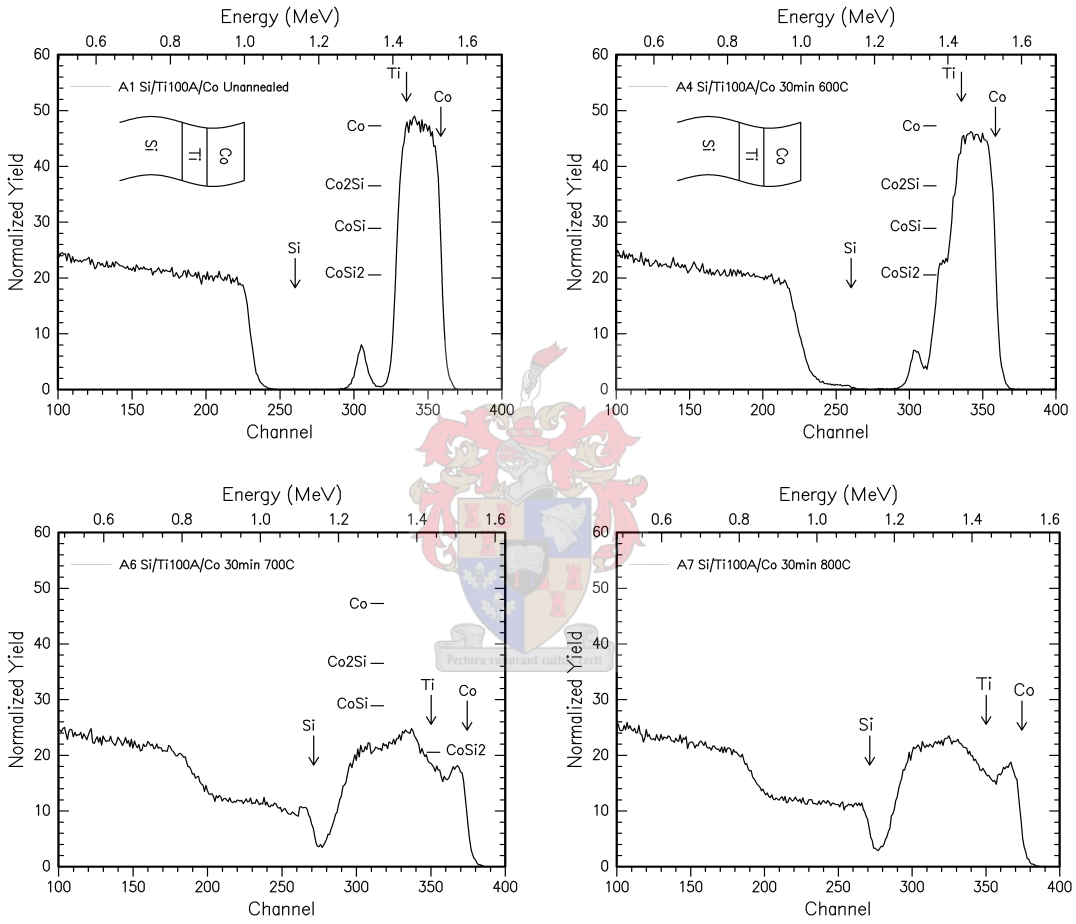

Figure 5. 14. RBS spectra of identical Si<100>|Ti(100Å)|Co(1200Å) samples annealed for 30 min at 600, 700 and 800˚C. At 600˚ $CoSi_2$ started to form, but most of the Co remained unreacted. At 700 or 800˚C very non-uniform $CoSi_2$ has formed.

For the 100 Å Ti diffusion barrier the reaction between the Co and the Si only started after heating for 30 min at 600˚C (sample A4 **Fig. 5.14**) and the height of the Co signal in the RBS spectrum indicates that $CoSi_2$ had started to form as first phase, but that most of the Co remained unreacted. Annealing at 700 or 800˚C formed very non-uniform $CoSi_2$. (samples A6 and A7 **Fig. 5.14**).

5.5 Summary and conclusions

Chapter 5 reported on the effect of the use of Ta and Ti diffusion barrier layers on silicide formation in the Co-Si system and a summary of the results of the investigation is given in **Table 5.1.**

The use of the thinner (10, 20 and 30 Å) Ta diffusion barriers for the Co-Si system retarded the Co diffusion for annealing temperatures of up to 560˚C. At 560˚C CoSi started to form as first phase. The presence of the Ta barrier lowers the effective concentration of the Co at the growth interface, thus skipping the formation of the Co_2Si precursor phase. Annealing for 1h at 560˚C formed a mixture of mostly CoSi and some $CoSi_2$ (as confirmed by XRD measurements). Nearly complete and more uniform $CoSi_2$ formation was found after annealing for one hour at 640˚C. The thicker (100 Å) Ta barrier layers retarded the diffusion of Co atoms through the barrier layer for temperatures of up to about 650˚C. Annealing at 700˚C formed mostly $CoSi_2$, but the height of the Co RBS signal indicated the presence of some CoSi. Heating at 800˚C formed non-uniform $CoSi_2$. The position of the Ta RBS signal in all spectra indicates that the Ta is not at the surface of the sample after silicide formation, but is spread throughout the silicide. It is interesting to note that both the $CoSi_2$ formation temperature of 560˚C through the thin Ta barrier and 700˚C through the thicker Ta barrier are higher than the formation temperature of $CoSi_2$ (about 550˚C) without a barrier present. Another group **[80,81]** also reported that the presence of a Ta diffusion barrier raised the formation temperature of both the CoSi and $CoSi_2$ phases.

In **Chapter 4** it was seen that during Ni-silicide formation through Ta barriers the Ta barrier moves completely to the surface with hardly any spreading taking place. However, during Co-silicide formation through Ta barriers a considerable amount of Ta spreading takes place in the silicide.

The addition of Ta capping layers of different thicknesses *in conjunction* with a 30 Å Ta diffusion barrier layer did not significantly change or improve the silicide formation of the Si|Ta(30Å)|Co system. Only the 60 Å Ta capping layer aided the formation of CoSi as first phase at 540˚C and slightly improved the thickness uniformity of the $CoSi_2$ that formed at 640˚C. Generally the use of Ta capping layers resulted in less uniformity of thickness for all the silicides that formed.

Table 5. 1. Co-silicide formation through Ta and Ti diffusion barrier layers.

COBALT-SILICIDE FORMATION THROUGH BARRIER LAYERS			
BARRIER	**TEMP (˚C)**	**SILICIDE FORMATION**	**THICKNESS UNIFORMITY**
Ta 10 - 30 Å	500	no reaction	
	560	30 min no reaction 1h CoSi and $CoSi_2$	non-uniform
	600	$CoSi_2$ some CoSi	non-uniform
	640	$CoSi_2$	uniform
	700	$CoSi_2$	uniform
	800	$CoSi_2$	uniform
Ta 100 Å	600	no reaction	
	700	$CoSi_2$ some CoSi	non-uniform
	800	$CoSi_2$	non-uniform
Ta 30 Å (30 Å cap)	560	no reaction	
	600	CoSi and $CoSi_2$	non-uniform
	640	CoSi and $CoSi_2$	non-uniform
Ta 30 Å (60 Å cap)	520	no reaction	
	540	first phase CoSi	non-uniform
	560	CoSi and $CoSi_2$	non-uniform
	600	CoSi and $CoSi_2$	very non-uniform
	640	$CoSi_2$	uniform
Ta 30 Å (100 Å cap)	600	no reaction	
	640	CoSi and $CoSi_2$	very non-uniform
Ta 30 Å (150 Å cap)	560	no reaction	
	600	CoSi and $CoSi_2$	very non-uniform
	640	CoSi and $CoSi_2$	non-uniform
Ti 10 - 30 Å	400	no reaction	
	520	first phase CoSi	uniform
	560	CoSi some $CoSi_2$	uniform
	640	$CoSi_2$	uniform
	800	$CoSi_2$	uniform
Ti 100 Å	500	no reaction	
	600	$CoSi_2$ most Co unreacted	incomplete
	700	$CoSi_2$	very non-uniform
	800	$CoSi_2$	very non-uniform

The use of thinner (10, 20 and 30 Å) Ti barrier layers resulted in the skipping of the Co_2Si precursor phase and the formation of quite uniform first phase CoSi at 520˚C, which is slightly higher than the formation temperature (500˚C) of CoSi without a barrier present. Uniform $CoSi_2$ started forming at 560˚C and remained uniform at higher temperatures. The thicker (100 Å) Ti barrier lowered the effective concentration of Co at the growth interface to such an extent that $CoSi_2$ started to

form directly as first phase after annealing for 30 min at 600˚C, but most of the Co metal still remained unreacted. At 700 and 800˚C very non-uniform $CoSi_2$ formed. The Ti RBS signal is mostly not clearly visible at the Ti surface energy position, because the relatively low atomic number of Ti causes weaker back scattering form it, particularly when the Ti layer is thin. With the thicker Ti barrier the Ti RBS signal is visible at 800˚C, but quite broad, showing the spreading of the Ti into the $CoSi_2$.

In conclusion it can be said that the presence of a *thinner* Ta or Ti diffusion barrier layer lowers the effective concentration of Co at the growth interface and this results in the skipping of the formation of Co_2Si as first phase. The thin Ti barrier formed uniform CoSi as first phase at 520˚C, whereas the thin Ta barrier formed mainly $CoSi_2$ as first phase at 560˚C, although the height of the Co signal indicated the presence of some CoSi as well. This was confirmed by XRD measurements. The use of both Ti and Ta thin barriers formed uniform $CoSi_2$ at 560˚C and after thermal anneals at higher temperatures (up to 800˚C) the thickness of the di-silicide layer was uniform for both barriers.

The *thicker* Ta and Ti barriers were more effective in retarding the diffusion of the Co atoms than the thinner barriers, the thicker Ta barriers preventing any reaction from occurring up to quite high annealing temperatures (up to 700˚C for Ta and 600˚C for Ti). The $CoSi_2$ formation through the thicker Ti barrier at 600˚C, however, was still incomplete and at higher temperatures, (up to 800˚C) the di-silicide that formed through both thicker barriers was non-uniform. The thicker Ta and Ti barriers did not perform as well as the thinner ones at promoting the growth of uniform layers of $CoSi_2$ at higher temperatures.

Some general conclusions can be drawn for the formation of Co-silicides through Ta and Ti diffusion barriers. Firstly, no silicide formation at all occurred at temperatures below 520˚C and the Co-silicide formation was generally more uniform at all temperatures when thin barriers were used. The thin Ti barrier delivered better uniformity at lower temperatures, although generally the uniformity improved with an increase in temperature. In all cases $CoSi_2$ first formed at 560˚C or above, which is higher than the formation temperature of $CoSi_2$ without a barrier. Generally it was found that the thicker the barrier, the higher the temperature of Co-silicide formation. Finally, Ta capping layers did not seem to improve the quality of the formed silicide and in some cases resulted in greater non-uniformity.

Chapter 6

Fe-SILICIDE FORMATION THROUGH BARRIER LAYERS

6.1 Introduction

The Fe-Si phase- and corresponding EHF diagram are shown in **Fig. 6.1**. On the phase diagram four compound phases can be seen as well as two liquidus minima, situated on both sides of the $Fe_{50}Si_{50}$ position. The four compound phases are Fe_2Si, Fe_5Si_3, FeSi and $FeSi_2$. The silicides FeSi and $FeSi_2$ occur in several polymorphic structures that are not all stable under equilibrium conditions. Some of these phases are only formed in thin film structures on crystalline Si substrates where the equilibrium form of the mono-silicide is indicated as εFeSi and the equilibrium forms of the di-silicides are indicated as $\alpha FeSi_2$ and $\beta FeSi_2$.

The first phase to form in thin film studies is usually the εFeSi phase at a temperature of about 500˚C **[6].** The EHF model states that the first phase to form will be the one with the most negative effective heat of formation ($\Delta H'$) at the concentration of the liquidus minimum. In this case the system has to choose between the two liquidus minima namely at 1212 and 1220˚C and seems to opt for an effective concentration in the middle of the two liquidus minima, where FeSi is thermodynamically favoured. Subsequent phase formation depends on the relative thickness of the Fe and the Si. In the case of a Si substrate the system has an excess of Si and therefore the most Si rich $FeSi_2$ phase, i.e. $\beta FeSi_2$ forms as a second and final phase at a formation temperature of 550˚C **[6].**

The $\alpha FeSi_2$ phase is stable above 937˚C, has a tetragonal structure and is metallic. The $\beta FeSi_2$ phase is stable below 937˚C, orthorhombic in structure and is a semiconductor. $\beta FeSi_2$ has an indirect optical band gap of about 0.87 eV which is near the infra red region and this makes it suitable for a variety of applications like optical fiber links, light sources and infra red detectors, and which also explains this research into it's formation through diffusion barriers.

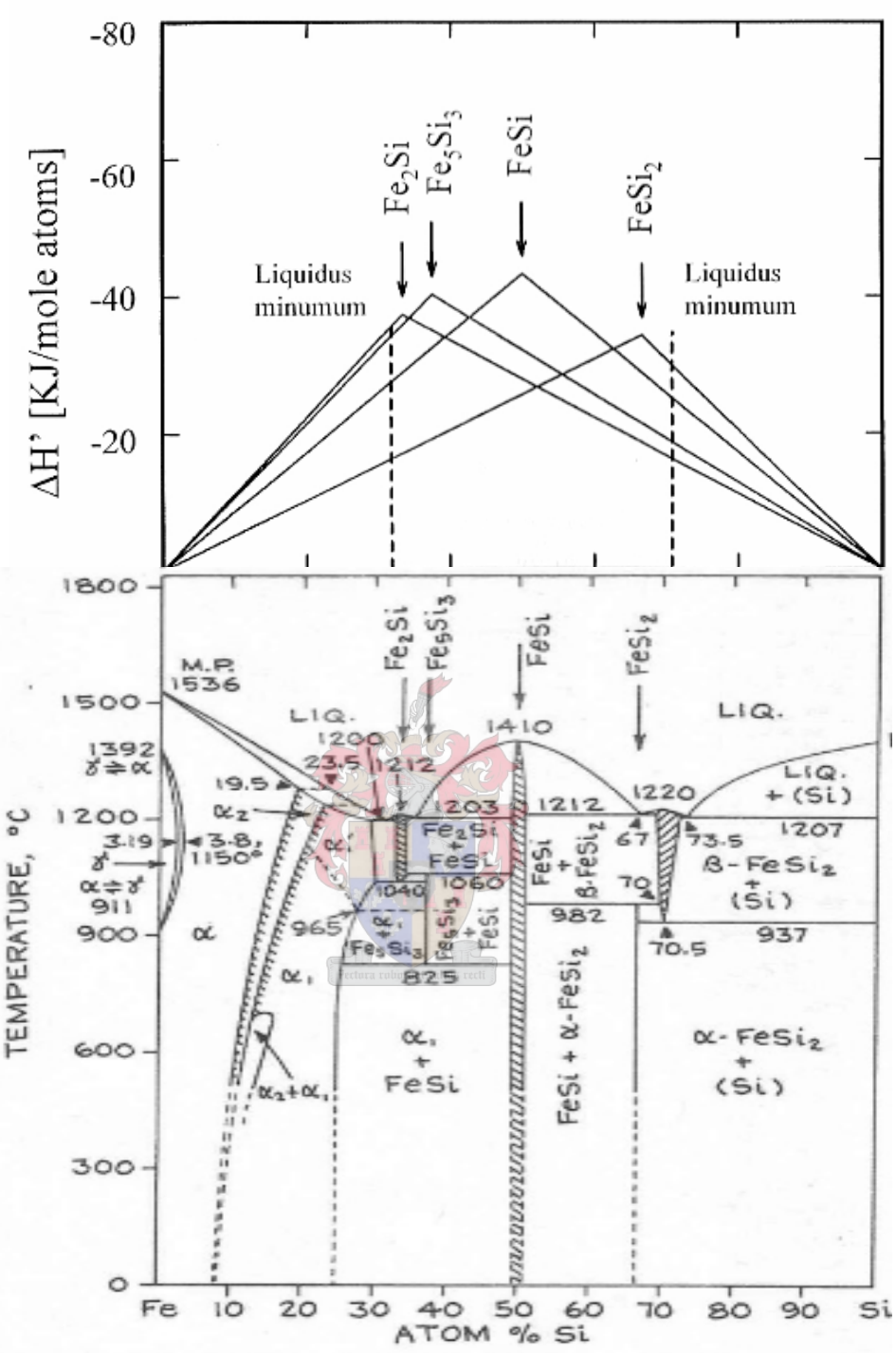

Figure 6. 1. EHF and phase diagram **[10]** of the Fe-Si system. Each triangle in the EHF diagram shows the amount of energy per mole of atom that will be generated if that phase were to form, as a function of composition. The effective concentration at the interface of a binary system is chosen to be that of the liquidus minimum. In this system there are two liquidus minima very close in temperature to each other, situated at 30 and 70 at.% Fe respectively.

In this study of iron-silicide formation, depositions and annealing were done in vacuum. The effects of both Cr and $CrSi_2$ diffusion barrier interlayers on the Fe-Si

system was investigated, the aim being to attempt to form uniform $\beta FeSi_2$ as first phase, instead of the normal $\varepsilon FeSi$ by controlling the effective Fe concentration at the growth interface. In this chapter the Fe-disilicide referred to as $FeSi_2$, is actually $\beta FeSi_2$, as annealing was done at temperatures of up to 800˚C, which is still well below the normal formation temperature of $\alpha FeSi_2$.

6.2 Si <100> | Cr | Fe system

As can be seen from **Table 2.6** in **Chapter 2** some research has previously been done using a Fe-Cr alloy as a diffusion barrier in the Si-Fe system **[52]**. The results of this research were discussed in **paragraph 2.5.** In this investigation of the effects of a Cr diffusion barrier on the formation of Fe-silicides the following Cr barrier systems were studied:

- 50 Å Cr barrier layer
- 100 Å Cr barrier layer

6.2.1 50 Å Cr barrier layer

The RBS spectra of samples of the Si<100>|Cr(50Å)|Fe(600Å) system annealed for 30 min at temperatures from 400 to 800˚C are shown in **Fig. 6.2**.

The 50 Å Cr was a successful diffusion barrier for Fe-silicide formation, with the Cr RBS signal only disappearing under the Fe signal at 500˚C (sample D3, **Fig. 6.2**) as proof that the Fe diffused through the barrier and started reacting with the Si substrate. The height of the Fe signal indicates that it was FeSi, the normal first phase, that formed. Annealing for 30 min at 600˚C forms $FeSi_2$ with some FeSi as indicated by the height of the Fe RBS signal and the sloping shoulders of the spectrum indicating non-uniformity. A 30 min anneal at 700˚C (sample D5) resulted in the complete formation of $FeSi_2$ of greater uniformity than was formed in the Si-Fe binary system after 30 min at 700˚C i.e. without the presence of a 50 Å diffusion barrier. (This comparison can be seen in **Fig. 6.3**.) At this point the Cr signal is visible at the Cr surface energy position, indicating that all of the Fe has diffused through the Cr barrier. This is a good example of the efficiency of a diffusion barrier to improve the quality of a silicide formed at a given temperature. At 800˚C (sample D7, **Fig. 6.2**) the Cr signal is not as noticeable at the Cr surface energy position, which indicates some intermixing of $CrSi_2$ and $FeSi_2$.

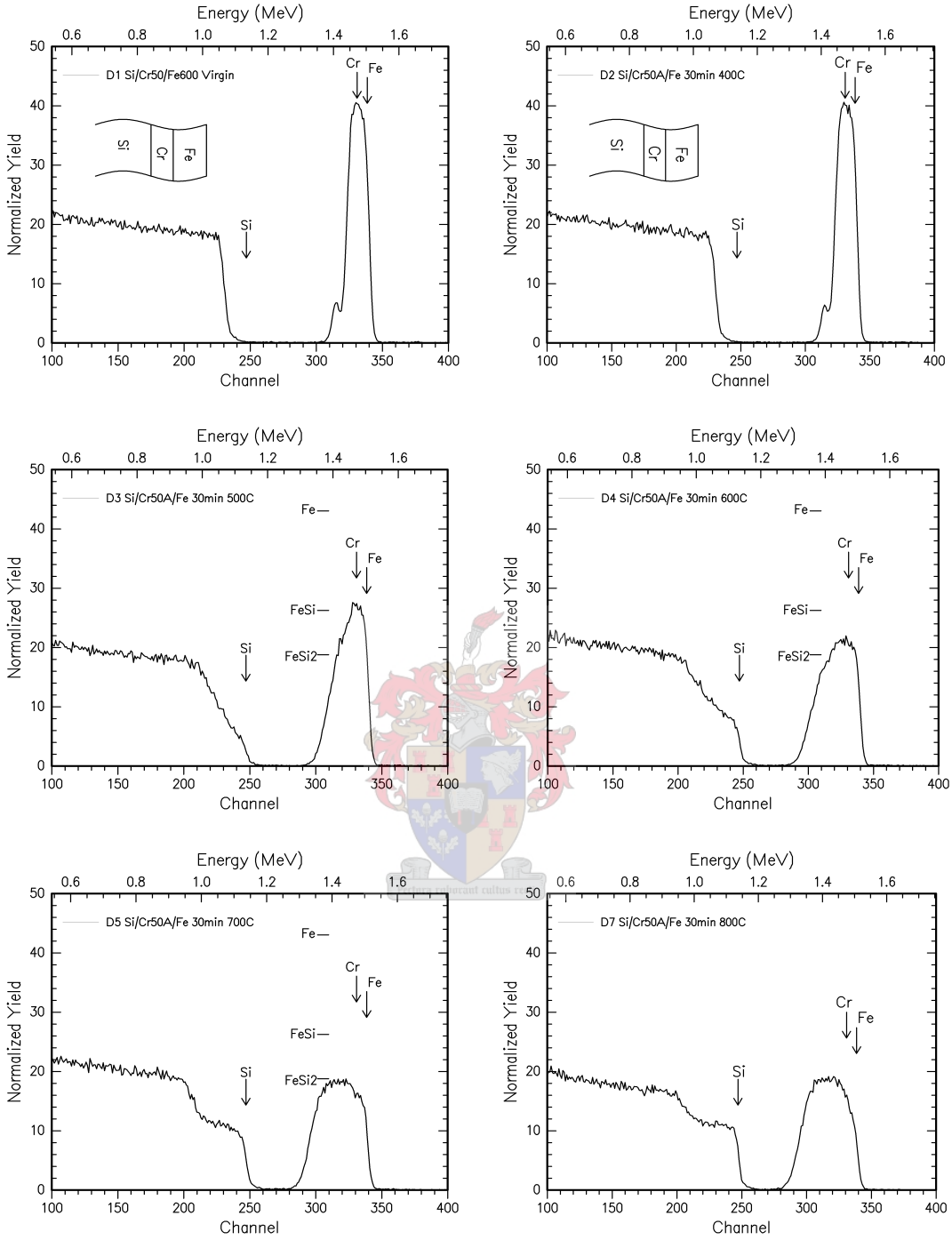

Figure 6. 2. RBS spectra of identical Si<100>|Cr(50Å)|Fe(600Å) samples annealed for 30 min at temperatures from 400 to 800˚C. First reaction occurred at 500˚C forming non-uniform FeSi and annealing for 30 min at 700˚C (sample D5) resulted in the complete formation of uniform $FeSi_2$.

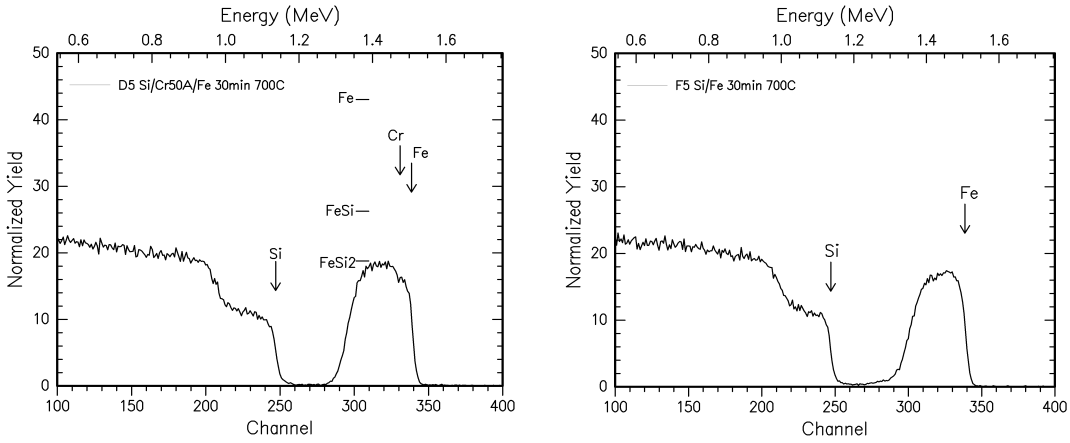

Figure 6. 3. Comparison of the RBS spectra of a Si|Cr(50Å)|Fe and a Si|Fe sample, both annealed at 700˚C for 30 min, showing clearly that the presence of a 50 Å Cr diffusion barrier improves the uniformity of the $FeSi_2$ that forms at this temperature.

6.2.2 100 Å Cr barrier layer

The RBS spectra of samples of the Si<100>|Cr(100Å)|Fe(600Å) system annealed for 30 min at temperatures from 400 to 800˚C are shown in **Fig. 6.4**.

The 100 Å Cr prevented any reaction between the Fe and the Si from occurring at temperatures of up to 400˚C, similar to the 50 Å Cr barrier. At 500˚C the Fe diffused through the barrier and reacted completely with the Si substrate to form non-uniform FeSi (sample E3 **Fig. 6.4**). Annealing for 30 min at 600˚C forms mainly $FeSi_2$, but there is also some FeSi present and the sloping shoulders of the spectrum indicates the non-uniformity. Heating at 700˚C (sample E5) resulted in the complete formation of $FeSi_2$, not quite as uniform as was found in the case of the 50Å Cr barrier (compare sample D5 **Fig. 6.2**), but still more uniform than without a diffusion barrier interlayer (compare sample F5 **Fig. 6.3**). At 800˚C the Cr signal is not visible at the surface energy position, indicating that the $CrSi_2$ and $FeSi_2$ has intermixed at this temperature (sample E7 **Fig. 6.4**).

It was not quite certain whether the diffusion barrier was Cr metal or perhaps $CrSi_2$, particularly at temperatures that are higher than the formation temperature of $CrSi_2$ (450˚C) or whether the Fe and Cr first intermix before silicide formation takes place. So it was decided to modify the experiments (using two samples of both the 50 and the 100 Å barrier) by doing a "double anneal": a first anneal for 60 min at 450˚C to form a $CrSi_2$ barrier from the deposited Cr barrier and then after that a second anneal for 30 min at temperatures of 500 and 600˚C respectively.

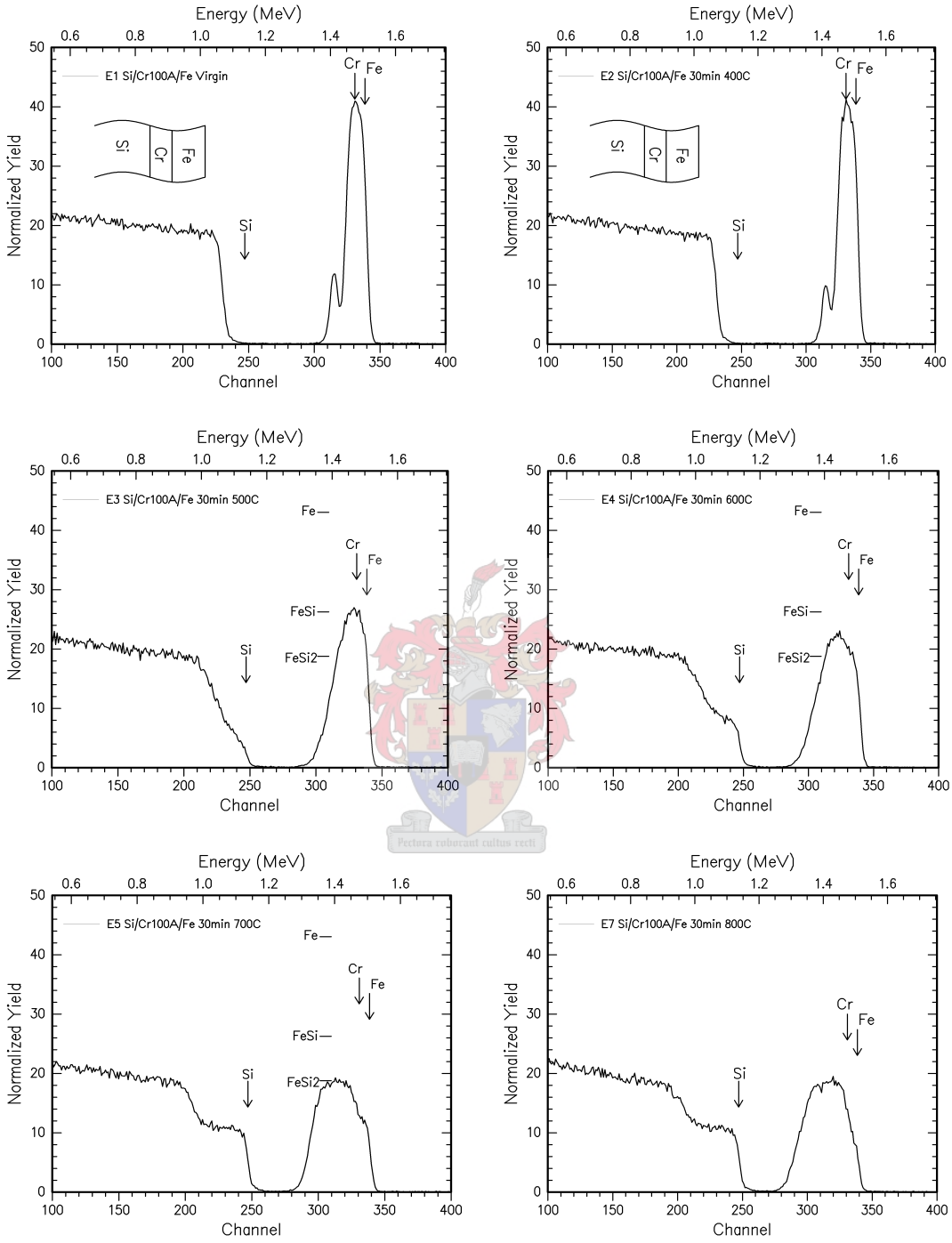

Figure 6. 4. RBS spectra of identical Si<100>|Cr(100Å)|Fe(600Å) samples annealed for 30 min at temperatures from 400 to 800˚C. First reaction only occurred at 500˚C (sample E3), forming non-uniform FeSi and annealing for 30 min at 700˚C (sample E5) resulted in the complete formation of uniform $FeSi_2$.

6.3 Si <100> | $CrSi_2$ | Fe system

6.3.1 $CrSi_2$ (Cr = 50 Å) barrier layer

The RBS spectra of two identical Si<100>|$CrSi_2$(Cr=50Å)|Fe(600Å) samples are shown in **Fig. 6.5.** The samples were firstly annealed for one hour at 450˚C to fully convert the deposited Cr layer into a $CrSi_2$ layer and then annealed again for 30 min at 500 and 600˚C respectively.

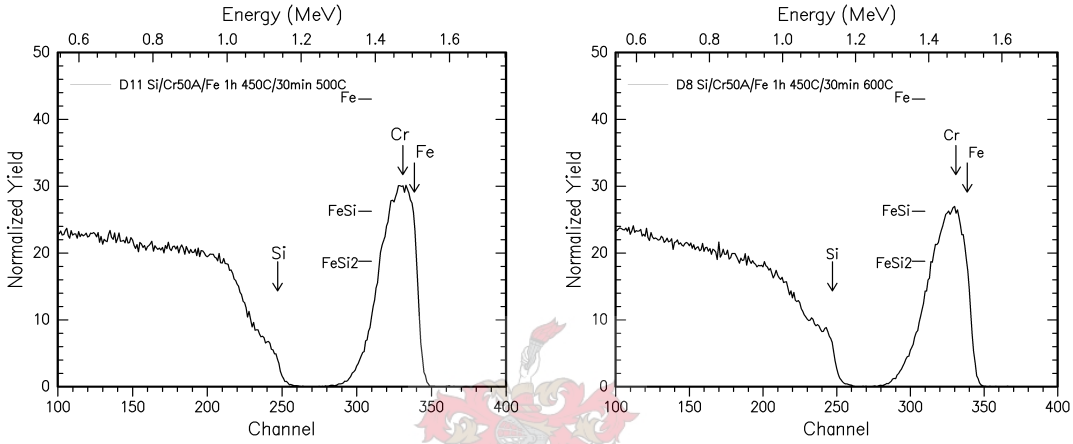

Figure 6. 5. RBS spectra of two identical Si<100>|Cr(50Å)|Fe(600Å) samples first annealed for 1h at 450˚C then annealed again for 30 min at 500 and 600˚C respectively.

The two step annealing that formed a $CrSi_2$ diffusion barrier produced non-uniform FeSi after annealing for 30 min at 500˚C, with the Cr signal visible at the surface energy position (sample D11 **Fig. 6.5**) At 600˚C an anneal of 30 min formed mainly FeSi (sample D8 **Fig. 6.5**).

6.3.2 $CrSi_2$ (Cr = 100 Å) barrier layer

The RBS spectra of two identical Si<100>|$CrSi_2$(Cr=100Å)|Fe(600Å) samples treated exactly like the two described in **paragraph 6.3.1** are shown in **Fig. 6.6.**

The use of the thicker (100 Å Cr) $CrSi_2$ barrier resulted in the complete formation of non-uniform FeSi at 500˚C (sample E11 **Fig. 6.6**) and a non-uniform mixture of FeSi and $FeSi_2$ at 600˚C (sample E8 **Fig. 6.6**). These results are similar to the case of the 50 Å $CrSi_2$ barrier.

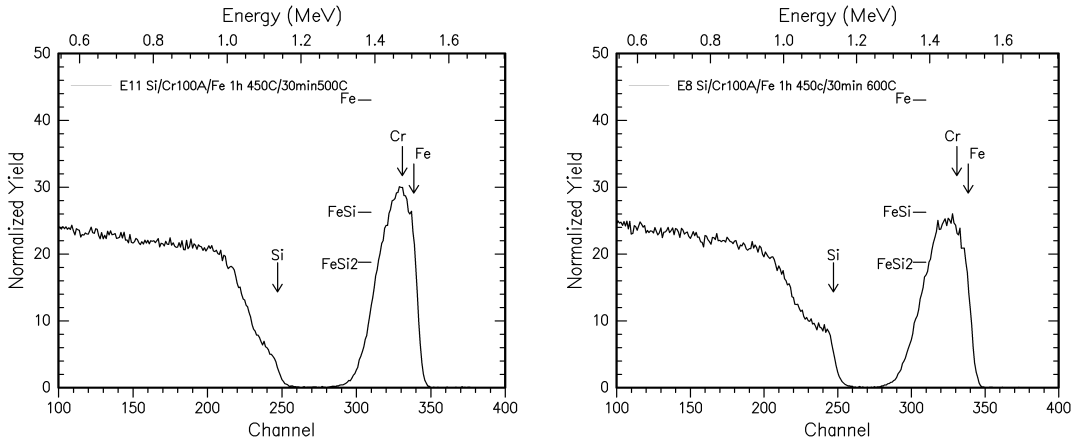

Figure 6. 6. RBS spectra of two identical Si<100>|Cr(100Å)|Fe(600Å) samples first annealed for 1h at 450˚C, then annealed again for 30 min at 500 and 600˚C respectively.

6.3.3 Comparison of Cr and $CrSi_2$ barriers

Fig. 6.7 compares the RBS spectra of two samples having the thin (50 Å) Cr and the thin $CrSi_2$ diffusion barrier annealed for 30 min at 500 and 600˚C.

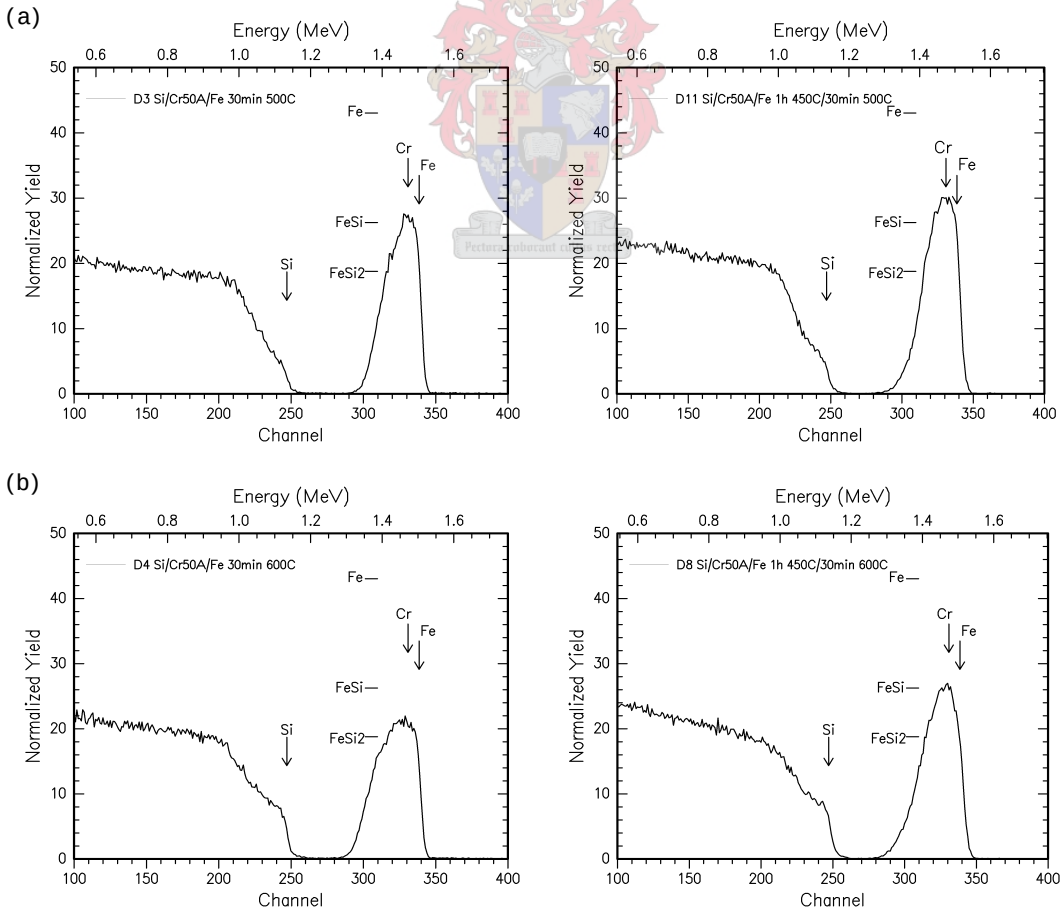

Figure 6. 7. Comparison of RBS spectra of samples with thin Cr (spectra on the left) and $CrSi_2$ (spectra on the right) barriers annealed for 30 min at (a) 500 and (b) 600˚C.

The use of the thin $CrSi_2$ (50Å Cr) diffusion barrier improved the uniformity of FeSi at 500˚C, with the Cr signal visible at the surface energy position (compare sample D11 with sample D3 **Fig. 6.7(a)**). At 600˚C there was hardly any $FeSi_2$ formation in the case of the $CrSi_2$ diffusion barrier, as can be seen by the height of the Fe signal, and the FeSi was more uniform (compare sample D8 with sample D4 **Fig. 6.7(b)**). It can be concluded from this that a thin $CrSi_2$ barrier is more efficient than a Cr one at improving the uniformity of FeSi formation at 500 and 600˚C.

A thicker $CrSi_2$ barrier proved more efficient than the thicker Cr barrier at improving the uniformity of FeSi at 500˚C, with the Cr signal visible at the surface energy position (compare sample E11 with sample E3 **Fig. 6.8(a)).** This result is similar to the case of the thin barriers. However, at 600˚C the use of the thicker Cr barrier formed mainly $FeSi_2$, whereas the thicker $CrSi_2$ barrier formed mainly FeSi (compare sample E4 with sample E8 **Fig. 6.8(b)**).

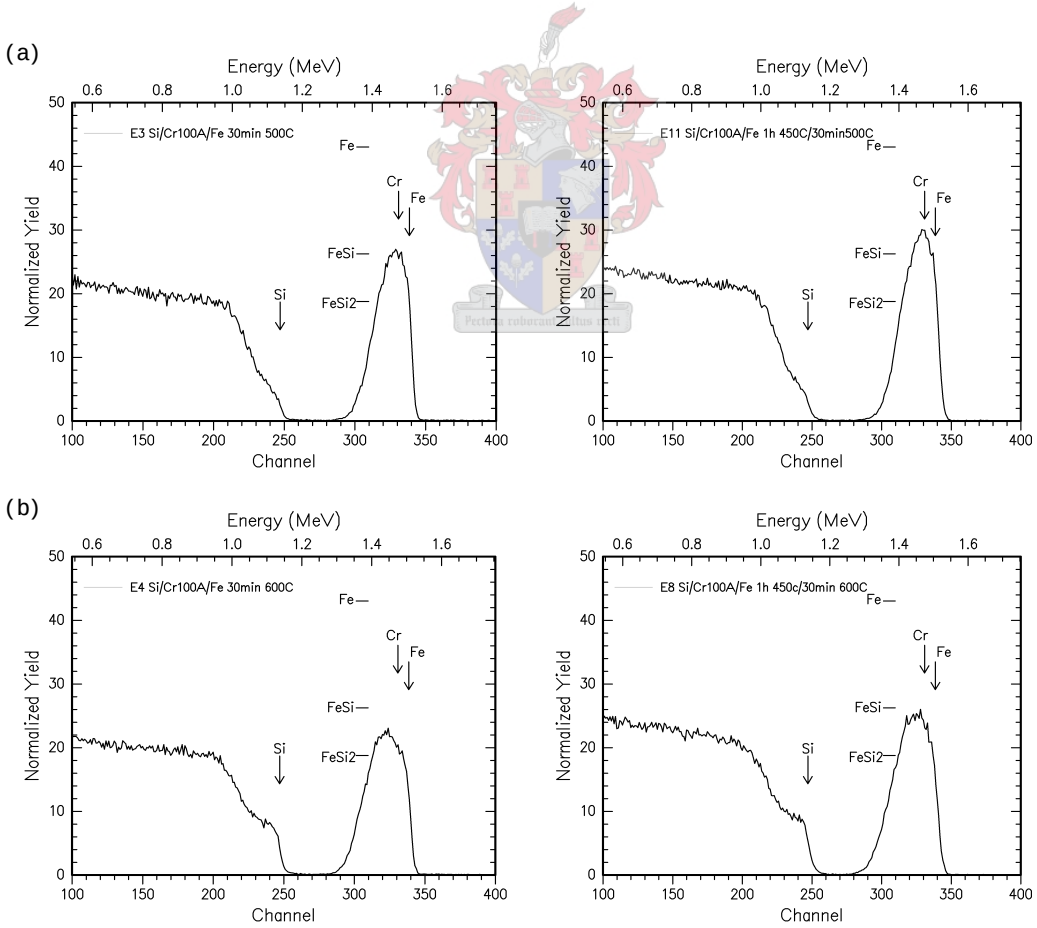

Figure 6. 8. Comparison of RBS spectra of samples with thicker (100 Å) Cr (spectra on the left) and $CrSi_2$ (spectra on the right) barriers annealed for 30 min at (a) 500 and (b) 600˚C.

6.4 Summary and conclusions

This chapter reported on the formation of Fe-silicides through Cr and $CrSi_2$ diffusion barrier layers and a summary of the results of the investigation is given in **Table 6.1.** Both the 50 and 100 Å Cr barriers showed very similar results. The Cr signal only disappeared under the Fe signal at 500˚C as proof that the Fe diffused through the barrier and started reacting with the Si substrate. There was, however, no change in the normal Fe-silicide phase formation sequence, as non-uniform FeSi was the first phase to form at 500˚C and thereafter $FeSi_2$ started to form at 600˚C. Annealing at 700˚C resulted in the complete formation of $FeSi_2$ of greater uniformity than was formed in the Si-Fe binary system without the presence of a diffusion barrier. At this temperature the Cr signal was not very noticeable at the surface energy position which indicated that the $CrSi_2$ and $FeSi_2$ had intermixed. The formation of uniform $FeSi_2$ at 700˚C is interesting, as this formation temperature is 100˚C lower than that reported by another group **[52],** who used a diffusion barrier consisting of a Fe-Cr alloy and found that the desired semiconducting β-$FeSi_2$ phase only formed after heating for 10 min at 800˚C.

Table 6. 1. Fe-silicide formation through Cr and $CrSi_2$ diffusion barrier layers.

IRON-SILICIDE FORMATION THROUGH BARRIER LAYERS			
BARRIER	**TEMP (˚C)**	**SILICIDE FORMATION**	**THICKNESS UNIFORMITY**
Cr 50 Å	400	no reaction	
	500	FeSi	non-uniform
	600	$FeSi_2$ some FeSi	non-uniform
	700	$FeSi_2$	uniform
	800	$FeSi_2$	less uniform
Cr 100 Å	400	no reaction	
	500	FeSi	non-uniform
	600	$FeSi_2$ some FeSi	non-uniform
	700	$FeSi_2$	uniform
	800	$FeSi_2$	non-uniform
$CrSi_2$ (Cr 50 Å)	500	FeSi	non-uniform
	600	FeSi some $FeSi_2$	non-uniform
$CrSi_2$ (Cr 100 Å)	500	FeSi	non-uniform
	600	FeSi some $FeSi_2$	non-uniform

The use of both a 50 and a 100 Å $CrSi_2$ diffusion barrier slightly improved the uniformity of FeSi at 500˚C when compared to the effect of a Cr barrier (although the FeSi that formed in all cases was rather non-uniform). The use of a thicker $CrSi_2$ barrier resulted in the formation of mainly FeSi at 600˚C, while at 600˚C the thicker Cr barrier formed mainly $FeSi_2$ (as second phase).

Generally the results using either a Cr or a $CrSi_2$ diffusion barrier did not differ much. The Cr as well as the $CrSi_2$ barriers examined here did not influence the order of the Fe-silicide phase formation sequence, but both formed non-uniform first phase FeSi at 500˚C, the $CrSi_2$ barriers (thin as well as thicker) having a slightly better effect, as the thickness of the FeSi that formed through it at 500˚C (although still non-uniform) was slightly more uniform than through the Cr barriers. The envisaged *first phase* formation of the semi-conducting β$FeSi_2$ phase was not achieved. The best results using Cr barriers were found at 700˚C, namely the (second phase) formation of uniform β$FeSi_2$.

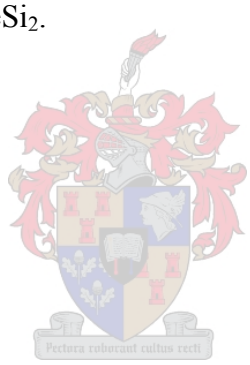

Chapter 7

SUMMARY AND CONCLUSIONS

In this study the formation of Ni-silicides, Co-silicides and Fe-silicides through different diffusion barrier interlayers was investigated. The diffusion barrier layers examined were Ta, Ti and Cr. In some cases the thickness of the barrier layer and the influence of a capping layer was investigated. The thin-film structures were prepared on single-crystal Si-substrates by Electron Beam Vacuum Deposition. The samples were vacuum annealed for times ranging from 10 - 60 min at temperatures ranging from 340 - 800°C. Sample characterization was done by conventional RBS, dynamic RBS, channeling RBS and X-ray diffraction.

The broader aim of the investigation was to experimentally determine the beneficial effects or influences (if any) that the various diffusion barriers would have upon the formation of the silicides of Ni, Co and Fe. In general it was envisaged that by the process of Concentration Controlled Phase Selection (CCPS) the presence of a diffusion barrier would retard the diffusion and thus change (lower) the effective concentration of the diffusing species (i.e. Ni, Co or Fe) at the growth interface to such an extent that certain precursor phases would be skipped and the more "desirable" phases would be formed, as first phase at a lower formation temperature than without the presence of a diffusion barrier. Furthermore, it would be ideal if the presence of a diffusion barrier at the growth interface would lead to improved thickness uniformity of all or some of the silicide phases that formed.

The more particular goals differed for each system. For the Ni-Si system the aim was to apply CCPS to try and form as the first phase, uniform, possibly epitaxial NiSi, at a lowered formation temperature by skipping first phase formation of Ni_2Si, as the physical properties (such as low resistivity, thermal stability) of NiSi renders it a more desirable phase. Another aim for this system was to possibly improve the uniformity and/or epitaxial quality of the NiSi. In previous studies $NiSi_2$ has been formed at 350°C as first phase by using a NiZr diffusion barrier to reduce the effective concentration of Ni at the growth interface **[116].** Fenske *et al***. [117-119]** found that the presence of a rather thick (~500 Å) Ti barrier resulted in the formation

of $NiSi_2$ as first phase at 475˚C, skipping the formation of both the Ni_2Si and the NiSi phases. The aim for the Co-Si system was to investigate if the use of other diffusion barriers (for instance Ta) would also lead to the skipping of one or both the Co_2Si and the CoSi precursor phases in favour of the more desirable $CoSi_2$ phase. In the Fe-Si system it was envisaged that the presence of a diffusion barrier would lead to the skipping of the εFeSi phase in favour of first phase formation of uniform $\beta FeSi_2$, a semiconductor with good optical properties in the infra-red region. The presence of a diffusion barrier could also possibly improve the thickness uniformity or epitaxiality of the FeSi and / or $FeSi_2$ phases.

Table 7.1 gives a comprehensive summary of the most relevant experimental results found in this investigation of silicide formation through diffusion barriers.

For Ni-silicide formation the use of a thin (20 Å) Ta diffusion barrier allowed no reaction even after annealing for 10 min at 400˚C, but RBS measurements showed that after annealing for 15 min at 400˚C uniform NiSi formed suddenly as first phase. XRD as well as dynamic RBS measurements confirmed this abrupt formation of NiSi instead of the normal first phase Ni_2Si. According to the EHF model this shows that the diffusion barrier interlayer reduces the effective concentration of the Ni atoms to a value where the effective heat of formation of NiSi is more negative than that of Ni_2Si and first phase formation of NiSi is thus thermodynamically favoured. The thickness uniformity of the first phase NiSi that formed through a 20 Å Ta barrier improved at higher temperature anneals (500 to 700˚C). A thicker (100 Å) Ta barrier also retarded the Ni diffusion and first phase, non-uniform NiSi only started to form at 500˚C. The thickness uniformity of the first phase NiSi that formed improved with an increase in annealing temperature up to 700˚C. However, the use of the 20 Å Ta barrier produced more uniform first phase NiSi in the 400 to 700˚C temperature range. In the RBS spectra of all annealed samples of the Si|Ta|Ni system, the Ta signal is clearly visible at the surface energy position, indicating that the Ni diffused through the Ta barrier and the barrier moved to the surface of the sample. No spreading of the Ta signal occurs, even at 800˚C, showing that the Ta does not diffuse back into the $NiSi_2$.

The use of a thin (30 - 50 Å) Cr barrier also allowed the formation of mainly NiSi at 400˚C, although XRD spectra also indicated the presence of some Ni_2Si.

Chapter 7 SUMMARY AND CONCLUSIONS

The uniformity of the NiSi improved at higher temperature anneals and at 800˚C the $NiSi_2$ formation was also quite uniform. The results were very similar when a $CrSi_2$ (Cr = 50 Å) barrier was used, the only difference being that the $NiSi_2$ that formed at 800˚C was non-uniform. Similar results were also obtained from samples with a thicker (100 Å) Cr barrier layer at lower temperatures, i.e. the formation of NiSi and some Ni_2Si as first phase at 400˚C, but in this case the first phase NiSi that formed at 500 to 700˚C was non-uniform and at 800˚C the $NiSi_2$ that formed was also non-uniform. In the RBS spectra of all samples of the Si|Cr|Ni system annealed in the 400 to 700˚C temperature range, the Cr signal is clearly visible at the surface energy position, indicating that the Ni diffused through the Cr barrier and the barrier moved to the surface of the sample. However, at 800˚C the Cr signal becomes less visible or disappears, particularly for the thinner Cr barriers, showing the intermixing of the $CrSi_2$ and the $NiSi_2$.

The use of a thin (30 - 50 Å) Ti barrier produced a mixture of Ni_2Si and NiSi as first reaction at 400˚C, but a 10 min anneal at 500˚C formed uniform NiSi as was confirmed by RBS and XRD measurements. The uniformity of the NiSi improved with an increase in annealing temperature up to 700˚C and at 800˚C uniform $NiSi_2$ formation occurred. In the case of the thicker (100 Å)Ti interlayer no reaction occured at 400˚C, showing that the thicker Ti barrier layer acts more effectively as a diffusion barrier for the Ni atoms. Non-uniform first phase NiSi formed at 500˚C and at temperatures above 750˚C the $NiSi_2$ that formed was non-uniform. The Ti RBS signal is clearly visible at the surface energy position for all samples of the Si|Ti|Ni system annealed in the 400 to 700˚C temperature range, indicating that the Ni has diffused through the Ti barrier. However, at 800˚C the Ti signal becomes less visible, showing the spreading or intermixing of the Ti into the $NiSi_2$.

During Ni-silicide formation through Ta, Cr and Ti diffusion barrier layers the thin (20 Å) Ta barrier was most effective as it allowed the sudden formation of uniform NiSi as first phase after annealing for only 15 min at 400˚C. The thin Cr barrier was less effective than Ta at 400˚C because, although it also formed mainly NiSi, a little Ni_2Si was also present. The thin Ti barrier formed a mixture of Ni_2Si and NiSi at 400˚C. At temperatures ranging from 500 to 700˚C the thin barriers (20 – 50 Å) all formed first phase uniform NiSi, with the uniformity improving with increased annealing temperature. All three thin barriers formed $NiSi_2$ at temperatures

of 750˚C and above, but the thin Ti barrier formed the most uniform di-silicide. The thicker Ta and Ti barriers were more effective in retarding the diffusion of the Ni atoms than the thinner barriers, as both the thicker Ta and Ti barriers prevented any reaction from occurring below 500˚C. However, the thicker Cr barrier allowed the formation of very non-uniform NiSi at 400˚C, which was similar to the case of the thin Cr barrier. The thicker Ta and Ti barriers formed first phase NiSi at higher temperatures (500 to 700˚C), although less uniform than the thinner barriers and the NiSi uniformity also improved with increased annealing temperature. The thicker Cr barrier did not perform as well at higher temperatures, not at retarding diffusion, nor at promoting the growth of first phase NiSi of uniform thickness. The $NiSi_2$ that formed at 800˚C through all three of the thicker barriers was non-uniform.

The general conclusions of the formation of Ni-silicides through Ta, Cr and Ti diffusion barriers can be summarized as follows: (i) Only the thin (20 Å) Ta barrier gave a uniform NiSi layer as first phase. In all other cases either some Ni_2Si was present and/or the NiSi layer was non-uniform. (ii) The Ni-silicide formation is more uniform at higher annealing temperatures and when thinner barriers are used. (iii) In all cases $NiSi_2$ formed at 800˚C, which is similar to the situation without a diffusion barrier. This is because the barrier moves to the surface of the sample during the formation of NiSi and it therefore does not act as a diffusion barrier any more when $NiSi_2$ starts to form. (iv) The thicker the barrier, the higher the temperature of Ni-silicide formation.

For Co-silicide formation the effect of Ta and Ti barrier layers, as well as a 30Å Ta barrier and Ta cap *combination* was investigated. The use of a thin (10 - 30Å) Ta diffusion barrier prevented silicide formation for thermal anneals up to 560˚C. The effective concentration of the Co at the growth interface is lowered, thus skipping the usual first phase formation of Co_2Si at 450˚C. At 560˚C a non-uniform mixture of CoSi and $CoSi_2$ formed, as was confirmed by XRD. The $CoSi_2$ that formed at temperatures ranging between 600 and 700˚C was of quite uniform thickness, but XRD measurements indicated that some CoSi was present as well. The thicker (100Å) Ta barrier layers retarded the diffusion of Co atoms through the barrier layer for temperatures of up to about 650˚C. Annealing at 700˚C formed mostly $CoSi_2$ (although some CoSi was present as well) and at 800˚C non-uniform $CoSi_2$ formed. The addition of Ta capping layers of different thicknesses in conjunction with a 30 Å

Ta diffusion barrier did not significantly improve Co-silicide formation. However, when a 60 Å Ta capping layer was used, non-uniform CoSi formed as first phase at 540 °C and the uniformity of the $CoSi_2$ between 600 and 700°C was slightly improved, although still non-uniform. The position of the RBS signal of the Ta barrier in all spectra of the Si|Ta|Co and Si|Ta|Co|Ta_{cap} systems indicates that the Ta from the barrier is not at the surface of the sample after silicide formation, but is spread throughout the silicide.

The use of thin (10 - 30 Å) Ti barrier layers resulted in the skipping of the Co_2Si precursor phase and the formation of quite uniform first phase CoSi at 520°C, which is slightly higher than the usual formation temperature (500°C) of CoSi without a barrier present. Uniform $CoSi_2$ started forming at 560°C and at higher annealing temperatures the $CoSi_2$ remained of uniform thickness. The use of a thicker (100 Å) Ti barrier lowered the effective concentration of Co at the growth interface to such an extent that $CoSi_2$ only started to form as first phase at 600°C, thereby skipping both the Co_2Si and the CoSi precursor phases. The $CoSi_2$ that formed through this barrier at 700 and 800°C was very non-uniform.

During Co-silicide formation through Ta and Ti diffusion barriers, the barrier layer lowers the effective concentration of Co at the growth interface and this results in the skipping of the formation of Co_2Si as first phase. The use of a thin Ti barrier resulted in the formation of uniform CoSi as first phase at 520°C and both the thin Ti and Ta barriers allowed $CoSi_2$ to form at 560°C. At higher temperatures (up to 800°C) the thickness of the di-silicide layer was uniform for both thin barriers. The thicker Ta and Ti barriers were more effective in retarding the diffusion of the Co atoms than the thinner barriers, because they prevented any reaction from occurring up to quite high annealing temperatures (up to 700°C for Ta and 600°C for Ti), although the thicker Ta and Ti barriers did not perform as well as the thinner ones at promoting the growth of uniform layers of $CoSi_2$ at higher temperatures.

The general conclusions for the formation of Co-silicides through Ta and Ti diffusion barriers can be summarized as follows: (i) No Co-silicide formation at all occurred below 520°C. (ii) The Co-silicide formation was generally more uniform at all temperatures when the thin barriers were used, the thin Ti barrier delivering better uniformity at lower temperatures (~520°C). (iii) Generally the uniformity improved with an increase in temperature (iv) In all cases $CoSi_2$ first formed at temperatures of

560˚C or higher. (v) Similar to the case of Ni-silicide formation, the thicker the barrier, the higher the temperature of Co-silicide formation. (vi) Ta capping layers did not improve the quality of the formed silicide and in some cases resulted in even greater non-uniformity.

For the formation of Fe-silicides through 50 and 100 Å Cr barriers, as well as $CrSi_2$ barriers, it was found that there was no change in the normal Fe-silicide phase formation sequence, as non-uniform FeSi was the first phase to form at 500˚C and then $FeSi_2$ started to form at 600˚C. However, with both the thin and the thick Cr barriers annealing at 700˚C resulted in the complete formation of $FeSi_2$ of greater uniformity than was formed in the Si-Fe binary system without the presence of a diffusion barrier. This was not so when $CrSi_2$ barriers were used, as the $FeSi_2$ that formed at 700˚C was non-uniform in this case. At this temperature the Cr signal was not very noticeable at the surface energy position, which indicated that the $CrSi_2$ and $FeSi_2$ had intermixed.

The conclusions that can be drawn for the formation of Fe-silicides through Cr and $CrSi_2$ diffusion barriers can be summarized as follows: (i) Both the thin and the thicker Cr as well as $CrSi_2$ barriers did not influence the order of the Fe-silicide phase formation sequence, but led to the formation of non-uniform first phase FeSi at 500˚C. (ii) First phase formation of the semi-conducting $\beta FeSi_2$ phase was not achieved. (iii) The results using the Cr and $CrSi_2$ barriers were very similar at temperatures below 600˚C. The $CrSi_2$ barrier had a slightly better effect, because the thickness of the FeSi that formed through it, though non-uniform, was slightly more uniform than through the Cr barriers. (iv) The best results obtained using Cr barriers was the formation of uniform $FeSi_2$ at 700˚C.

In this study dynamic real-time RBS has been used for the first time to prove without any doubt that diffusion barrier layers can be used to bring about “phase skipping”. These results have been interpreted in terms of the Effective Heat of Formation (EHF) model and are good examples of Concentration Controlled Phase Selection (CCPS). In general it was found that the thicker the diffusion barrier layer, the higher the temperature of silicide formation. Furthermore, silicide formation was generally found to be more uniform at higher annealing temperatures and when thinner diffusion barrier layers were used.

Table 7. 1. Summary of Ni, Co and Fe-silicide formation through diffusion barrier layers.

	Diffusion barrier	Ta		Cr		$CrSi_2$	Ti	
Ni-silicide formation	Barrier thickness (Å)	20	100	30-50	100	Cr=50	30-50	100
	* Temperature of first reaction (˚C)	15min 400	30min 500	400	400	400	400	500
	First phase formed	NiSi	NiSi	NiSi and some Ni_2Si	NiSi and Ni_2Si	NiSi and some Ni_2Si	NiSi and some Ni_2Si	NiSi
	NiSi thickness uniformity at 400˚C	uniform	-	non-uniform	very non-uniform	non-uniform	non-uniform	-
	NiSi thickness uniformity at 500˚C	uniform	non-uniform	uniform	non-uniform	uniform	uniform	non-uniform
	NiSi thickness uniformity at 600-700˚C	uniform	uniform	uniform	non-uniform	uniform	uniform	non-uniform
	**$NiSi_2$ thickness uniformity at 800˚C	uniform	non-uniform	uniform	non-uniform	non-uniform	uniform	non-uniform
	* NiSi formation temperature without barrier ~ 400˚C ** $NiSi_2$ formation temperature with and without barrier ~ 750˚C							

	Diffusion barrier	Ta		Ta 30 Å+Ta cap				Ti	
Co-silicide formation	Barrier thickness (Å)	10-30	100	30Å cap	60Å cap	100Å cap	150Å cap	10-30	100
	* Temperature of first reaction (˚C)	1h 560	700	600	540	640	600	520	600
	First phase formed	$CoSi_2$ and some CoSi	$CoSi_2$ some CoSi	CoSi and $CoSi_2$	CoSi	CoSi and $CoSi_2$	CoSi and $CoSi_2$	CoSi	$CoSi_2$
	CoSi thickness uniformity	non-uniform	non-uniform	non-uniform	non-uniform	very non-uniform	very non-uniform	uniform	-
	** $CoSi_2$ formation temperature	560	700	600	560	640	600	560	600
	$CoSi_2$ thickness uniformity at 600-700˚C	uniform	non-uniform	non-uniform	non-uniform	non-uniform	non-uniform	uniform	non-uniform
	$CoSi_2$ thickness uniformity at 800˚C	uniform	non-uniform	-	-	-	-	uniform	very non-uniform
	* CoSi formation temperature without barrier ~ 500˚C ** $CoSi_2$ formation temperature without barrier ~ 550˚C								

	Diffusion barrier	Cr		$CrSi_2$	
Fe-silicide formation	Barrier thickness (Å)	50	100	Cr=50	Cr=100
	* Temperature of first reaction (˚C)	500	500	500	500
	First phase formed	FeSi	FeSi	FeSi	FeSi
	FeSi thickness uniformity	non-uniform	non-uniform	non-uniform	non-uniform
	** $FeSi_2$ formation temperature	600	600	600	600
	$FeSi_2$ thickness uniformity at 700˚C	uniform	uniform	non-uniform	non-uniform
	$FeSi_2$ thickness uniformity at 800˚C	uniform	non-uniform	-	-
	* FeSi formation temperature without barrier ~ 500˚C ** $FeSi_2$ formation temperature without barrier ~ 550˚C				

Pectora roborant cultus recti

REFERENCES

[1] R. Pretorius, *MRS Proc*. **25**, 15 (1984).

[2] R. Pretorius and J.W. Mayer, *J. Appl. Phys*. **81**, 2448 (1997).

[3] R. Pretorius, T.K. Marais, and C.C. Theron, *A Review, Mat, Sci. and Eng* **R10**, 1 (1993).

[4] J.M. Poate, K.N. Tu and J.W. Mayer, Thin films –Interdiffusion and reactions (John Wiley and Sons, New York, 1978).

[5] R. Pretorius, *Vacuum*. **41**, 1038 (1990).

[6] M.A. Nicolet and S.S. Lau, in VLSI Electronics: Microstructural Science, edited by N. Einspruch (Academic Press, New York, 1983).

[7] R.M. Walser and R.W. Bené, *Appl. Phys. Lett*. **28**, 624 (1976).

[8] B.Y. Tsaur, S.S. Lau, J.W. Mayer and M.A. Nicolet, *Appl. Phys. Lett*. **38**, 922 (1981).

[9] R.W. Bené, *Appl. Phys. Lett*. **41**, 529 (1982).

[10] O. Kubaschewski and C.B. Alcock, Metallurgical Thermochemistry (Pergamon Press, Oxford, 1979).

[11] K. Maex and M. van Rossum, Properties of Metal Silicides, published by INSPE, the Institution of Electrical Engineers, London 1995.

[12] R.T. Tung, *Mater. Chem. Phys*. **32**, 107 (1992).

[13] G.B. Kim, J.S. Kwak, H.K. Baik, S.M. Lee, S.H. Oh and C.G. Park, *Appl. Phys. Lett*. **77**, 1443 (2000).

[14] A.Vantomme, M.A. Nicolet, G. Bai and D.B. Fraser, *Appl. Phys. Lett*. **62**, 243 (1993).

[15] R.T. Tung, *Appl. Phys. Lett*. **68**, 3461 (1996).

[16] M.W. Kleinschmit, M. Yeadon and J.M. Gibson, *Appl. Phys. Lett*. **75**, 3288 (1999).

[17] R.T. Tung, *Appl. Surf. Sci.* **117**, 268 (1997).

[18] M.L.A. Dass, D.B. Fraser and C.S. Wei, *Appl. Phys. Lett*. **58**, 1308 (1991).

[19] R.T. Tung and F. Schrey, *Appl. Phys. Lett*. **67**, 2164 (1995).

[20] R.T. Tung, *Mater. Res. Soc. Proc.* **427**, 491 (1991).

[21] C. Cabral, L.A. Clevenger, G.B. Stephenson, S. Bauer, G. Morales and K.F. Ludwig, *Applications of Syncrotron Radiation Techniques to Materials Science II*, **375**, 253 (1995).

[22] J. Cardenas, S.L. Zhang, B.G. Svensson and C.S. Petersson, *Silicide Thin films Fabr. Prop. and Appl.* **402**, 155 (1996).

[23] J. Cardenas, S.L. Zhang, B.G. Svensson and C.S. Petersson, *J. Appl. Phys*. **80**, 762 (1996).

[24] C. Detavernier, R.L. Vanmeirhaeghe, F. Cardon, K. Maex, W. Vandervorst and B. Brijs, *Appl. Phys. Lett*. **77**, 3170 (2000).

[25] M. Falke, B. Gebhardt, G. Beddies, S. Teichert and H.J. Hinneberg, *Microelectr. Eng*, **55**, 171 (2001).

[26] S.L. Hsia,T.Y. Tan, P. Smith and G.E. Mcguire, *J. Appl. Phys*. **70**, 7579 (1991).

[27] F. Hong, B.K. Patnaik, B.Z. Li, P. Liu, Z. Sun and G.A. Rozgonyi, *Phase Transformations in Thin films – Thermodynamics and Kinetics*, **311**, 305 (1993).

[28] S.L. Hsia, T.Y. Tan, P. Smith and G.E. Mcguire, *J. Appl. Phys*. **72**, 1864 (1992).

[29] G.B. Kim, H.K. Baik, and S.M. Lee, *Appl. Phys. Lett*. **69**, 3498 (1996).

[30] G.B. Kim, J.S. Kwak, H.K. Baik and S.M. Lee, *J. Appl. Phys*. **82**, 2323 (1997).

[31] G.B. Kim, J.S. Kwak, H.K. Baik and S.M. Lee, *J. Vac. Sci. & Technol. B*, **18**, 2576 (2000).

[32] J.R. Kim, K.S. Bae and Y.S. Cho, *J. Mat. Sci. Lett*. **16**, 473 (1997).

[33] Y. Kwon, C. Lee, H.K. Kang and D.L Bae, *J. of the Korean Physical Soc.* **34**, S499 (1999).

[34] Y. Kwon and C. Lee, *Mat. Sci. and Eng. B Solid State Materials for advanced Technology* **65**, 187 (1999).

[35] Y. Kwon and C. Lee, *Materials Chemistry and Physics* **63**, 202 (2000).

[36] Y.J. Kwon and C. Lee, *Thin Solid Films*, **380**, 127 (2000).

[37] A. Lauwers, A. Vercaemst, M. Vanhove, K.K. Larsen, R. Verbeeck, R. Vanmeirhaeghe, K. Maex and M. Vanrossum, *Silicides, Gemanides and their interfaces*, **320**, 59 (1994).

[38] B.Z. Li, W.J. Wu, K. Shao, Z.G. Gu, G.B. Jiang, W.N. Huang, H. Fang, Z. Sun, P. Liu, and Z.Y. Zhou, *Advanced metallization for devices and circuits* **337**, 449 (1994).

[39] D.J. Millar, T.I. Selinder and K. E. Gray, *Silicide Thin films- Fabric. Prop. and Applic*. **402**, 161 (1996).

[40] S. Ohmi and R.T. Tung, *Advanced Interconnects and contacts* **564**, 117 (1999).

[41] C.M. Osburn, J.Y. Tsai and J. Sun, *J. Electr. Mat*. **25**, 1725 (1996).

[42] T.I. Selinder, T.A. Roberts, D.J. Miller, M.A. Beno, G.S. Knapp, K.E. Gray, S. Ogawa, J.A. Fair and D.B. Fraser, *J. Appl. Phys*. **77**, 6730 (1995).

[43] A. Steegen, C. Detavernier, A. Lauwers, K. Maex, R.L. Vanmeirhaeghe and F. Cardon, *Microelectronic Engineering* **55**, 145 (2001).

[44] R.T. Tung and S. Ohmi, *Thin Solid films* **369**, 233 (2000).

[45] A.Vantomme, M.A. Nicolet, G. Bai and D.B. Fraser, *Appl. Surf. Sci*. **73**, 117 (1993).

[46] A. Vantomme, M.A. Nicolet, and N.D. Theodore, *J. Appl. Phys*. **75**, 3882 (1994).

[47] H.M. Weng, G. Qin, R.D. Han, S.L. Wu, P. Liu, C.L. Lin, B.Z. Li and S.C. Zou, *Positron Annihilation ICPA-10 Pts 1 and 2* **175**, 233 (1995).

[48] A. Vantomme, S. Degroote, J. Dekoster and G. Langouche, *Appl. Surf. Sci*. **91**, 24(1995).

[49] W.J. Wu, B.Z. Li, K. Shao, Z. Sun, Z.G. Gu, W.N. Huang, G.B. Jiang and Z.Y. Pingliu Zhou, *Second Int. Conference on Thin Film Phys and Applc*. **2364**, 494 (1994).

[50] S.L. Zhang, J. Cardenas, F.M. Dheurle, B.G. Svensson and C.S. Petersson, *Appl. Phys. Lett.* **66**, 58 (1995).

[51] R. Pretorius, A.M. Vredenberg and F. W. Saris and R. de Reus, *J. Appl. Phys*. **70**, 3636 (1991).

[52] M. K. Moodley, K. Bharuth-Ram, H. De Waal and R. Pretorius, *Hyperfine Interactions* **139**, 589 (2002).

[53] M. Falke, B. Gebhardt, G. Beddies, S. Teichert and H.J. Hinneberg, *Thin Solid Films* **336**, 201 (1998).

[54] P. Liu, B.Z. Li, Z.Y. Zhou, C.L. Lin and S.C. Zou, *Mat. Lett.* **17**, 383 (1993).

[55] P. Liu, B-Z. Li, Z. Sun, Z-G. Gu, W-N. Huang, Z-Y. Zhou, R-S. Ni, C-L. Lin, S.C. Zou, F. Hong and G. A. Rozgonyi, *J. Appl. Phys*. **74**, 1700 (1993).

[56] M.L.A. Dass, D.B. Fraser and C-S. Wei, *Appl. Phys. Lett*. **58**, 1308 (1991).

[57] M. Lawrence, A. Dass, D.B. Fraser and C-S. Wei, *Appl. Phys. Lett.* **58**, 1308 (1991).

[58] T.I. Selinder, D.J. Miller and K.E. Gray, *Appl. Phys. Lett*. **67**, 1597 (1995).

[59] A. Alberti, F. Lavia and F. Rimini, *J. Vac. Sci. & Technol. B*, **17**, 1448 (1999).

[60] J.S. Maa and C.H. Peng, *Microstructure Evolution During Irradiation* **439**, 263 (1997).

[61] F. Hong, G.A. Rozgonyi and B. Patnaik, *Appl. Phys. Lett*. **61**, 1519 (1992).

[62] F. Hong and G.A. Rozgonyi, *J. Electrochem. Soc*. **141**, 3480 (1994).

[63] R.T. Tung and F. Schrey, *Silicide Thin films Fabr. Prop. and Appl.* **402**, 173 (1996).

[64] R.T. Tung, D.J. Howard, S. Ohmi, M. Caymax and K. Maex, *Mater. Res. Soc. Proc*. **514**, 427 (1998).

[65] C. Detavernier, R.L. Vanmeirhaeghe, F. Cardon and K. Maex, *Thin Solid Films* **386**, 19 (2001).

[66] J. Heo and H. Jeon, *Thin Solid Films* **379**, 265 (2000).

[67] M.W. Kleinschmit, M. Yeadon and J.M. Gibson, *Advanced Interconnects and Contacts* **564**, 135 (1999).

[68] M.W. Kleinschmit, M. Yeadon and J.M. Gibson, *Advanced Microelectronic Processing Techniques* **4227**, 9 (2000).

[69] Y. shin, C. Bea and H. Jeon, *J. Mat. Sci. Lett*. **18**, 731 (1999).

[70] R.T. Tung, *Japanese Journal of Applied Physics Part 1* **36**, 1650 (1997).

[71] R.T. Tung, *Appl. Phys. Lett.* **72**, 2538 (1998).

[72] C. Detavernier, R.L. Vanmeirhaeghe, F. Cardon, R.A. Donaton and K. Maex, *Appl. Phys. Lett*. **74**, 2930 (1999).

[73] C. Detavernier, R.L. Vanmeirhaeghe, F. Cardon, R.A. Donaton and K. Maex, *Microelectr. Eng*. **50**, 125 (2000).

[74] C. Detavernier, R.L. Vanmeirhaeghe, F. Cardon, K. Maex, H. Bender and S.Y. Zhu, *J. Appl. Phys*. **88**, 133 (2000).

[75] G.B. Kim, J.S. Kwak, H.K. Baik and S.M. Lee, *J. Vac. Sci. & Technol.* **17**, 162 (1999).

[76] G.B. Kim, J.S. Kwak, H.K. Baik and S.M. Lee, *J. Appl. Phys.* **85**, 1503 (1999).

[77] P.C. Kluth, C. Detavernier, Q.T. Zhao, J. Xu, H.P. Bochern, S. Lenk and S. Manti, *Thin Solid Films* **380**, 201 (2000).

[78] J.S. Byun, J.M. Seon, K.S. Youn, H.S. Hwang, J.W. Park and J.J. Kim, *J. Electrochemical Soc.* **143**, L56 (1996).

[79] Y.M. Makogon, S.M. Voloshko, O.P. Pavlova, S.I. Sidorenko, O.V. Zelenin, M.O. Vasylyev and S. Teichert, *Metallofizika I Noveishie Tekhnologii* **23**, 1455 (2001).

[80] G. Briskin, J. Pelleg and M. Talianker, *Thin Solid Films* **288**, 132 (1996).

[81] J. Pelleg, *Thin Solid Films* **325**, 60 (1998).

[82] J.S. Byun, S.B. Kang, H.J. Kim, C.Y. Kim and K.H. Park, *J. Appl. Phys*. **74**, 3156 (1993).

[83] J.S. Byun, W.S. Kim, M.S. Choi, H.J. Cho and H.J. Kim, *Silicides, Gemanides and their Interfaces* **320**, 379 (1994).

[84] J.S. Byun, D.H. Kim, W.S. Kim and H.J. Kim, *J. Appl. Phys*. **78**, 1725 (1995).

[85] D.H. Lee, D.H. Ko, J.H. Ku, S. Choi, K. Fujihara, H.K. Kang, S.H. Oh, C.G. Park and H.J. Lee, *Jap. J. Appl. Phys –Part 1* **40**, 2712 (2001).

[86] M.J. Kim, H.J. Choi, D.H. Ko, J.H. Ku, S. Choi, K. Fujihara and C.W. Yang, *J. of the Korean Pysical Soc*. **40**, 737 (2002).

[87] C. Franklyn, J. Aspeling, W. Strydom and R. Malunga, *Nuclear Inst. and Meth. in Phys. Research* **190**, 742 (2002).

[88] B. Gebhardt, M. Falke, H. Giesler, S. Teichert, G. Beddies and H.J. Hinneberg, *Microelectronic Engineering* **37**, 43 (1997).

[89] E.T. Kim, Y. Kwon and C. Lee, *J. of Neuroscience Methods* **100**, 17 (2000).

[90] F.M. Yang and M.C. Chen, *J. Vac. Sci. and Technol. B*, **9**, 1497 (1991).

[91] C. Detavernier, R.L. Vanmeirhaeghe, F. Cardon, K. Maex, H. Bender, B. Brijs and W. Vandervorst, *J. Appl. Phys*. **89**, 2146 (2001).

[92] J.S. Byun and H.J. Kim, *J. Appl. Phys*. **78**, 6784 (1995).

[93] C. Detavernier, R.L. Vanmeirhaeghe, F. Cardon, K. Maex, *Physical Review B* **62**, 12045 (2000).

[94] C. Detavernier, R.L. Vanmeirhaeghe, F. Cardon and K. Maex, *Thin Solid Films*, **384**, 243 (2001).

[95] K. Prabhakaran, K. Somitomo and T. Ogino, *Appl. Surf. Sci.* **11**7, 280 (1997).

[96] J.P.W.B. Duchateau, A.E.T. Kuiper, M.F.C. Willemsen, A. Torrisi and G.J. Vanderkolk, *J. Vac. Sci. & Technol.-B* **9**, 1503 (1991).

[97] D. Kim and H. Jeon, *Thin Solid Films* **346**, 244 (1999).

[98] S.G. Park and H. Jeon, *J. of Korean Phys. Soc*. **34**, S526 (1999).

[99] J.J. Jeong, S. Ghosh, J. Lim and C.Lee, *Mat. Sci. and Eng. –B*, **96**, 240 (2002).

[100] B.Z. Li, X.P. Qu, G.P. Ru, N. Wang and P. Chu, *Nucl. and growth processes in materials* **580**, 117 (2000).

[101] X.P. Qu, G.P. Ru, Z.Y. Han, B.L. Xu, B.Z. Li, N. Wang and P.K. Chu, *J. Appl. Phys.* **89**, 2641 (2001).

[102] C. Detavernier, R.L. Vanmeirhaeghe, H. Bender, O. Richard, B. Brijs and K. Maex, *J. Appl. Phys.* **92**, 1207 (2002).

[103] H.S. Rhee and B.T. Ahn, *J. Electrochem. Soc*. **146**, 2720 (1999).

[104] J. P. Gambina and E. G. Colgan, *Mat. Chem. Phys*. **52**, 99 (1998).

[105] F. Deng, K. Ring, Z.F. Guan, S.S. Lau, W.B. Dubbelday, N. Wang and K.K. Fung, *J. Appl. Phys*. **81**, 8047 (1997).

[106] J. Chen, J.P. Colinge, D. Flandre, R. Gillon, J.P. Raskin and D Vanhoenacker, *J. Electrochem. Soc*. **144**, 2437 (1997).

[107] T. Ohguro, S. Nakajima, M. Koike, T. Morimoto, A. Nishiyama, Y. Ushiku, T. Yoshitomi, M. Saito and H. Iwai, *IEEE Trans. Electron Devices*, **41**, 2305 (1994).

[108] D. Mangelinck, J.Y. Dai, J. S. Pan and S.K. Lahiri, *Appl. Phys. Lett*. **75**, 1736 (1999).

[109] J.F. Liu, H.B. Chen, J.Y. Feng and J. Zhu, *Appl. Phys. Lett*. **77**, 2177 (2000).

[110] J.F. Liu, J.Y. Feng and J. Zhu, *J. Appl. Phys*, **90**, 745 (2001).

[111] J.F. Liu, J.Y. Feng and J. Zhu, *Appl. Phys. Lett*. **80**, 270 (2002).

[112] F. Corni, B.G. Gregorio, G. Ottaviani, G. Queirolo and J.P. Follegot, *Appl. Surf. Sci.* **73**, 197 (1993).

[113] J.F. Liu, H.B. Chen and J.Y. Feng, *J. Cryst. Growth* **220**, 488 (2000).

[114] R.N. Wang and J.Y. Feng, *J. Phys. – Condensed Matter*, **15**, 1935 (2003).

[115] C.J. Tsai, P.L. Chung and K.H. Yu, *Thin Solid Films* **365**, 72 (2000).

[116] R. de Reus, H.C. Tissink and F.W. Saris, *J. Mater. Res*. **5**, 341 (1990).

[117] U. Falke, F. Fenske, S. Schulze and M. Hietschold, *Physica Status Solidi A-Applied Research* **162**, 615 (1997).

[118] M. Hietschold, S. Schulze, U. Falke, F. Fenske and W. Wolke, *Appl. Surf. Sci.* **102**, 156 (1996).

[119] F. Fenske, A. Schopke, S. Schulze and B. Selle, *Appl. Surf. Sci.* **104**, 218 (1996).

[120] J.-H. Lee, G.A. Rozgonyi, B.K. Patnaik, D. Knoesen, D. Adams, P. Balducci and A. S. Salih, J. Appl. Phys. **73**, 4023 (1993).

[121] J.S. Maa, Y. Ono, D.J. Tweet, F.Y. Zhang and S.T. Hsu, *J. Vac. Sci. & Technol. A-Vac. Surf. and Films*, **19**, 1595 (2001).

[122] S.K. Saha, R.S. Howell and M.K. Hatalis, *Thin solid Films*, **347**, 278 (1999).

[123] M. Garciamendez, F.F. Castillon, G.A. Hirata, M.H. Farias and G. Beamson, *Appl. Surf. Sci.* **161**, 61 (2000).

[124] Y.W. Ok, C.J. Choi and T.Y. Seong, *J. Electrochem. Soc.* **150**, 385 (2003).

[125] H. Yang, R.F. Pinizzotto, L. Luo and F. Namavar, *Appl. Phys. Lett.* **62**, 2694 (1993).

[126] C. Cabral, L.A. Clevenger, J.M.E. Harper, F.M. Dheurle, R.A. Roy, K.L. Saenger, G.L. Miles and R.W. Mann, *J. Mat. Research* **12**, 304 (1997).

[127] Cabral, L.A. Clevenger, J.M.E. Harper, R.A. Roy, K.L. Saenger, G.L. Miles and R.W. Mann, *Thin films – Stucture and Morphology* **441**, 295 (1997).

[128] S.L. Cheng, J.J. Jou, L.J. Chen and B.Y. Tsui, *J. Mat. Research* **14**, 2061 (1999).

[129] S.L. Cheng, J.J. Jou, L.J. Chen and B.Y. Tsui, *Mat. Chem. and Phys.* **54**, 346 (1998).

[130] W. Kaplan, A. Mouroux, S.L. Zhang and C.S. Petersson, *Microelectr. Eng.* **37**, 461 (1997).

[131] A. Mouroux, S.L. Zhang, W. Kaplan, S. Nygren, M. Ostling and C.S. Petersson, *Appl. Phys. Lett.* **69**, 975 (1996).

[132] A. Mouroux, W. Kaplan, S.L. Zhang and S. Petersson, *Microelectr. Eng.* **37**, 449 (1997).

[133] A. Mouroux and S.L. Zhang, *J. Appl. Phys.* **86**, 704 (1999).

[134] M. Roux, A. Mouroux and S.L. Zhang, *Advanced Interconnects and Contacts*, **564**, 53 (1999).

[135] S.L. Zhang, C. Lavoie, C. Cabral, J.M.E. Harper, F.M. D'Heurle and J. Jordan-sweet, *J. Appl. Phys.* **85**, 2617 (1999).

[136] Z.B. Zhang, S.L. Zhang, D.H. Zhu, H.J. Xu and Y. Chen, *Int. J. Modern Phys.* **16**, 205 (2002).

[137] A. Mouroux, S.L. Zhang, W. Kaplan, S. Nygren, M. Ostling and C.S. Petersson, *Adv. Metallization for Future ULSI* **427**, 511 (1996).

[138] H. Jeon, H. Won, Y. Kim, J. Lee and R.J. Nemanich, *J. Korean Pysical Soc.* **40**, 903 (2002).

[139] F. Lavia, F. Mammoliti, M.G. Grimaldi, S. Quilici and F. Meinardi, *Microelectr. Eng.* **55**, 123 (2001).

[140] F. Lavia, S. Privitera, F. Mammoliti, M.G. Grimaldi, *Microelectr. Eng.* **60**, 197 (2002).

[141] F. Lavia, F. Mammoliti, G. Corallo, M.G. Grimaldi, D.B. Migas and L. Miglio, *Appl. Phys. Lett.* **78**, 1864 (2001).

[142] A. Mouroux, S.L. Zhang and S. Petersson, *Physical Review B – Condensed Matter* **56**, 10614 (1997).

[143] R.N. Wang, J.Y. Feng and Y. Huang, *J. Crystal Growth* **253**, 280 (2003).

[144] H. Jeon, B. Jung, Y.D. Kim, W.C. Yang and R.J. Nemanich, *J. Appl. Phys.* **88**, 2467 (2000).

[145] B. Jung, Y.D. Kim, W. Yang, R.J. Nemanich and H. Jeon, *Adv. Interconnects and Contacts* **564**, 59 (1999).

[146] B. Jung, Y.D. Kim, H. Jeon, W. Yang and R.J. Nemanich, *J. Korean Physical Soc.* **35**, S769 (1999).

[147] A.S. Ozcan and K.F. Ludwig, *Magnetic and Electronic films –Struc.Text. and Appl*. **721**, 43 (2002).

[148] S.L. Zhang, F.M. Dheurle, C. Lavoie, C. Cabral and J.M.E. Harper, *Appl. Phys. Lett.* **73**, 312 (1998).

[149] J. Aberg, S. Persson, P.E. Hellberg, S.L. Zhang, U. Smith, F. Ericson, M. Engstrom and W. Kaplan, *J. Appl. Phys*. **90**, 2380 (2001).

[150] A.T.S. Wee, A.C.H. Huan, T. Osipowicz, K.K. Lee, W.H. Thian, K.L. Tan and R. Hogan, *Thin Solid Films* **283**, 130 (1996).

[151] S. Yoon and H. Jeon, *J. Korean Physical Soc*. **34**, 365 (1999).

[152] C.C. Theron, A. Falepin, S. DeGroote, J. Dekoster, A. Vantomme, G. Langouche, H. S. DeWaal and R. Pretorius, *Nucleation and Growth Processes in Mat*. **580**, 123 (2000).

[153] R.N. Wang and J.Y. Feng, *J. Crystal Growth* **422**, 206 (2002).

[154] H.C. Swart and G.L.P. Berning, *Appl. Surf. Sci*. **78**, 77 (1994).

[155] R.S. Rastogi, V.D. Vankar and K.L. Chopra, *Thin Solid Films*, **206**, 34 (1991).

[156] C.C. Theron, J.A. Mars, C.L. Churms, J. Farmer and R. Pretorius, *Nucl. Instr. Methods in Phys. Research-B* **139**, 213 (1998).

[157] J.S. Choi, S.H. Peak, Y.S. Hwang, S.G. Kang, H.C. Cho, J.E. Oh, T.E. Shim, S.I. Lee, J.K. Lee and J.G. Lee, *J. Appl. Phys*. **74**, 1456 (1993).

[158] F. Mahmood, H. Ahmed and M. Suleman, *J. Mat. Sci*. **28**, 3155 (1993).

[159] L.C. Feldman and J.W. Mayer, Fundamentals of Surface and Thin Film Snalysis (North-Holland, New York, 1986).

[160] W.K. Chu, J.W. Mayer and M.A. Nicolet, Backscattering Spectrometry (Academic Press, New York, 1978).

[161] L.R. Doolittle, *Nucl. Instr. Meth. in Phys. Research-B*, **9**, 344 (1985).

[162] R. Steadman, Crystallography (University of Bradford, Bradford, 1995).

[163] P. Villars and L.D. Calvert, Pearson's Handbook of Crystallographic Data for Intermetallic Phases (Academic Press, New York, 1998).

[164] C.L. Churms, *C.C. Millar: A Crystallographic Calculator*, iThemba Labs, South Africa (1996).

APPENDIX A

Phase identification by X-ray diffraction

A.1 Plane spacing

The value of d, the distance between adjacent crystallographic planes in the set (hkl), may be found from the following equations **[162]:**

Cubic
$$\frac{1}{d^2}=\frac{h^2+k^2+l^2}{a^2}$$

Tetragonal
$$\frac{1}{d^2}=\frac{h^2+k^2}{a^2}+\frac{l^2}{c^2}$$

Hexagonal
$$\frac{1}{d^2}=\frac{3}{4}\left(\frac{h^2+hk+k^2}{a^2}\right)+\frac{l^2}{c^2}$$

Rhombohedral
$$\frac{1}{d^2}=\frac{\left(h^2+k^2+l^2\right)\sin^2\alpha+2\left(hk+kl+hl\right)\left(\cos^2\alpha-\cos\alpha\right)}{a^2\left(1-3\cos^2\alpha+2\cos^3\alpha\right)}$$

Orthorhombic
$$\frac{1}{d^2}=\frac{h^2}{a^2}+\frac{k^2}{b^2}+\frac{l^2}{c^2}$$

Monoclinic
$$\frac{1}{d^2}=\frac{1}{\sin^2\beta}\left(\frac{h^2}{a^2}+\frac{k^2\sin^2\beta}{b^2}+\frac{l^2}{c^2}-\frac{2hl\cos\beta}{ac}\right)$$

Triclinic
$$\frac{1}{d^2}=\frac{1}{V^2}\left(S_{11}h^2+S_{22}k^2+S_{33}l^2+2S_{12}hk+2S_{23}kl+2S_{13}hl\right)$$

In the above equation for triclinic crystals the symbols are defined by the following equations **[162]:**

V = volume of unit cell (see A.2 below)

$$S_{11} = b^2c^2 \sin^2 \alpha$$
$$S_{22} = a^2c^2 \sin^2 \beta$$
$$S_{33} = a^2b^2 \sin^2 \gamma$$
$$S_{12} = abc^2 \left(\cos\alpha \cos\beta - \cos\gamma\right)$$
$$S_{23} = a^2bc\left(\cos\beta \cos\gamma - \cos\alpha\right)$$
$$S_{13} = ab^2c\left(\cos\gamma \cos\alpha - \cos\beta\right)$$

A.2 Cell volumes

The following equations gives the volume of the unit cell **[162]:**

Cubic $V = a^3$

Tetragonal $V = a^2c$

Hexagonal $V = \dfrac{\sqrt{3}a^2c}{2}$

Rhombohedral $V = a^3\sqrt{1 - 3\cos^2\alpha + 2\cos^3\alpha}$

Orthorhombic $V = abc$

Monoclinic $V = abc\sin\beta$

Triclinic $V = abc\sqrt{1 - \cos^2\alpha - \cos^2\beta - \cos^2\gamma + 2\cos\alpha\cos\beta\cos\gamma}$

A.3 Diffraction directions

The Bragg law can be combined **[159]** with the plane spacing equation and then the diffraction angle can be predicted. For example, if the crystal is cubic, then

$$\frac{1}{d^2} = \frac{h^2 + k^2 + l^2}{a^2}$$

and $$\lambda = 2d \sin\theta$$

The combination of these two equations yields the following equation

$$\sin^2\theta = \frac{\lambda^2}{4a^2}\left(h^2 + k^2 + l^2\right)$$

and the reflections of the (110) planes in terms of the angle of the incident X-ray beam will then occur at

$$\sin^2\theta_{110} = \frac{\lambda^2}{2a^2}$$

A.4 X-ray and crystallographic data of Ni-silicide phases

Table A.1 gives the crystal parameters of different Ni-silicide phases as obtained from Pearson's Handbook of Crystallographic Data for Intermetallic Phases **[163].**

Table A. 1. Crystal parameters of different Ni-silicide phases.

Compound	Crystal system	Space group	Prototype	Lattice constants (Å)		
				a	b	c
Si	cubic	cF8 Fd$\underline{3}$m	C	5.428		
Ni	cubic	cF4 Fm$\underline{3}$m	Cu	3.523		
NiSi	orthorhombic	Op8 Pnma	MnP	5.18	3.34	5.62
NiSi	cubic	cP8 $P2_13$	FeSi	4.446		
$NiSi_2$	cubic	cF12 Fm$\underline{3}$m	CaF_2	5.406		
Ni_2Si	orthorhombic	oP12 Pnma	Co_2Si	5.0	3.73	7.04
Ni_2Si	hexagonal	hP6 $P6_3/m$	Ni_2Si	3.805		4.89
Ni_3Si	cubic	cP4 Pm$\underline{3}$m	$AuCu_3$	3.504		
Ni_3Si	cubic	cP2 Pm$\underline{3}$m	ClCs	2.808		
Ni_3Si	cubic	cF4 Fm$\underline{3}$m	Cu	3.526		
Ni_3Si_2	orthorhombic	oC80 $Cmc2_1$	Ni_3Si_2	12.22	1.080	6.924

The XRD data shown in **Table A.2** was acquired by making use of the C.C. Millar Crystallographic Computer Simulation Program **[164].**

Table A. 2. Characteristic lines used for phase identification in the Ni-silicide system. The intensity in powder of the two or three strongest powder diffraction lines are given in each case.

Phase	Crystal system	Strong lines in 2θ	hkl values	Intensity in powder (%)
Si (C)	cubic	28.46	111	100
		47.30	220	67
Ni	cubic	44.49	111	100
		51.83	200	47
Ni_2Si	orthorhombic	39.50	112	34
		42.51	103	
		44.39	202	
		45.61	211	100
		48.77	020	33
		53.49	203	
NiSi	orthorhombic	31.10	011	77
		31.80	002	
		34.60	200	
		35.71	111	
		36.32	102	
		38.22	201	
		44.20	210	
		45.63	112	88
		47.21	211	99
		51.83	103	
		64.88	022	
		69.19	104	
$NiSi_2$	cubic	28.57	111	81
		47.51	220	100

A.5 X-ray and crystallographic data of Co-silicide phases

Table A.3 gives the crystal parameters of different Co-silicide phases as obtained from Pearson's Handbook of Crystallographic Data for Intermetallic Phases **[163].**

Table A. 3. Crystal parameters of different Co-silicide phases.

Compound	Crystal system	Space group	Prototype	Lattice constants (Å)		
				a	b	c
Si	cubic	cF8 Fd$\underline{3}$m	C	5.428		
Si	cubic	cI16 I a$\underline{3}$	Si	6.636		
Co	cubic	cF4 Fm$\underline{3}$m	Cu	3.544		
Co	hexagonal	hP2 $P6_3/mmc$	Mg	2.507		
Co	hexagonal	hP46 $P6_3mc$	Co	8.320		
CoSi	cubic	cP8 $P2_13$	FeSi	4.442		
$CoSi_2$	cubic	cF12 Fm$\underline{3}$m	CaF_2	5.365		
Co_2Si	orthorhombic	oP12 Pnma	Co_2Si	4.918	3.738	7.109
Co_2Si_3	tetragonal	tP20 P$\underline{4}$c2	Ru_2Sn_3	5.234		8.543
Co_3Si	hexagonal	hP8 $P6_3/mmc$	Ni_3Sn	4.976		4.069

The XRD data shown in **Table A.4** was acquired by making use of the C.C. Millar Crystallographic Computer Simulation Program **[164].**

Table A. 4. Characteristic lines used for phase identification in the Co-silicide system. The intensity in powder of the two or three strongest powder diffraction lines are given in each case.

Phase	Crystal system	Strong lines in 2θ	hkl values	Intensity in powder (%)
Si (Si)	cubic	33.09	211	93
		47.40	222	
		65.94	332	
		69.28	422	
Co	cubic	44.20	111	100
		51.50	200	46
Co_2Si	orthorhombic	21.95	101	100
		25.03	002	36
		42.28	103	16
CoSi	cubic	45.61	210	100
		50.25	211	49
		66.35	310	
$CoSi_2$	cubic	28.78	111	79
		33.36	200	
		47.90	220	100
		70.07	400	15

A.6 X-ray and crystallographic data of Fe-silicide phases

Table A.5 gives the crystal parameters of different Fe-silicide phases as obtained from Pearson's Handbook of Crystallographic Data for Intermetallic Phases **[163].**

Table A. 5. Crystal parameters of different Fe-silicide phases.

Compound	Crystal system	Space group	Prototype	Lattice constants (Å)		
				a	b	c
Si	cubic	cF8 Fd3m	C	5.428		
Fe	cubic	cI2 Im3m	W	2.937		
Fe	cubic	cF4 Fm3m	Cu	3.666		
ε-FeSi	cubic	cP8 $P2_13$	FeSi	4.448		
β-$FeSi_2$	orthorhombic	oC48 Cmca	$FeSi_2$	9.63	7.791	7.833
α-$FeSi_2$	tetragonal	tP3 P4/mmm	$FeSi_2$	2.695		5.09
Fe_2Si	hexagonal	hP6 P3ml	Fe_2Si	4.052		5.085
Fe_2Si	cubic	cP2 Pm3m	ClCs	2.81		
Fe_2Si	cubic	cF16 Fm3m	BiF_3	2.808		
Fe_5Si_3	hexagonal	hP16 $P6_3/mcm$	Mn_5Si_2	6.755		4.717

The XRD data shown in **Table A.6** was acquired by making use of the C.C. Millar Crystallographic Computer Simulation Program **[164].**

Table A. 6. Characteristic lines used for phase identification in the Fe-silicide system.

Phase	Crystal system	Strong lines in 2θ	hkl values	Intensity in powder (%)
Si (C)	cubic	28.46	111	100
		47.30	220	67
Fe (W)	cubic	43.51	110	100
		79.89	211	28
FeSi	cubic	28.07	110	20
		34.56	111	16
		45.12	210	100
		79.84	321	27
β-$FeSi_2$	orthorhombic	29.19	220	100
		37.57	312	34
		45.96	331	33
α-$FeSi_2$	tetragonal	17.40	001	84
		49.18	102	100

Pectora roborant cultus recti

APPENDIX B

Dynamic RBS data acquisition

The data-acquisition procedure used for dynamic RBS **[156]** is basically the same as that for conventional RBS measurements. The data is not stored as individual RBS events, as this could lead to data storage problems because of the vast amounts of data involved, but it is stored in "time-slices" of 10 or 30 seconds each.

The charge accumulated during each time-slice is also recorded and is used to charge normalize all the spectra in a given run, in case any beam current fluctuations occur during the run. The beam current can also be influenced by the on and off switching of the heating elements and this effect was corrected by requiring that the integral number of counts in a certain energy window of some constant part of the spectrum, for example the substrate, be constant for the given run. The counts in each spectrum are then adjusted by a correction factor so that the integral over the energy window for that spectrum is equal to the average of all the spectra.

The temperature is measured by an Eurotherm controller and transmitted to the data acquisition computer as an analog signal. This signal is then fed into a single channel analyser and converted to a digital value. Appropriate filters were installed onto the transmission lines to make the signal more stable, because the temperature measurement is sensitive to pick-up noise In practice this means that a statistical fluctuation, resulting from the temperature signal and not from an actual fluctuation in the temperature, was introduced into the temperature measurement. In this way the temperature can be controlled to ± 1˚C for isothermal anneals. The temperature is sampled ten times per time-slice, which for a 10 s slice means a sampling rate of 1 Hz.

Resistance measurements are made simultaneously by using a separate PC that is fitted with a PH-IB interface card. This PC controls a digital multimeter and sends the measured resistance values to the main data acquisition computer via a RS-232 serial cable.

APPENDIX C

RUMP Simulation of Ta double peak structure

The input data for the RUMP computer program that was used to simulate the double Ta RBS peaks that occurred in the Si|Ta|Ni RBS spectrum discussed in **Chapter 4, paragraph 4.2.1.5,** is given below. The simulation was done according to the following sample structure:

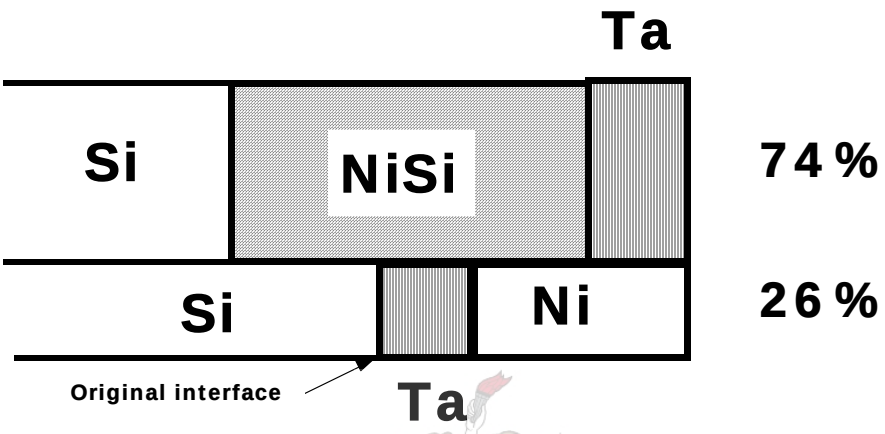

Two separate layers were simulated, the top layer receiving 74 % and the bottom layer 26 % of the total incident charge. The two RBS spectra were then added together.

Input data

```
RBS  File:   A:\tani0011.rbs
  Identifier:  D3 Si/Ta20A/Ni 30min 500C
  LTCT Text:   Irradiation time (sec): 309
  Date:        Mon May 14 16:01:51 2001
  Beam:        2.000 MeV   4He+     20.00 uCoul  @ 64.00 nA
  Geometry:        IBM  Theta:  -10.00  Phi:   15.00  Psi:    5.00
  MCA:         Econv:   4.050   59.130  First chan:  0.0  NPT:  504
  Detector:    FWHM: 20.0 keV  Tau:  5.0   Omega: 1.150
  Correction:  1.0303
  #         Thickness         Sublayers     Composition  . . .
   1           4.20  /CM2        auto         Ta   1.000
   2 (L)    1113.26  /CM2        auto         Si   1.000     Ni  1.689
*  3           4.10  /CM2        auto         Ta   1.000
   4 (L)     919.11  /CM2        auto         Si   2.000     Ni  1.145
                  with fuzzing of 855.06 in 9 steps
   5       30000.00     A        auto         Si   1.000
```